Seawater Intrusion Modeling with Single-Density Codes

Nathan R. Hatch

ISBN 000-00-0000-000-0

TU Delft

Seawater Intrusion Modeling with Single-Density Codes

by

Nathan R. Hatch

to obtain the degree of Master of Science

at the Delft University of Technology,

to be defended publicly on Wednesday February 25, 2021 at 4:00 PM.

Student number:	4776496	
Project duration:	January 1, 2020 – February 25, 2021	
Thesis committee:	Prof. dr. ir. M. Bakker,	TU Delft, supervisor
	Dr. G. Schoups,	TU Delft
	Dr. B. van Breukelen,	TU Delft
	Dr. S. Kraemer	US EPA

This thesis is confidential and cannot be made public until March 31, 2021.

TU Delft

Preface

I want to first thank my advisor, Mark Bakker, for this opportunity to build my skills and deepen my knowledge of groundwater modeling codes and seawater intrusion. It is a great complement to my Masters at Delft where I was able to build on my skill-set and enrich my education and perspective. Mark was helpful and critical in just the right ways, helping me think through it and figure it out with appropriate guidance. During the course of the thesis, I really expanded my abilities and consideration both through the fine details of modeling and the high-level perspective critical to ensuring a model that fulfills its purpose.

I also want to thank my family and friends who have been so supportive throughout this entire process. My family always makes effort to be helpful-however that may be required. My friends also have been such a positive influence during my time at Delft and are one of my proudest experiences. Without these kinds of people that I have been so fortunate to have found, this product would not be what it is today and I would not have learned and grown as much as I have. Specifically, I want to thank Force Elektro, the ultimate frisbee club, for providing such great friendship and an important outlet to keep myself sane and healthy during my studies. I have developed a fond association and relationship with The Netherlands, and Delft that I look forward to building upon and maintaining. I learned so much even going beyond water management.

Nathan R. Hatch
February, 2021

Summary

Saltwater intrusion modeling is an important tool for coastal water resource managers and engineers to understand the threat to their water supply and to plan for different scenarios. Seawater intrusion can be a complex phenomenon that typically comes with limited-to-no monitoring information regarding the location of the saltwater plume or the interface between the saltwater and the freshwater. Many coastal aquifers are at risk due to unsustainable levels of groundwater extraction, decreasing river flows and natural recharge, and sea level rise (IPCC, 2019; Kummu et al., 2016). These issues benefit from models that can help managers make decisions to protect their residents and resources.

Seawater intrusion modeling can be divided into two categories: miscible flow models and immiscible flow models (Bobba, 1993; Werner et al., 2013). Miscible flow models typically use numerical methods to solve fully coupled flow and transport equations (e.g. SUTRA (Voss and Provost, 2010), SEAWAT (Langevin et al., 2008)). They model the transport of chloride and density-driven flows related to the saltwater-freshwater interaction. These processes require sufficient grid discretization and small time-steps. Put together, this results in models that are computationally expensive and take a long time to complete and run. Combined with limited monitoring information also creates a problem with parameterization that increases the uncertainty of these models (Carrera et al., 2009, Werner et al., 2013). Immiscible flow models neglect mixing between saltwater and freshwater and can sometimes be solved with analytical solutions. Immiscible flow models typically solve for the position of the interface between the saltwater and the freshwater. There are transient interface models that predict the changing location of an interface in response to variable boundary conditions and steady-state interface models that are used to determine the final position of the interface for a given set of boundary conditions. Another issue facing steady interface models is how to deal with moving saltwater (Shamir and Dagan, 1971; Mercer at al., 1980). In cases where mean sea level is not equal everywhere in the model, the saltwater will be moving beneath the freshwater and the heads between known boundary conditions will vary.

Bakker and Schaars (2013) present a method for solving for the steady interface location using single-density groundwater codes such as MODFLOW (Harbaugh et al., 2000; Harbaugh, 2005). Steady-state models are suitable for scenario analysis functionality (Cheng et al., 2000; Manteglou, 2003). This method is able to take the ability of numerical models to represent complex environments

while maintaining fast and precise solutions. This is done through a transformation of an existing single-density groundwater flow model. The transformation for single-layer and multi-layer models involves scaling the horizontal hydraulic conductivity by the density factor, α (Equation 3.14), the inverse scaling of the model layer thicknesses and vertical hydraulic conductivity by α (Equations 3.15-3.17), and the flipping of the model layers about mean sea level (Equations 3.15-3.16). The method is expedient and relatively simple to implement–especially in comparison to creating a standalone miscible flow seawater intrusion model. FloPy, a Python package designed to work with MODFLOW models was used through Jupyter Notebooks to implement this method efficiently. Using GUIs (Graphical User Interfaces) for the implementation of this method would be very difficult so the use of Python-enabled MODFLOW model manipulation is a critical component to this research displaying the potential of FloPy as a MODFLOW tool. This approach is applied to three different coastal aquifer models to evaluate the performance of the method when applied to real-world models. This thesis also attempts to address the issue of moving saltwater through an iterative approach where the saltwater head and freshwater head are modeled separately.

The first model this method is applied to is in the area of Los Angeles, California, USA. This first model is relatively coarse yet the area is geologically complex with many faults and folds. The method is applied successfully to a pre-development version of the model and gives realistic results for the interface position based on the boundary conditions. A critical pumping exercise is performed using the method to demonstrate its capability of solving for different scenarios. From this model, the results reveal that the faults running across the middle of the model act as major impediments to both freshwater flow from inland areas and to seawater intrusion pushing farther inland. The critical pumping rate for the hypothetical well location is 1,305,000 ft^3/d (44 af/d, 54,283 m^3/d). Reichard (2003) reports that the total net pumping in the basin is 10 times this amount for the period from 1971-2000 but most of those wells are on the inland side of the main faults as well as a barrier of injection wells.

The second model this method is applied to is the island of Terschelling, a part of the Frisian Islands, in the Netherlands. This island has simple model layers that are horizontal except for the model top which represents the island's topography of dunes and polders. Terschelling also has two different sea levels in different parts of the model which provides an opportunity to attempt to solve for moving saltwater. Bakker and Schaars' (2013) method is applied to estimate the interface position successfully. The model includes existing wells and supports the idea that the pumping rates on the island are sustainable. The critical pumping rate of these wells is determined to be approximately 75 times greater than the pumping rate used in the original model. The iterative method to solve for moving saltwater is attempted but ultimately unsuccessful. The method creates inactive zones in the freshwater model that are within the bounds of the original active area of the model. It becomes impossible to expand the

inactive zones and consequently, the active model area contracts unrealistically resulting in a deeper and steeper interface than what is realistic. The iterative approach needs to be modified to resolve this problem,

The third model this method is applied to is of the Alamitos Gap, straddling the southern boundary of the first model in Southern California, USA. This model is complex with fine grid cells, high variability in vertical hydraulic conductivity and model layer elevations, and a large inactive zone representing the impact of regional faults and outcrops. This inactive zone disconnects 12 of the 13 model layers from the ocean so that the only connection to the sea is through the top layer. This type of disconnect between the sea and the model ultimately invalidates the method of Bakker and Schaars (2013) as the method requires a connection to the sea so that the saltwater head in the saltwater can be approximated as equal to sea level. Therefore, it is not possible to compute an interface position for this model.

Several challenges were faced when implementing the Bakker and Schaars method method to these models. It was important to understand the boundary conditions, their purpose for each model, and how they work when the model is flipped about sea level. In some cases, the boundary conditions may not apply when the model is flipped. For instance, the Terschelling model had drain cells that had to be removed because they would remove too much water in the transformed model. A related challenge was the issue of starting heads and fixed-head-boundaries. The layer bottoms are mostly higher than the original model (with the common exception being the original uppermost layer); this means that starting heads and fixed heads must be above those layer bottoms which may be different than the original boundary conditions. For example, in the Alamitos Gap model, there were fixed-head-boundaries on the inland side of the model that were below sea level. This was possible because there is a series of injection wells and faults that prevents seawater from flowing inland. When the model was flipped, these below-sea-level boundary conditions caused model failure and the boundary conditions had to be adjusted or the adjustment of saturated thickness is not applied in this area.

The method works well and is quite efficient. It is a powerful tool for broad management of coastal aquifers through scenario analysis that is cheap and expedient. For further research, it is recommended to compare results to other seawater intrusion modeling tools (e.g., SEAWAT, SWI2) in the same locations and further developing the procedure to facilitate easy implementation. Seawater intrusion modeling will benefit greatly from improved monitoring efforts and technologies. Technologies such as aerial electromagnetic mapping provide optimism for improvement in the future (Auken et al., 2010, Gottschalk et al., 2020). The method of Bakker and Schaars (2013) paired with improved monitoring offers potential for efficient futures in coastal aquifer modeling and management.

Contents

List of Figures

List of Tables

1 Introduction

1.1. Motivation

1.1.1. Saltwater Intrusion

Seawater, or saltwater, intrusion refers to the movement of saltwater into a freshwater aquifer. The variability of hydrogeologic settings, source of saline water, sea levels, and history of groundwater withdrawals and surface drainage all influence the extent of saltwater intrusion (Barlow, 2003).

Seawater intrusion is of interest primarily because it can cause the abandonment of wells or a general decrease of freshwater storage in coastal aquifers. Coastal areas have high population densities which may be vulnerable to seawater intrusion (Kummu et al., 2016). Rising sea levels and increasing water demand leading to increased groundwater extraction also threaten to increase seawater intrusion (IPCC, 2019).

While monitoring of seawater intrusion can be difficult and is often limited, water resource managers still need to protect their inland water supplies. Seawater intrusion modeling is a valuable tool for the protection and maintenance of coastal freshwater supplies but it can be a complex process that comes with many challenges.

1.1.2. Approaches to Seawater Intrusion Modeling

Seawater intrusion modeling can be categorized into two distinct groups: interface models and miscible flow models (Bobba, 1993; . Interface models neglect dispersion and diffusion and assume that saltwater moves through the aquifer by advection only. Interface models assume a zero thickness of the mixing zone between the saltwater and freshwater. Miscible flow models consider a finite thickness of the mixing zone where the salinity and, hence, the density of water varies continuously. Analytical solutions exist for some relatively simple interface problems whereas numerical solutions are used to simulate more complicated interface models and represent miscible flow.

1.1.2.1. Interface Models

Interface models are often used for steady conditions to determine the equilibrium position of the interface. Further simplifications usually involve adoption of the Dupuit approximation so that head in the freshwater zone is only a function of horizontal coordinates. The freshwater head can then be converted to a depth through the Ghyben-Herzberg relation, which is a linear expression of interface depth as a function of freshwater head. The interface can be understood to represent the location where the concentrations of freshwater and seawater are approximately 50% each.

There are many exact solutions to steady interface flow problems, some based on the Strack potential. The Strack potential allows for solutions to be written as one expression where the potential is a function of the horizontal coordinates regardless of the interface position. While the Strack potential is valid for piecewise homogeneous aquifers, interface solutions become difficult to obtain in multi-aquifer systems which lead to nonlinear differential equations. There are few exact solutions to interface flow where both freshwater and seawater are moving as the analytical problem becomes much more complicated. Transient interface flow in multi-aquifer systems may be simulated with finite difference models, for example using the SWI package in MODFLOW (Bakker et al, 2013).

The SWI package is based on the Dupuit approximation so it does not require vertical discretization of aquifer layers. SWI computes the salinity distribution through time by application of continuity of flow for water of different salinities, while neglecting additional mixing of different salinities during the simulation. Consequently, the SWI package requires three orders of magnitude less computational effort than the codes that solve for fully combined flow and transport equations. However, SWI requires parameterization of the model through specification of the initial interface position and some algorithm-specific parameters. SWI may take significant computational time to simulate the steady position of the interface.

1.1.2.2. Miscible Flow Models

Miscible flow models rely on numerical solution techniques. Most codes used to solve miscible flow solve a coupled system of variable density flow and solute transport equations. This is numerically complicated and computationally expensive. Finite element or finite difference methods are applied to solve these problems and small time steps are usually required to limit issues with numerical dispersion. To obtain accurate solutions of solute transport, significantly fine discretization of the model grid is also required. Popular codes to simulate variable density flow include: SEAWAT (Langevin et al., 2008), SUTRA (Voss and Provost, 2010), and FEFLOW (Diersch and Kolditz, 2002). All of these codes solve the coupled flow and transport equations and all the associated complexities such as the evolution of mixing zones and density inversions. The SWI package can be considered a miscible flow model but it does not solve the full coupled flow and transport equations (Bakker and Schaars, 2005).

1.1.3. Challenges to Seawater Intrusion Modeling

Seawater intrusion modeling comes with many challenges related to computational effort, parameterization, and calibration. A brief overview of some of the challenges that seawater intrusion modeling face is presented here.

1.1.3.1. Computational Effort

Miscible flow models are able to more accurately represent the complexity of many real-world seawater intrusion settings. They require fine discretization and solutions of complex equations. Because of this, computational requirements are significant especially when attempting to run models until steady-state conditions are reached. Even the SWI package can face some of these problems. Analytical models do not face the computational challenges that variable-density models do, but they are typically limited in the complexity of the scenario they can simulate.

1.1.3.2. Parameter Uncertainty

There is significant difficulty encountered when calibrating seawater intrusion models. Automatic calibration tools are rarely applied to saltwater intrusion models and uncertainty estimation is commonly omitted from saltwater intrusion studies (Carrera et al., 2009). Seawater intrusion models can be sensitive to a number of parameters and evaluating parameters is very difficult and often requires extensive simplification. This leads to very high uncertainty for seawater intrusion model parameters (Werner et al., 2013). The SWI package is also sensitive to a few parameters and this creates some uncertainty in the simulations.

1.1.3.3. Comparison between Model Types and their Uses

The different model types present different advantages and disadvantages. Analytical models can provide exact solutions to seawater intrusion problems, but when problems get complicated (transience, heterogeneity, multi-layer aquifer systems), the equations become too difficult to solve analytically (Sikkema and Van Dam, 1982). Numerical techniques can be used to solve complex sets of equations to represent realistic and complicated environments, but the computational effort and parameter uncertainty pose significant hurdles.

1.1.3.4. Aquifer Management Modeling

When it comes to coastal aquifer management, steady-state solutions are used for their scenario analysis functionality (Cheng et al., 2000; Manteglou, 2003). This empowers interface models and exacerbates the problems variable-density flow models have. However, interface models tend to give unrealistic results in areas where dispersion plays a significant role and tend to overestimate the extent of seawater intrusion. Pool and Carrera (2011) showed that the mixing zone is wider and more seaward than interface models predict when large dispersivity is present. The SWI package may be viewed as middle-ground as it has been demonstrated that it performs reasonably well when compared with codes that solve fully combined equations except in situations where dispersion is large, when vertical hydraulic conductivity is less than 1% of horizontal hydraulic conductivity, and in some cases of inversion for transient modeling (Dausman et al, 2010). The SWI package requires significantly large computational times when solving for steady-state conditions desired for aquifer management.

Considering the computational expense and the conservative results of interface models, the use of interface models is often sufficient for management of coastal aquifers. However, it seems the use of numerical methods is necessary to represent real-world seawater intrusion problems. Bakker and Schaars (2013) formulated an approach to use numerical solvers for regular flow to solve for the steady interface position without the need of a transient simulation.

1.1.3.5. Moving Saltwater

While interface models may present the best tool for steady-state modeling for coastal aquifer management, they often assume that the saltwater is not moving. In some real-world situations, this is not true. On islands, there may be differences in the sea level from one side of the island to the other which would cause movement of the saltwater which translates to an uncertain saltwater head between the known sea levels. The few solutions available to deal with moving saltwater seem to be less suitable for complex environments so there is a modeling gap here (Shamir and Dagan, 1971; Mercer et al., 1980). The original solution put forth by Bakker and Schaars (2005) also assumes that saltwater is not moving. There is a need for solutions to moving saltwater problems that find a way to take advantage

of the computational abilities of numerical methods without the expensive complications that come with most miscible flow models.

1.2. Objectives

Objective 1:

The first objective of this thesis is to evaluate whether the method in Bakker and Schaars (2013) is able to be applied to real-world coastal aquifers by using single-density groundwater codes (MODFLOW).

Objective 2:

The second objective of this thesis is to evaluate whether the interface can be estimated when saltwater beneath the freshwater is also moving using a novel iterative technique.

Bakker and Schaars (2013) propose a technique that utilizes single-density groundwater codes to solve for the position of the steady interface through a simple mathematical transformation of a coastal groundwater model. The problem of finding the freshwater-saltwater interface is mathematically the same as finding the phreatic surface in unconfined flow. Bakker and Schaars (2013) use algorithms in MODFLOW that have been developed to solve for the phreatic surface (including methods to deal with cells that go dry) to compute the position of the interface. This technique was applied to simple situations in their original research. In this thesis, the approach of Bakker and Schaars (2013) is applied to complex multi-layer aquifer systems. In this research, Flopy (Bakker et al., 2016) is used to manipulate the MODFLOW models through the use of Jupyter Notebooks. Furthermore, the Bakker and Schaars method is used to demonstrate how it can be used as a management tool with pumping optimization situations included.

Regarding Objective 2, a new method is developed to simulate the steady interface for aquifers where the saltwater is moving. Most interface models cannot deal with instances of both saltwater and freshwater movement, but this proposed methodology–outlined in Section 2.4–attempts to solve for those instances.

1.3. Outline

The thesis begins in Chapter 2 with an explanation of the methodology. In this section, some basic examples are used to demonstrate how the Bakker and Schaars (2013) method works to estimate the position of the steady interface.

In Chapter 3, the method is applied to three different settings: 1) Los Angeles, California, USA, 2) Terschelling, The Netherlands, and 3) Alamitos Gap, California, USA. These models were chosen because they represented real-world coastal aquifers with varying degrees of complexity and also because they were readily available for use. For each model, the model setting and parameters are explained prior to the application to explain the context. The results of the steady-state interface modeling are then shown for each model and evaluated. For the Terschelling model, the method to estimate the interface when saltwater is moving is also tested.

Chapter 4 discusses the implications of the findings of the research and goes into some recommendations for future research on this topic to substantiate findings or answer new questions that are raised. The results are discussed in the context of the research objective and some of the challenges that seawater intrusion modeling faces. Within that same chapter, the thesis is concluded by summarizing the findings of the thesis in the context of the original research objective. The conclusion reflects on the main questions with regard to saltwater intrusion modeling.

2

Methodology

For this project, the methodology of Bakker and Schaars (2013) is followed and applied to various pre-constructed MODFLOW models. Only flow models using MODFLOW 2000 (Harbaugh et al., 2000) or MODFLOW 2005 (Harbaugh, 2005) are used for the applications in this thesis, but MODFLOW 6 (Langevin et al., 2017) can be used as well. FloPy (Bakker et al., 2016) is used to manipulate the models.

2.1. Main Approximations

The methodology applied has several limitations as well as approximations. The four main approximations are listed below.

1. The transition zone between saltwater and freshwater is approximated as an interface.
2. The system is at steady-state.
3. The pressure in the aquifer is hydrostatic and the Dupuit approximation is adopted.
4. The saltwater is not moving.

Approximation 1: The Transition Zone This approximation addresses the 'transition zone' which refers to the zone in an aquifer where there may be mixing between fresh and saltwater. In some aquifer

systems with higher hydraulic conductivity or more dynamic systems (e.g., strong tidal systems) there may be a wide zone of mixing where the density of water varies more gradually from that of saltwater to freshwater. Such wide transition zones can limit the ability of a sharp interface model to accurately reflect the location of the border between fresh and saltwater.

Approximation 2: Steady-State This approximation addresses the state of the model to be steady. In reality, the conditions controlling flow and seawater intrusion may be dynamic leading to a moving interface or a slightly different location of the interface since terms may be imprecisely averaged. Dynamic effects can not be represented by the model.

Approximation 2 can be made here for conditions in which operational management is the focus for which steady-state models to serve as justified conservative estimates based on long-term operations.

Approximation 3: The Dupuit Approximation The approximation of hydrostatic pressure implies that pressure increases linearly with depth in accordance with the density. This is an important approximation to simplify the solutions, for without this approximation, there could be different heads at different depths within a single layer causing for a much more complicated solution and also an inability to apply the Ghyben-Herzberg method.

This approximation holds when the water table is gently sloping or in general, the vertical head gradient is small.

Approximation 4: Saltwater is Not Moving The approximation that saltwater is static is important because it allows for an approximation of constant saltwater head everywhere in the model. If the seawater were moving, this could cause the interface to react differently and thus, have a different position, due to spatially varying saltwater heads.

This approximation holds most of the time in coastal continental aquifers where the ocean only interacts from one side, In island aquifers, this approximation holds when the sea level around the island is constant; if this is not true then the seawater will be moving and affect the interface position.

2.2. Step-by-Step Approach

A regular MODFLOW (Harbaugh, 2005) model is used for application of the approach of Bakker and Schaars (2013) to simulate steady interface flow. It is common to set the datum of a coastal aquifer model equal to mean sea level (MSL). Each model layer will have its respective aquifer properties including horizontal hydraulic conductivity, vertical conductivity(or leakance), and storage parameters like storativity or specific yield. Each layer will also have a defined thickness and corresponding bound-

ary conditions (wells, rivers, etc.).

The freshwater thickness is a linear function of the head in steady-state Dupuit approximation models. MODFLOW assumes a linear relationship between head and saturated thickness for the simulation of unconfined conditions. The head solution of the transformed model can then use the Ghyben-Herzberg relationship between head and depth-to-interface below sea level to map the steady seawater interface.

Bakker and Schaars (2013) were able to reformulate Dupuit interface flow so that the mathematical formulation is identical to the formulation of unconfined flow in MODFLOW. The following step-by-step approach can be applied to simulate steady Dupuit interface flow with a regular MODFLOW model by putting the model upside-down (flipping about the vertical datum) and by transforming scaled parameters.

Here, a simple step-by-step approach for applying the Bakker and Schaars methodology is given to solve for the steady interface position. The next section will demonstrate the application of some basic examples; a full derivation of the procedure is available in Bakker and Schaars (2013).

---

1 Flip the model upside down (including boundary condition packages) about sea level.

2 Scale the bottom and top of each of the model layers.

3 Scale the hydraulic conductivity both,(horizontal and vertical).

4 Obtain the head solution from the transformed model.

5 Calculate the interface depth using the Ghyben-Herzberg equation (Equation 2.1).

2.3. Explanation of Basic Scenarios

Four examples are used to demonstrate and illustrate the methodology from Bakker and Schaars (2013):

1 Steady unconfined interface flow in a deep aquifer

2 Steady unconfined interface flow in an aquifer with a finite bottom

3 Steady confined interface flow

4 Steady interface flow in multi-layer systems

For all systems, a Cartesian x, y, z coordinate system is adopted with the z direction pointing vertically up. The origin of the z-axis is referred to as the datum and z_s is the sea-level which is approximated as constant. The density of freshwater and saltwater are ρ_f and ρ_s, respectively. The Dupuit approximation is used allowing for the depth of the steady interface below sea level to be calculated using the Ghyben-Herzberg approximation as:

$$D = \alpha(h - z_s) \tag{2.1}$$

where h is defined as the freshwater head:

$$h = \frac{p}{\rho_f g} + z \tag{2.2}$$

where p is defined as the pressure of the water. The density factor α is defined as:

$$\alpha = \frac{\rho_f}{\rho_s - \rho_f} \tag{2.3}$$

2.3.1. Steady Unconfined Interface Flow in a Deep Aquifer

Consider a one-layer model with unconfined interface flow conditions in a deep aquifer (Figure 2.1) in which the interface never reaches the aquifer bottom. Two parameters must be transformed: the hydraulic conductivity, k, and the aquifer bottom, z_b. The top of the aquifer must be set high enough so that the head does not reach it.

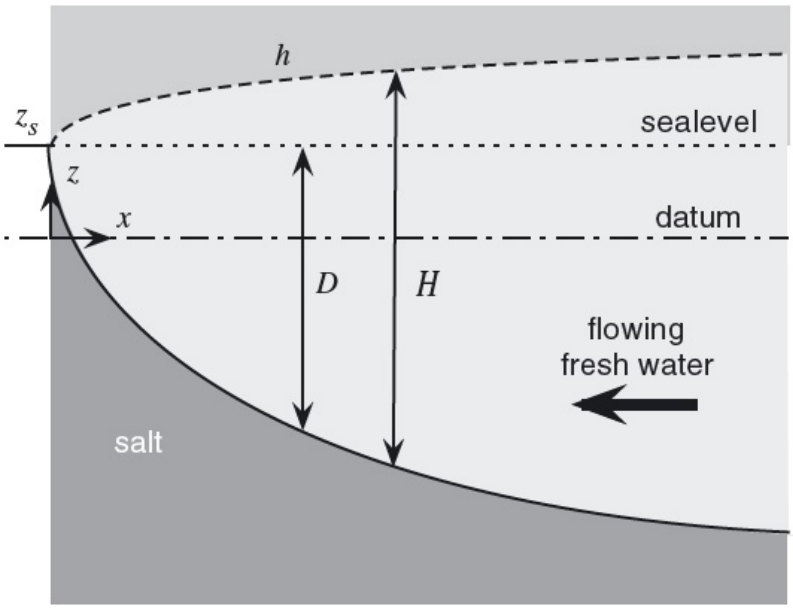

Figure 2.1: Problem definition of steady unconfined interface flow with deep bottom (Bakker and Schaars, 2013)

$$\tilde{k} = (\alpha + 1)k \tag{2.4}$$

$$\tilde{z}_b = z_s \tag{2.5}$$

2.3.2. Steady Unconfined Interface Flow in an Aquifer with a Finite Bottom

In this system, there are two types of flow: normal unconfined flow, and unconfined interface flow (see Figure 2.2). There will be normal unconfined flow to the right of the toe, and to the left of the toe, there will be interface flow. This system is modeled as a two layer model with low enough resistance to vertical flow between them such that the heads in both layers are equal. The transformed parameters for each layer are as follows (numbering referring to model layer starting from the top). The transformed model with the interface is shown in Figure 2.3.

$$\tilde{k}_1 = k \tag{2.6}$$

$$\tilde{z}_{b1} = z_s + (z_s - z_b)/\alpha \tag{2.7}$$

$$\tilde{k}_2 = (\alpha + 1)k \tag{2.8}$$

$$\tilde{z}_{b2} = z_s \tag{2.9}$$

$$\tilde{z}_{t2} = z_s + (z_s - z_b)/\alpha \tag{2.10}$$

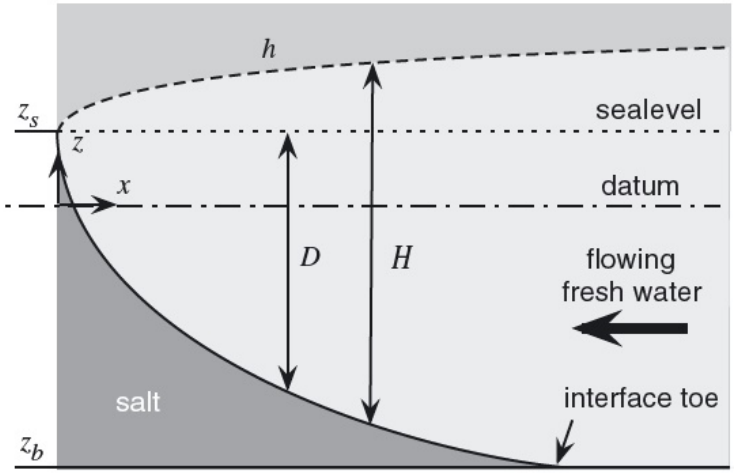

Figure 2.2: Problem definition of steady unconfined interface flow with finite bottom (Bakker and Schaars, 2013)

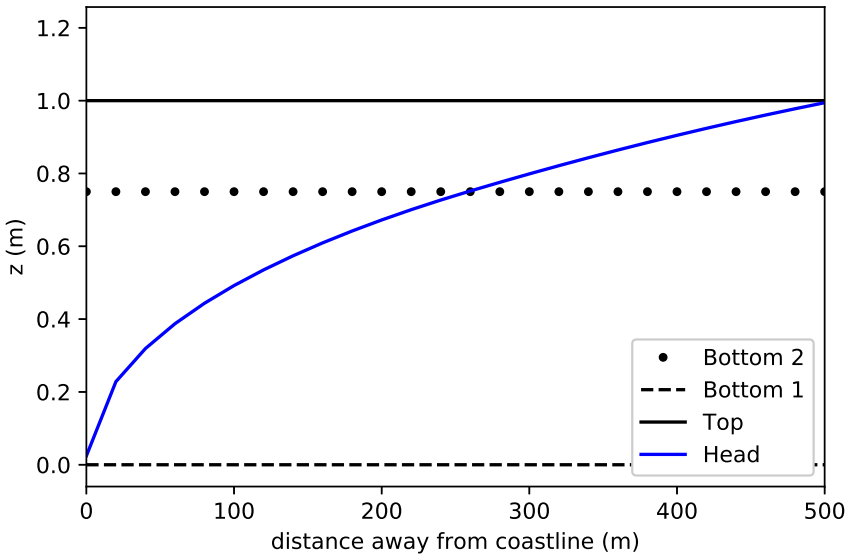

Figure 2.3: Transformed conceptual model with interface on one side of unconfined shallow island

2.3.3. Steady Confined Interface Flow

In a steady confined interface flow, there are three different types of interface flow regimes. First, when the head is between the sea level and $(z_s - z_t)/\alpha)$, there will be no interface flow, so H will be 0. Second, H is then head-dependent when it is varying between 0 and the aquifer thickness. Third, H is equal to the aquifer thickness. The following three parameters must be transformed.

$$\tilde{k} = \alpha k \tag{2.11}$$

$$\tilde{z}_b = z_s + (z_s - z_t)/\alpha \tag{2.12}$$

$$\tilde{z}_t = z_s + (z_s - z_b)/\alpha \tag{2.13}$$

2.3.4. Steady Interface Flow in Multi-Layer Systems

In a multi-layer system, the model layers must be flipped so that transformed layer $j = M + 1 - i$, where i is the layer of the original domain and M is the total number of layers in the model. The same

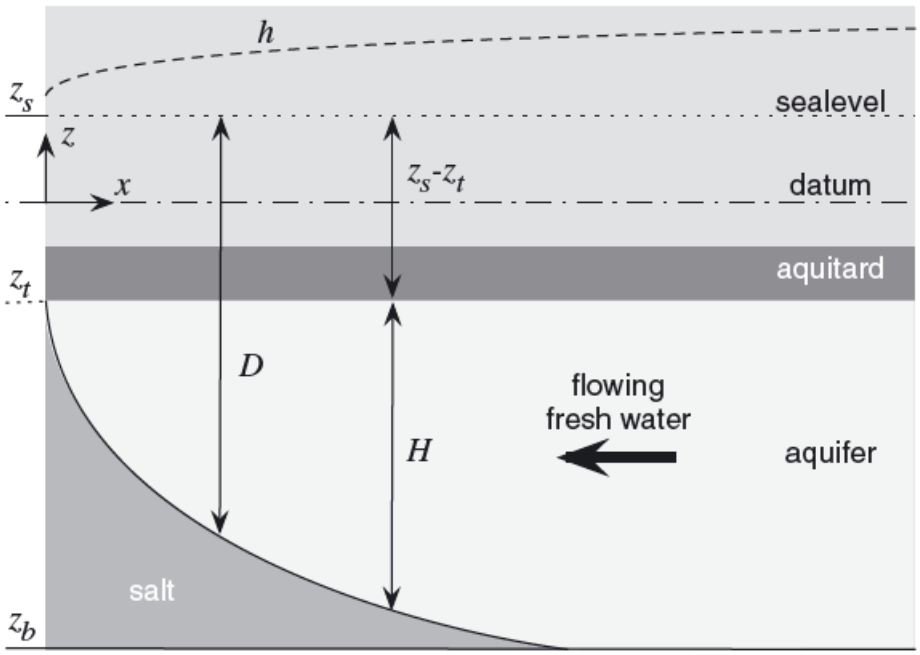

Figure 2.4: Problem definition of steady confined interface flow (Bakker and Schaars, 2013)

transformations as in the previous example shown in Equations 2.11-2.13 are applied to each layer i.

$$\tilde{k}_i = \alpha k_j \tag{2.14}$$

$$\tilde{z}_{bi} = z_s + (z_s - z_{tj})/\alpha \tag{2.15}$$

$$\tilde{z}_{ti} = z_s + (z_s - z_{bj})/\alpha \tag{2.16}$$

$$\tilde{k}_{vi} = k_{vj}/\alpha \tag{2.17}$$

2.4. Model Implementation and Results

Python Jupyter Notebooks were written using FloPy (Bakker et al., 2016) to model the four scenarios described above. Each will be described in such a way to understand how to implement these techniques using regular MODFLOW. In all of the models, the density factor, α, which is used in every version of the transformations, is set to 40 with ρ_s, saltwater density, and ρ_f, freshwater density, equal to 1025 kg/m^3 and 1000 kg/m^3, respectively. All packages use the MODFLOW BCF (Block-Centered Flow) package; the LPF (Layer-Property Flow) package can also be used. The Python scripts for these examples can be found in the Appendix.

2.4.1. Steady Unconfined Interface Flow in a Deep Aquifer

A MODFLOW model was created using the transformed parameters (Equations 2.4 and 2.5) and applied to a circular island with uniform recharge.The following parameters are defined:

- the radius of the island, R, is set to 1000 m
- hydraulic conductivity, k, is 10 m/d which means that $\tilde{k}$ is 410 m/d
- the head is fixed along the shore to h_0 which is set to 1/41 (1/(α+1)) m above sea level
- z_s is 0 m which means that $\tilde{z}_b$=0 m
- Areal infiltration, N, is 1 mm/d

The grid cells are set to 20 m by 20 m. The layer type in the BCF package is set to 1 for unconfined flow. A scenario with a well is also demonstrated where the well is located a distance, p = 200 m, to the right of the center of the island. The discharge of the well, Q is 200 m^3/d and the radius of the well is r_w = 0.3 m.

The exact solution to this problem may be solved using the method of images for a circle (Strack 1989, equation 2.18).

$$\phi = -\frac{N}{4}(x^2 + y^2 - R^2) + \frac{Q}{4\pi}\ln\frac{r^2R^2}{[(z - R^2/p^2) + y^2]p^2} + \frac{k(\alpha+1)}{2}h_0^2 \tag{2.18}$$

where $\phi(x, y)$ is the discharge potential and the radial distance from the well is at least r_w:

$$r = \max(\sqrt{(x-p)^2 + y^2}, r_w) \tag{2.19}$$

The head may be obtained from the potential solution.

$$h = z_s + \sqrt{\frac{2}{k(\alpha+1)}\phi} \tag{2.20}$$

The results for the island with no well are shown in Figure 2.5. The results for the case with a well are shown in Figure 2.6. The situation with the well demonstrates how the exact solution results in a greater upconing than the MODFLOW solution, which is to be expected as MODFLOW cells are much larger than the diameter of the well. The rest of the results compare very well with the exact solution.

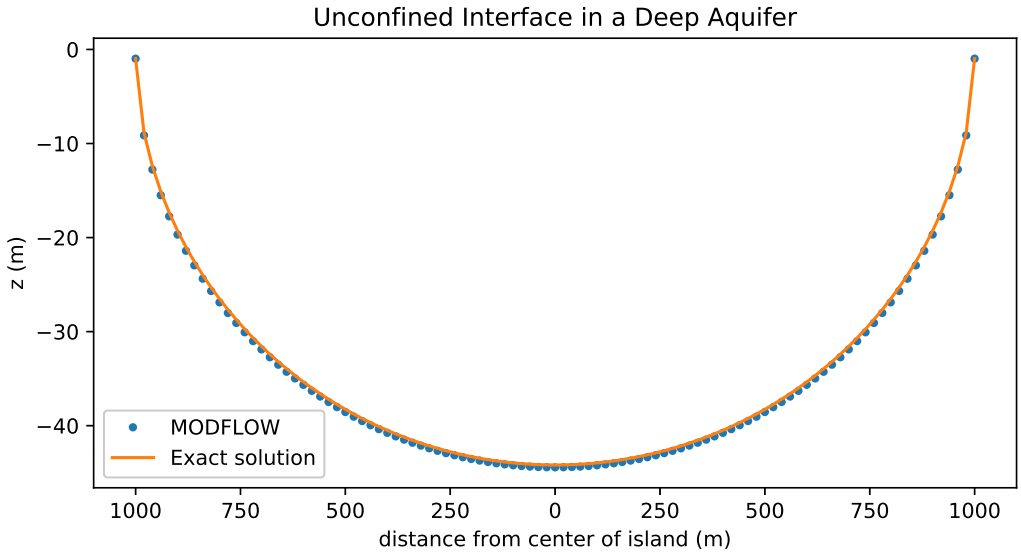

Figure 2.5: Interface position for deep, unconfined aquifer with no well

2.4.2. Steady Unconfined Interface Flow in an Aquifer with a Finite Bottom

A MODFLOW model using the same circular island with areal recharge of the previous example was used, but without pumping and a finite aquifer thickness. All of the other parameters are the same including the same discretization except the bottom of the aquifer is set to -30 m. The obtained parameters for the solution are described below. The layer type in layer 2 is set to 3 which represents unconfined or confined conditions. The top of the second layer, $\tilde{z}_{t2}$, is set to 0.75 m and the vertical leakance is set to 1 d^{-1}.

Layer	$\tilde{k}$ (m/d)	$\tilde{z}_b$ (m)	Layer Type (BCF)
1	10	0.75	1
2	410	0	3

Table 2.1: Transformed parameters of the MODFLOW model representing steady interface flow in an aquifer with a finite bottom

The exact solution may be obtained with the Strack potential from equation 2.18 and is valid when ϕ is smaller than ϕ_{toe}, as computed in equation 2.21. When ϕ is greater than ϕ_{toe}, flow is regular and unconfined and head can be computed using equation 2.22. The results of both the exact solution and the MODFLOW solution are shown in Figure 2.8. The MODFLOW toe location differs only 1% from the exact toe location.

$$\phi_{toe} = \frac{k(\alpha+1)}{2\alpha^2}(z_s - z_b)^2 \tag{2.21}$$

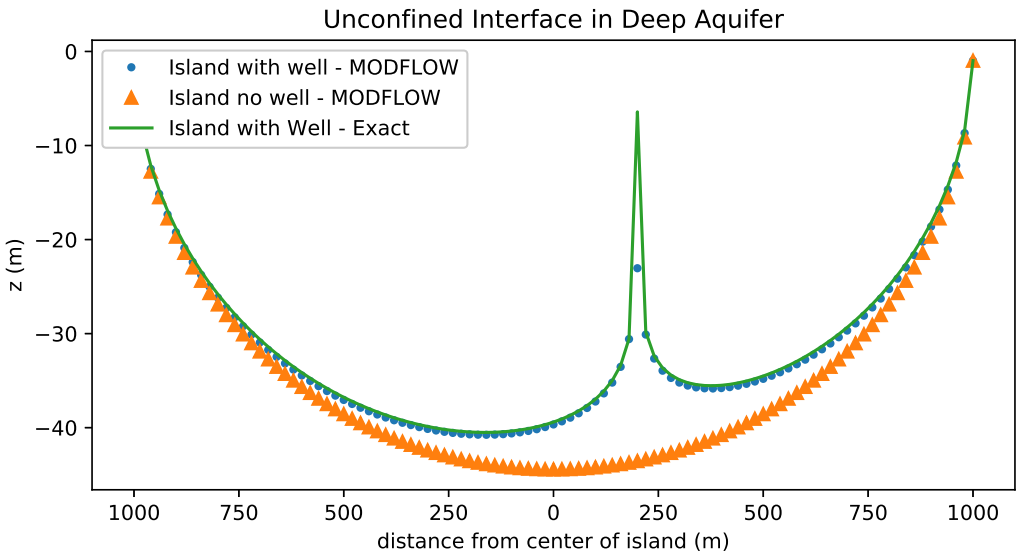

Figure 2.6: Interface position for deep, unconfined aquifer with a well

$$h = \sqrt{\frac{2}{k}[\phi - \frac{\alpha + 1}{\alpha}(z_s - z_b)^2]} \tag{2.22}$$

2.4.3. Steady Confined Interface Flow

A One-Dimensional MODFLOW model is created to simulate uniform flow in a confined aquifer. The model is discretized into one row of 150 cells of length and width 10 m. The exact solution using the Strack potential may be obtained with equation 2.23. The following parameters and their transforms are used.

- z_s is set to 0 m so $\tilde{z}_b$ is then 0 m
- z_t is set to 0 m
- z_b is - 40 m which means $\tilde{z}_t$ is 1 m
- k is 10 m/d so $\tilde{k}$ is 400 m/d
- h_0 is fixed at the coast to be 1/40 m so that D_0 is 1 m
- Inflow, Q_0, is set on the right side of the model to 0.2 m^2/d

$$\frac{k(D^2 - {D_0}^2)}{2\alpha} = Q_0 x \tag{2.23}$$

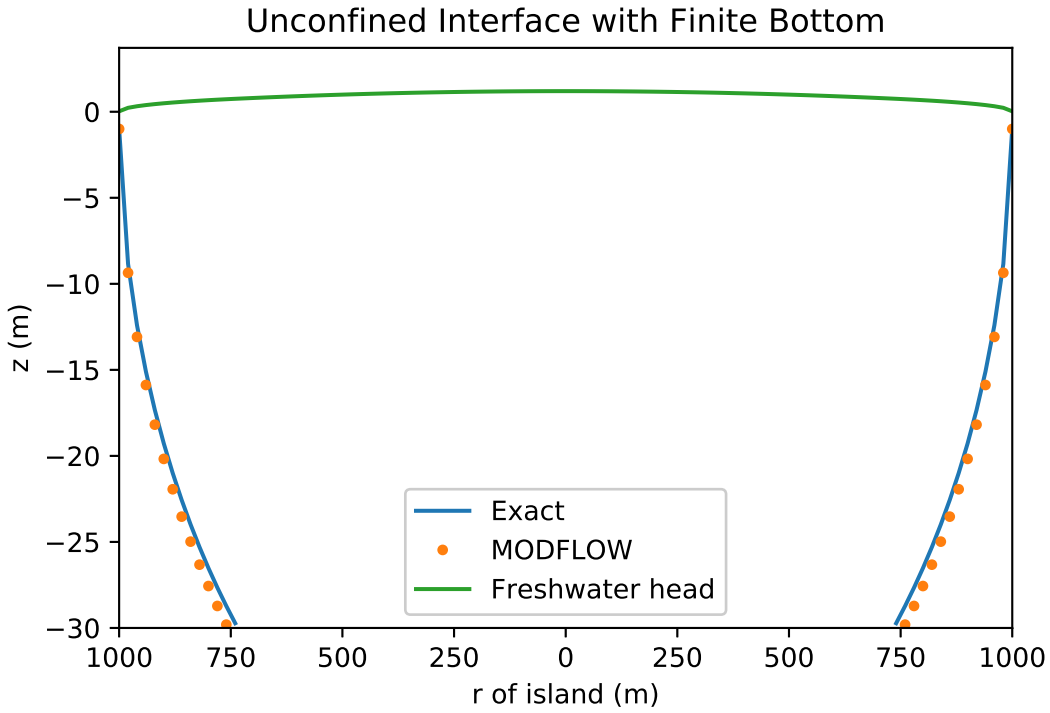

Figure 2.7: Interface position for unconfined aquifer with a finite bottom

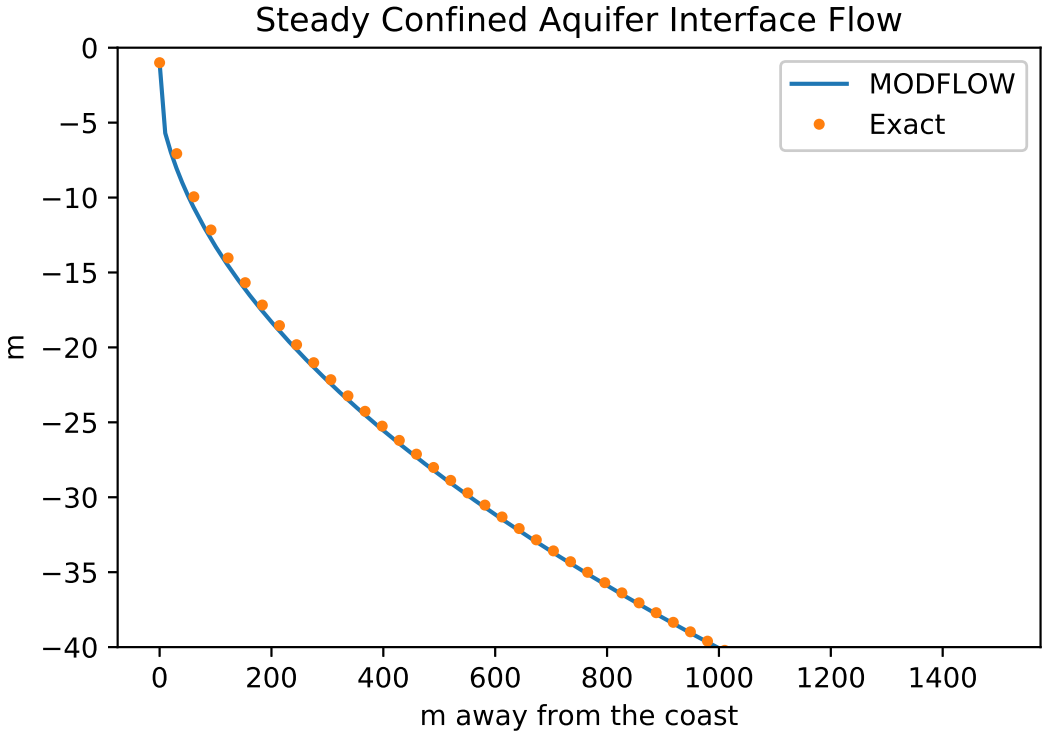

Figure 2.8: Interface Position for Steady Confined Aquifer

The results for this scenario are shown in Figure 2.8. The visual comparison between the exact and MODFLOW solution is good and the computed toe locations vary by less than 0.1 m.

2.4.4. Steady Interface Flow in Multi-Layer Systems

A two-layer MODFLOW model is created to represent a two-layer aquifer system. Both aquifers are 20 m thick with k = 10 m/d, separated by an aquitard 4 m thick (converting to transformed thicknesses and $\tilde{k}_i$ of 0.5 m and 400 m/d, respectively. The model is simulated with four different resistances (c=25 d^{-1}; 500 d^{-1}; 1000 d^{-1}; 2000 d^{-1} corresponding to k_v=0.16 m/d; $8*10^{-3}$ m/d; $4*10^{-3}$ m/d; $2*10^{-3}$ m/d). The aquitard is represented by using the BCF VCONT parameter which is equal to the leakance. Inflow on the right side of the model is set to 0.2 m^2/d in both layers and the sea level is fixed to z_s = 0 m. The model is discretized with a single row of 50 cells of 40 m length and width. Half of the model extends below the ocean bottom.

The results of the different scenarios with varying resistances are shown in Figure 2.9. What can be drawn from this is that the interface position in the top aquifer is insensitive to the resistance but the greater the resistance, the further seaward the freshwater zone is able to extend in the lower layer.

Layer	$\tilde{k}$ (m/d)	$\tilde{z}_b$ (m)	$\tilde{z}_t$ (m)	Layer Type (BCF)
1	400	0.5	1	1
2	400	0	0.5	3

Table 2.2: Transformed parameters of the MODFLOW model representing steady interface flow in a multi-layer aquifer system

2.4.5. Limitations

The first main limitation comes in situations where the top aquifer is unconfined. When the model is inverted about the z-axis, the top layer now will have other layers on top of it which precludes it from being represented as unconfined. A suitable approximation is to represent flow as confined or to use MODFLOW's option for confined/unconfined flow by setting the layer type in the MODFLOW groundwater flow package (BCF: 2 or 3; LPF: >0) .

The second limitation involves situations where saltwater may become disconnected from the salt-water directly connected to the ocean. This occurs when the application of the Ghyben-Herzberg re-lationship ends up computing such a disconnected interface. Good examples of this are: (1) extreme upconing far away from the ocean-originated interface such that there is no source of seawater actually to be extracted by that well that could rise above the aquifer base and (2) aquifer base elevation drops that expose the interface at further inland locations as computed using Ghyben-Herzberg, but in reality are not connected to the ocean-based saltwater.

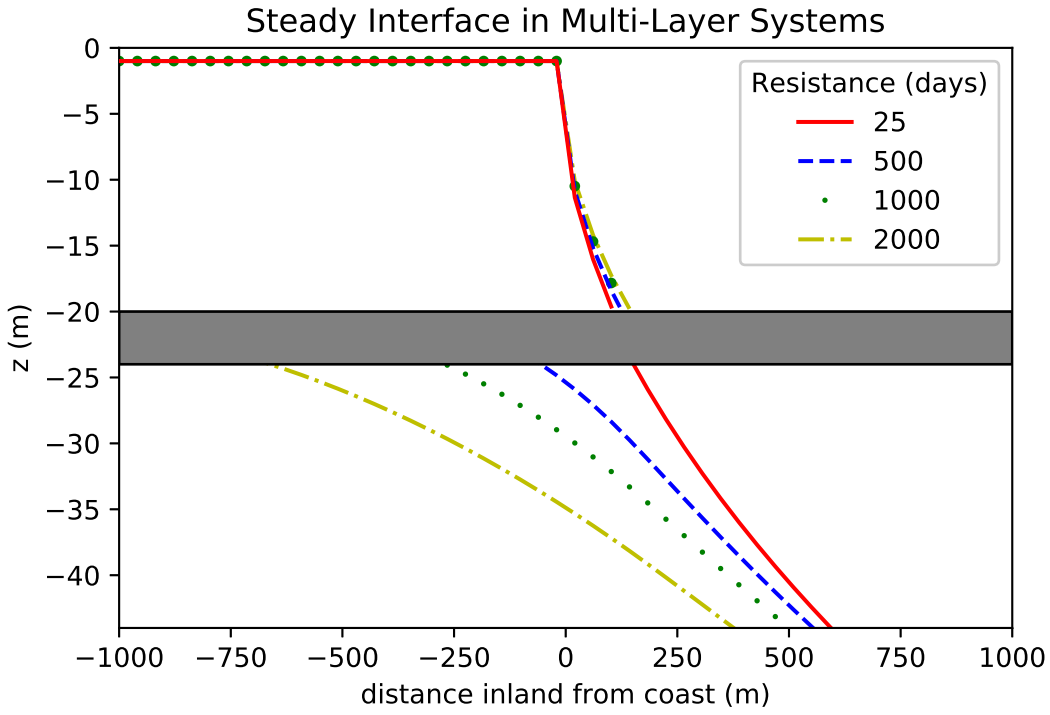

Figure 2.9: Interface position for a two-layer model with different resistance values (x=0 m represents the coastline)

Bakker and Schaars (2013) propose different solutions to this such as modifying the relationship between transmissivity and head or to workaround it by raising the base of the aquifer on an *ad-hoc* basis. These isolated pockets of saltwater need to be evaluated carefully.

2.4.6. Boundary Condition Package Implementation

A variety of packages exist in MODFLOW to represent the different hydrogeologic features such as pumping from wells, surface-water interactions, and geologic settings. The way these packages will be manipulated to fit within the transformed models' schemes is described below.

The **WEL, RCH, GHB, CHD, HFB, RIV,** and **DRN** packages are all implemented in the transformed model by inverting which layer they are in so that they are in the same corresponding layer as in the original model. For example, recharge will now be infiltrating into the bottom-most layer as it is usually located on the top layer of a model. There are packages that are not described here and that is because they were not used in the models considered in this thesis.

2.5. Pumping Optimization

The maximum amount of pumping before seawater reaches the well is determined for different wells in each model–whether included through the original model or added through scenario testing. When

a single well is being evaluated, the following procedure is followed:

1 An arbitrarily low discharge is chosen for a well.

2 The transformed model is run with the new well discharge and all other parameters unchanged.

3 If the resulting head is above the layer bottom, the cell is still fresh and the discharge is increased by a fixed amount, ΔQ, and the model is run again; If the resulting head in the cells next to and below the cell containing the well is lower than the bottoms in those cells, the last discharge is recorded as the critical pumping rate.

The procedure for optimizing multiple wells at the same time can be quite complex so instead the discharge of each well was set to be proportionate to the transmissivity of the layer of each respective well. The following equation describes the set-up principle.

$$Q_{w,i} = \sum_{i=1}^{n} Q_{w,i} \frac{T_i}{\sum_{i=1}^{n} T_i} \tag{2.24}$$

where Q_w refers to the discharge of a well; i refers to the index of the well; T refers to the transmissivity of the layer in which the relevant well is in; and, n refers to the total number of wells.

When multi-well optimization is used, the total discharge is what is really being optimized but the discharge from each well can be reported to illustrate the relationship between the different wells' pumping.

2.6. Iterative Procedure for Regions with Different Sea Levels

Earlier in this chapter–in section 2.1, an approximation was used in which the saltwater is not moving. However, this does not always hold for steady flow, for example, in situations regarding islands where there may be different sea levels around the island. In this case, the seawater will be moving from high mean sea level to low mean sea level. This causes a problem for the interface because now the saltwater head between the different levels is unknown. With no single fixed sea level to use anymore, the model also needs a different datum defined. The difference in head must be accounted for to determine how the interface will adjust based on this situation with moving saltwater. The datum is set as just below the lowest of the heads that represent the various sea levels around the island. This is because when the model is flipped and transformed, a negative head used as a boundary condition will be impossible to run. Therefore, all boundary condition fixed heads must be above the zero-elevation point.

A new iterative procedure is developed to solve for the head between the different sea-levels. This process allows for a steady-state solution of the interface position under variable sea-level conditions. As in earlier approximations, the system is still approximated as steady.

A procedure here is given to determine these unknown heads:

1 An initial interface is determined by using the Bakker-Schaars transformed model with constant sea levels set to the minimum fixed-head boundary.

2 The calculated interface is used to redefine the top of an untransformed model so that only the seawater is modeled using the variable sea levels. That model is then run with the different sea-levels implemented which gives the saltwater head everywhere in the model.

3 The calculated interface is used conversely to redefine the bottom of an untransformed model with the different sea-levels implemented so as to only represent the freshwater, resulting in the freshwater head everywhere in the model.

4 A new interface depth is computed using the resulting heads where $h_s(x, y)$ is the saltwater head at location x, y and $h(x, y)$ is the freshwater head at location x, y:

$$D = \alpha(h - h_s) \tag{2.25}$$

5 The new interface is compared with the interface used in steps 2 and 3. If there is a difference between the two beyond an acceptable tolerance, then the new interface is used to begin the procedure from step 2 and 3 (An acceptable tolerance is defined by the RMSE (root mean square error) where the maximum acceptable RMSE is 0.05 m). If the RMSE is less than 0.05 m, the interface is accepted.

2.6.1. Example

To demonstrate how the procedure works, a simple example is given. A one-layer model discretized as one row with 100 columns is created. The hydraulic conductivity is constant for the original model set to 10 m/d. The aquifer thickness of the original model is set to 70 m where the bottom of the model is -70 m and the datum is set to sea level. The sea level on the left is set to h_0 = 1/α m AMSL and the sea level on the right is set to 1/α + Δh m AMSL where Δh is specified as 0.25 m.

First, the interface is estimated using the transformed model without accounting for the sea level difference so sea level is h_0 everywhere, resulting in the interface in Figure 2.10. In this transformed model the model thickness is now 70/α m and k is now 400 m/d.

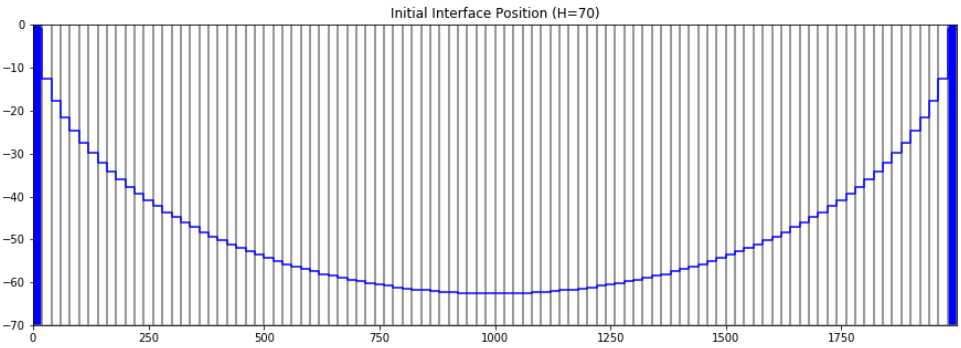

Figure 2.10: First estimate of seawater interface based on constant sea level

This interface is then specified as the top of the saltwater model (Step 2) and the bottom of the freshwater model (Step 3). It is important only to include relevant boundary conditions in each of the models. The cross-sections of the two different models used to calculate the different contributions of seawater and freshwater are shown in Figures 2.11 and 2.12.

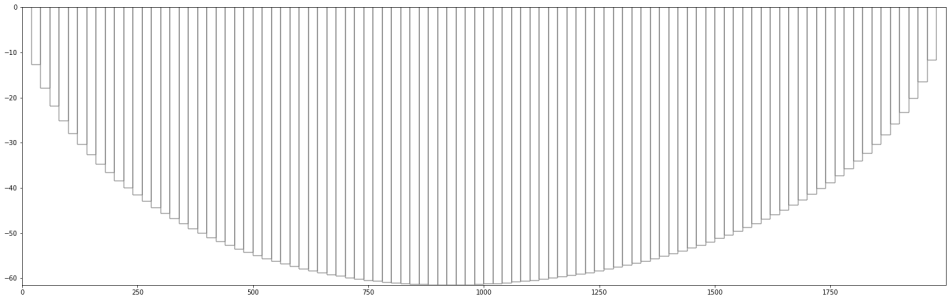

Figure 2.11: Normal model with original interface used as model bottom to represent freshwater head

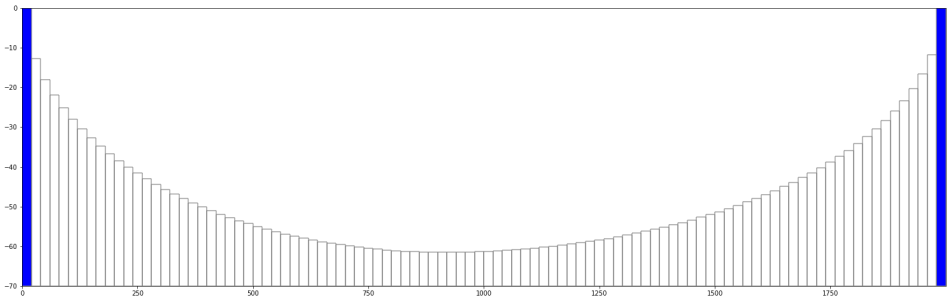

Figure 2.12: Normal model with original interface used as model top to represent saltwater head

Finally, a new interface is calculated using Equation 2.25 and plotted in Figure 2.13 along with the first interface estimate. The RMSE is then calculated and for this example, the first RMSE is 2.6 m. Thus, this new interface should replace the first estimate and the models should be run again with this

new adoption so as to iterate a second instance. The steps are repeated, setting the interface to the models' top and bottom, for each respective model. The final iteration resulted in an interface that had an RMSE between the prior interface and the new one of 0.05 m, which satisfies the criteria and is accepted as the accurate interface. The differences between the final interface and the original based on constant sea level (the sea level on the right is 1 m higher than the sea level on the left) are shown in Figure 2.13. The maximum difference in the depth of the interface is 0.73 m.

Figure 2.13: Comparison between last interface solution and original interface guess for an aquifer with a bottom of 70 m below AMSL (blue: initial interface for constant sea level, red: final interface with different sea levels)

Even in a deep aquifer where the interface doesn't touch the bottom, the thickness of the aquifer layer can impact how variable sea levels can alter the interface position. This is because of the impact it will have on the movement of the saltwater in the model that represents only the saltwater head. The layer thickness will be thicker for the saltwater head if the aquifer itself is also thicker, which can impact the results as the model simulates this saltwater head as confined. This impact is demonstrated in the same example but with the aquifer thickness specified as 120 m so the depth of the aquifer is -120 m AMSL. All other conditions of the model setup are unchanged. Figure 2.14 shows the initial interface position for this model. The initial interface for constant sea level is the same as for the example with a thickness of 70 m. After the procedure is followed, a final interface is found. Figure 2.15 shows the results of the final interface position compared with the initial interface position. It shows that the difference is not as great as when the model thickness is less. The fact that the maximum difference in depth to interface between initial and final results is 0.35 m as compared 0.73 m in the original examples further demonstrates this relationship.

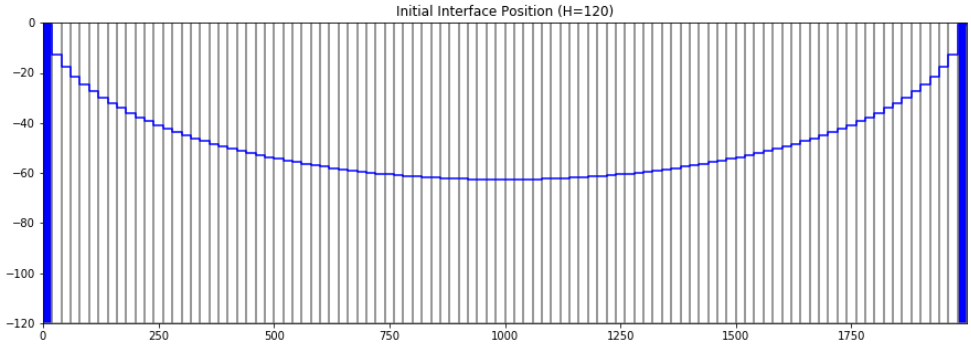

Figure 2.14: First estimate of seawater interface based on constant sea level for model with thickness 120 m

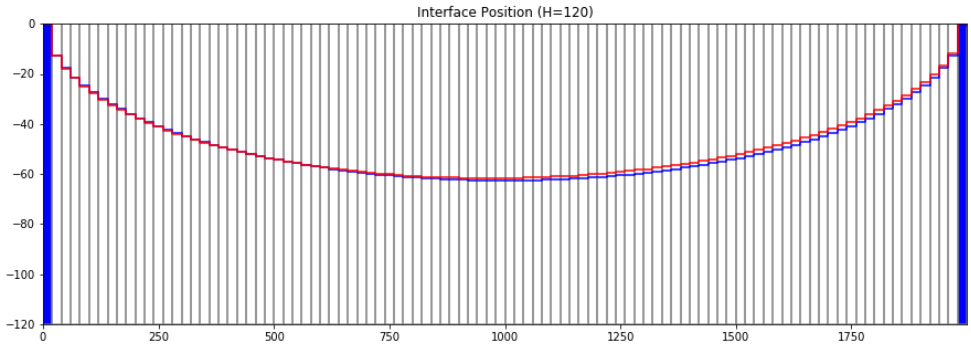

Figure 2.15: Comparison between last interface solution and original interface guess for an aquifer with a bottom of 120 m below AMSL (blue: initial interface for constant sea level, red: final interface with different sea levels)

3

Interface Modeling and Results

3.1. Los Angeles, USA

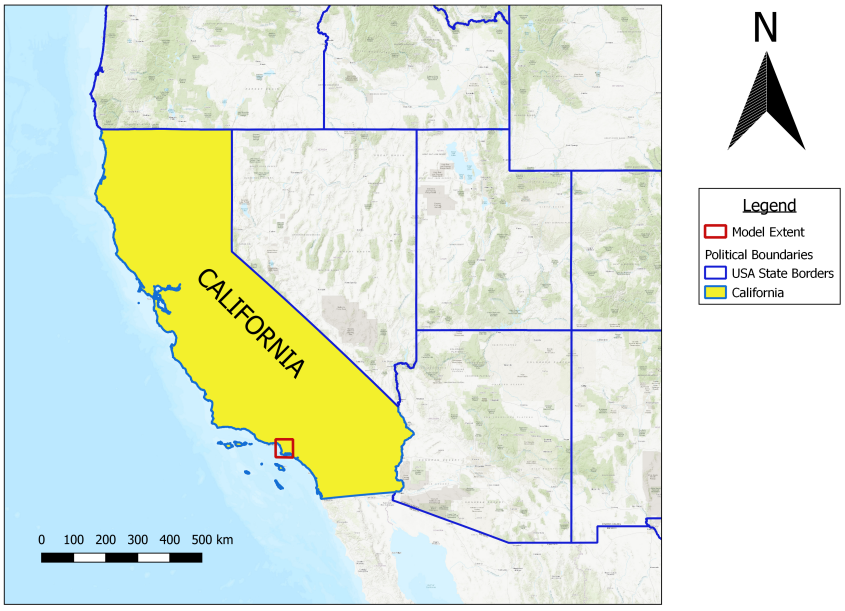

Figure 3.1: Map showing geographic context (western United States) of the Los Angeles model outlined in red

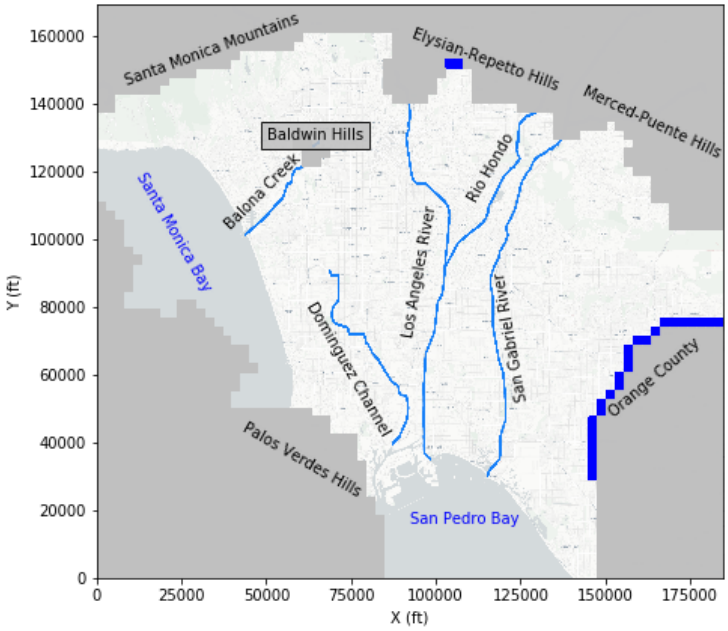

Figure 3.2: Map of model area (boundary is red square in Figure 3.1 with no-flow boundary in grey, rivers marked by blue lines, and major geographic features labeled

3.1.1. Area Description

The Central and West Coast Basins in Los Angeles County, California are the focus of this model. These basins lie within the greater metropolitan area of Los Angeles, California, USA. To the north of the model domain, the Santa Monica Mountains bound the model; to the northeast, the Elysian, Repetto, Merced, and Puente Hills form the boundary; to the southeast, the Orange County forms the boundary; to the southwest and west, the Palos Verdes Hills and, beyond, the Pacific Ocean form the boundary. The model interacts with the ocean to the south through San Pedro Bay and to the west through Santa Monica Bay. The total onshore area of the basin is approximately 480 mi^2 (1243 km^2). The area is drained by three rivers: the Los Angeles River, the San Gabriel River, and the Rio Hondo. The Dominguez Channel, a man-made feature, and Balona Creek also transport surface water that interacts with the groundwater. Figure 3.2 shows the main geographic features described here in the context of the model area.

The geology of the basin can be divided into five different layers: four aquifers and one underlying impermeable unit. The four aquifers are (from youngest to oldest): the Recent Aquifer, the Lakewood Aquifer, the Upper San Pedro Aquifer, and the Lower San Pedro Aquifer. The below-boundary layer is called the Pico Unit (Yerkes et al., 1965, Biddle, 1991). The Newport-Inglewood Uplift (NIU) fault system is a dominating geologic influence in the area caused by tectonic activity from the transverse

fault between the Pacific and North American tectonic plates. The NIU is the cause for faults and folds that generally trend to the northwest. The faults act as an impediment to horizontal flow in the aquifer system and also cause a series of predominantly anticlinal folds. Only the San Pedro formations and Lakewood aquifer system are affected by the NIU. They were materially influenced through a series of uplift and erosion then resubmergence and deposition followed by again uplift and alluvial deposition. Ultimately the effect of the NIU and this series of geologic events is compressional shortening of the affected geologic units and a series of faults that impede flow. This can be seen in the thickness of the aquifer layers in the model increasing away from the sea. The faults are mostly believed to help keep seawater intrusion at bay due to their prevention of lateral flow although there may be evidence they have leaks. The Recent Aquifer is unaffected by the NIU and is a thinner layer deposited after the major faulting had occurred.

Groundwater plays an important role supplying 4 million local residents of the Central and West Coast basins with 40% of their water supply. Over-development of the groundwater supply in the early twentieth century led to severe lowering of the groundwater levels and consequent seawater intrusion. To help protect these coastal aquifers, management actions were taken including implementing active managed recharge through the use of spreading grounds and restrictions on groundwater pumping during critical periods. The managing agencies in the basin actively use injection wells and recharge as a way to supplement and treat their water supply. The area is still dependent on imported water to meet their demand. In the 1960s, injection barrier wells were installed in three strategic locations to mitigate the effects of seawater intrusion and protect the inland freshwater. However, there is concern that these barriers are not completely effective and the geology of the basins and their faults is more complex than originally understood.

3.1.2. Model Description

A single-density MODFLOW model (Harbaugh et al., 2000) of the area was built by Reichard et al. (2003) of the US Geological Survey. This model was re-implemented and adapted by Dr. Stephen Kraemer of the US Environmental Protection Agency (EPA) with adjustments of adding features to represent the Los Angeles River, the Rio Hondo, and the San Gabriel River with fixed head data. Kraemer also removed all wells in an attempt to replicate pre-development conditions and this version is used for the analysis here. A brief description of the model is presented here. Further details can be found in Reichard et al. (2003).

The model is run with an altered, proprietary version of MODFLOW 2000 that included an improved procedure for dealing with unconfined flow with dry cells as developed by Bedekar et al. (2013). The model has 64 rows, 70 columns, and four layers to represent the four geologic zones described earlier,

excluding the lowermost, impermeable Pico Unit. The cell area is 2,640 ft by 2,640 ft. Layer one is modeled as unconfined (BCF layer type 1) and all other layers are modeled as unconfined/confined (BCF layer type 3: T is variable). Figures A.1-A.4 show the spatial pattern of hydraulic conductivity in the model and Figures A.5-A.8 in show the range of bottom elevations for each layer (see Appendix A). Figures 3.3-3.4 show the main features of the model with geographic descriptions. Figures 3.5-3.7 show cross-sections of the original model to also demonstrate the variability in bottom elevations. The bottom elevations show some of the complexity of different eras of uplift, erosion, and deposition through the different high and low points for each layer (Figure A.7 shows a good example). The top of the model is specified as a constant 339 ft AMSL. It is important to state that the model is aimed to be representative of pre-development conditions (roughly early 19th century) before significant seawater intrusion became a problem. Mendenhall (1905) describes broad areas of the coastal plain being artesian prior to groundwater development.

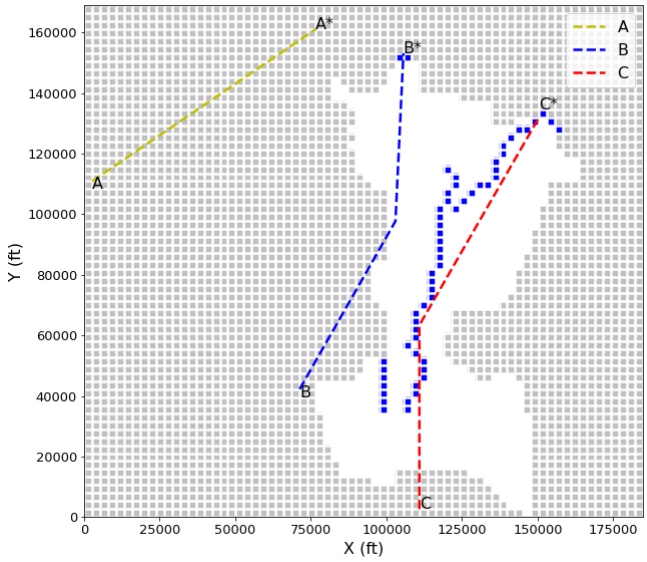

Figure 3.3: Map of layer 1 main boundary conditions (grey: inactive, blue: constant head) of LA Model with cross-sectional lines to be plotted

3.1.2.1. Boundary Conditions

The lateral model-boundary to the north, east, and southwest is surrounded by Tertiary deposits and is simulated as impermeable and represented as inactive conditions as shown in Figures 3.8-3.10. The Baldwin Hills within the model domain are also modeled as no-flow cells. The smaller areal extent of the Recent Aquifer is used for the representation of model layer 1. Both layer 1 and 2 feature surficial boundary conditions since the aquifer represented by layer 1 has such a limited extent. The Pico Unit beneath the San Pedro formations makes up the bottom of the model and is considered to be no-flow.

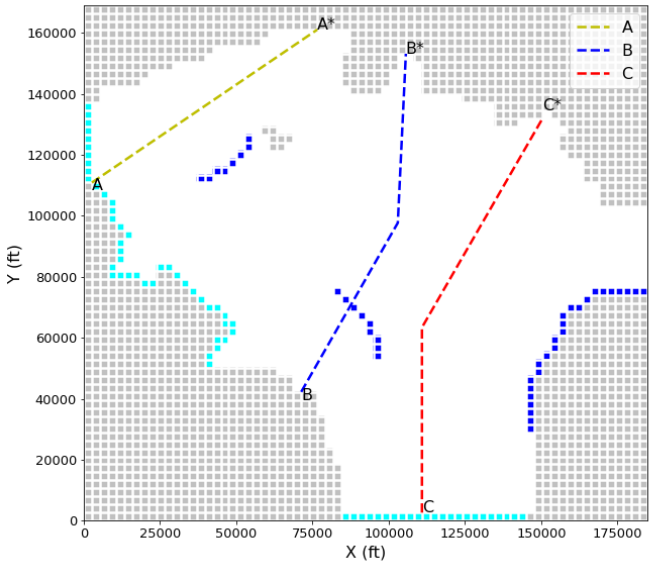

Figure 3.4: Map of layer 2-4 main boundary conditions (grey: no-flow, blue: constant head, light blue: outer cells of GHB representing ocean) of LA Model with cross-sectional lines to be plotted

The model uses four boundary conditions packages to represent the system for a pre-development scenario: General Head Boundary (GHB), Horizontal Flow Boundary (HFB), Recharge (RCH), and Constant Head (CHD).

The boundary conditions for the model are shown in Figures 3.8 through 3.10. Blue cells represent fixed heads (CHD), light blue represents GHB cells, orange circles represent the locations of the HFB cells, and light grey cells represent no-flow boundaries or inactive cells.

General Head Boundary (GHB) GHB cells are used to represent the off-shore ocean cells to model the impact of the overlying seawater. At the offshore cells, GHB cells' heads are specified for the top layer to be zero (sea level). In the lower layers, the heads representing the ocean boundary are specified to be the freshwater head equivalent of the overlying saltwater if the top of the corresponding layer is below sea level (head = layer top/α. The GHB conductance values are set to 10^4 ft^2/d for layer 1, ranging from 8.64 to 10^4 ft^2/d in layer 2, and ranging from 259 to 518 ft^2/d in layers 3 and 4.

Constant Head (CHD) Constant head boundaries are used at the Los Angeles-Orange County border to represent groundwater flow to and from the Orange County groundwater basin to the east as well as flow through both the Los Angeles and Whittier Narrows in the north of the model. The CHD heads for the Narrows were applied using the average measured water level during the original model simulation period (1971-2000) . It should be noted that during this period, the water levels are quite constant in this area. The specified heads representing flow to and from Orange County were determined using the average of the minimum and maximum annual measured water level data from that area. Water levels

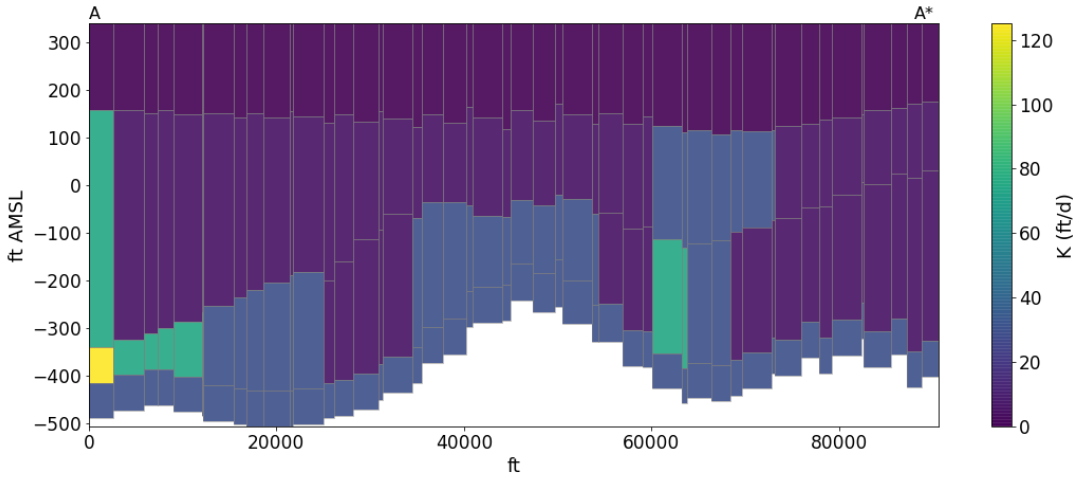

Figure 3.5: Cross-section of Los Angeles model along line A colored by hydraulic conductivity

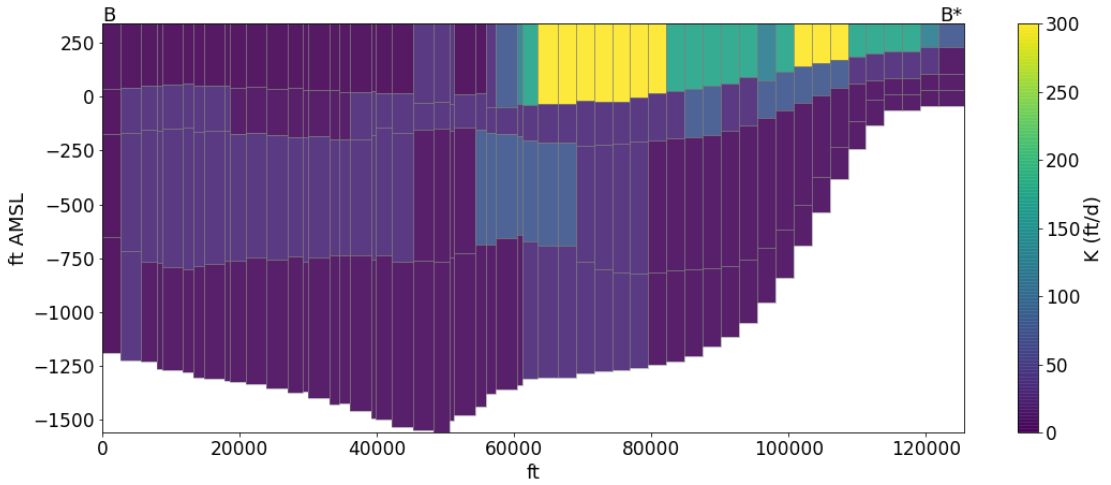

Figure 3.6: Cross-section of Los Angeles model along line B colored by hydraulic conductivity

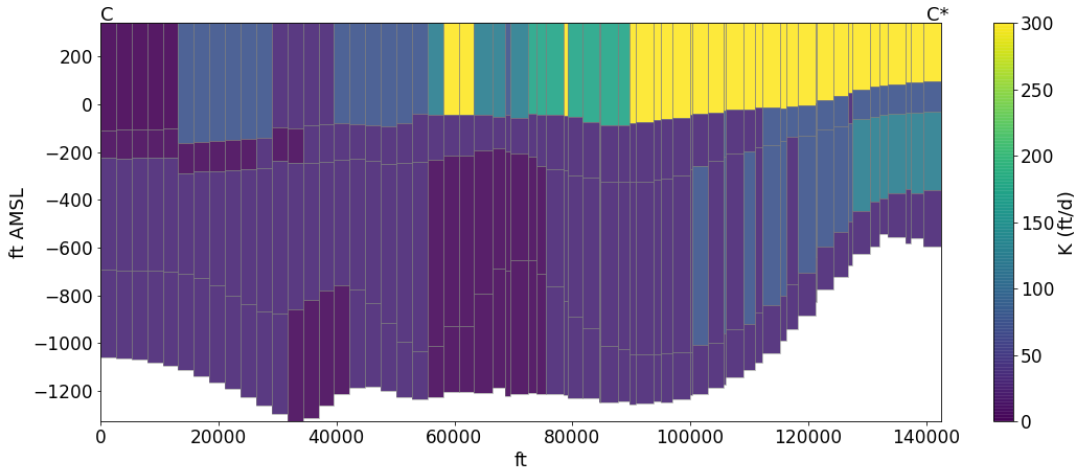

Figure 3.7: Cross-section of Los Angeles model along line C colored by hydraulic conductivity

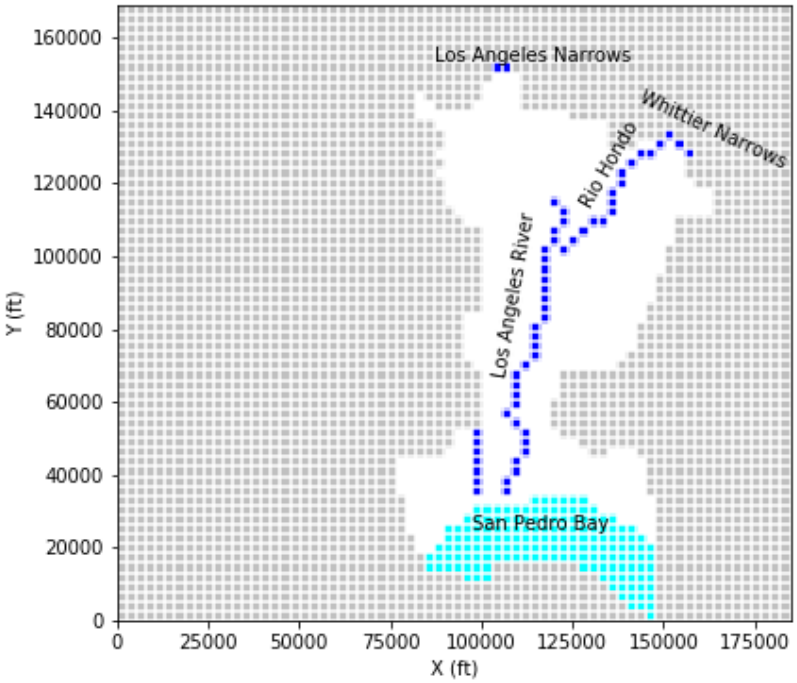

Figure 3.8: Boundary Conditions within model domain for layer 1 with relevant landmarks for Los Angeles model: grey cells: no-flow; light blue cells: GHB cells; blue cells: fixed-head or CHD cells; orange circles: HFB locations

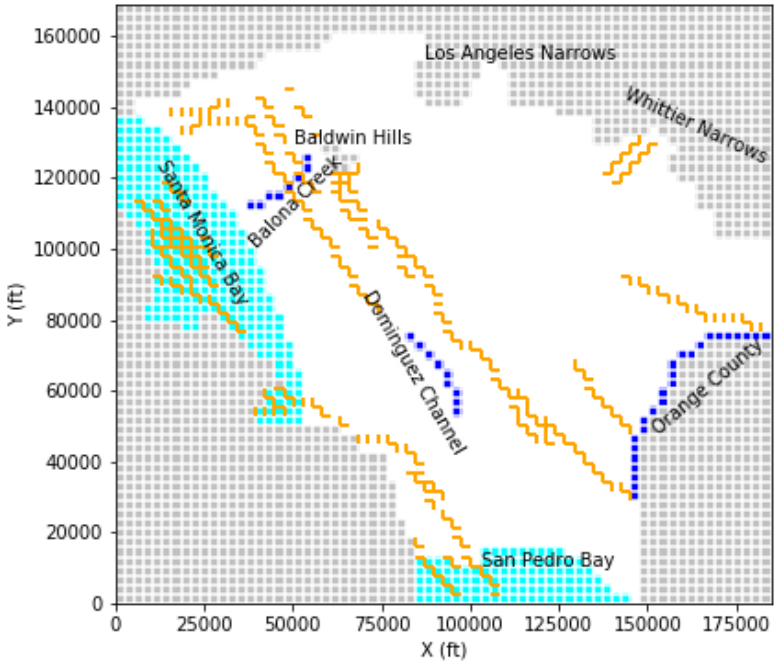

Figure 3.9: Boundary Conditions within model domain for layer 2 with relevant landmarks for Los Angeles model: grey cells: no-flow; light blue cells: GHB cells; blue cells: fixed-head or CHD cells; orange circles: HFB locations

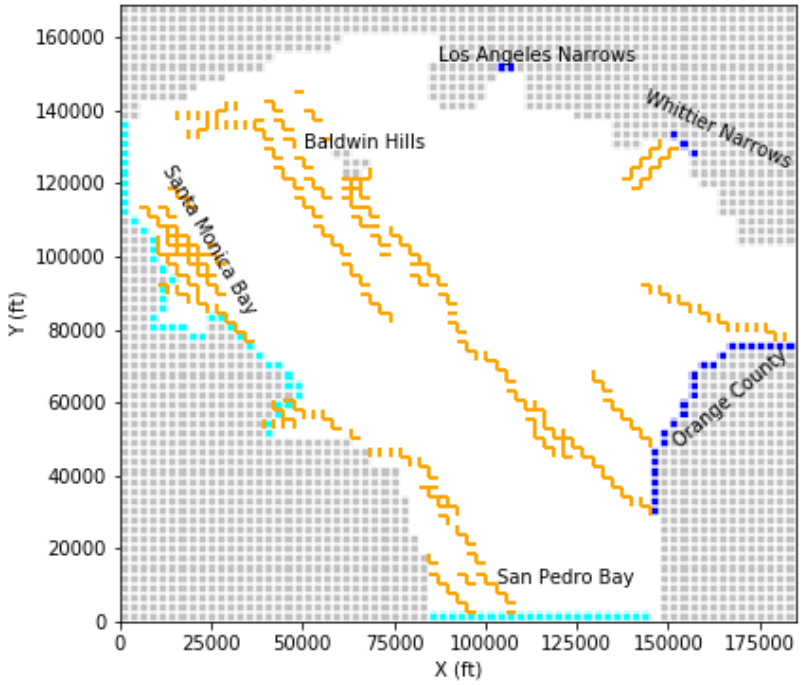

Figure 3.10: Boundary Conditions within model domain for layers 3 and 4 for Los Angeles model: grey cells: no-flow; light blue cells: GHB cells; blue cells: fixed-head or CHD cells; orange circles: HFB locations

from those measurements are assumed to represent the heads in layer 3. The relative differences between model layer 3 with model layers 2 and 4 at multiple well monitoring sites are used to estimate the specified heads in layers 2 and 4 at these positions where lateral flow occurs.

CHD fixed head cells are also used to represent surface water features such as channels that are not included in the original Reichard et al. (2003) model but added in subsequent adjustments by Kraemer (Kraemer, S.R., US EPA, personal communication). In the original Reichard model, the surface water channels are lined with concrete but in a pre-development model, these streams have a natural connection to the subsurface that can be represented by fixing heads with input from phreatic contours from Mendenhall (1905). In layer 1, the Los Angeles River and the Rio Hondo which connects with the Los Angeles River are represented by CHD cells (Figure 3.8). These rivers are represented by CHD cells that are specified at 200 ft AMSL at the northernmost point of the Los Angeles River decreasing downstream to 0 ft AMSL where the river meets the San Pedro Bay. In layer 2, the Dominguez Channel and Balona Creek are represented with CHD cells (Figure 3.9). All of the layer 2 CHD cells are fixed to 20 ft AMSL.

Recharge (RCH) Recharge varies from 0 to 0.01 ft/d, as shown in Figure 3.11. Recharge is included to represent mountain-front recharge on the model active area perimeter and direct precipitation and

irrigation return flow on the model interior. Mountain-front recharge is higher than the interior precipitation recharge. Recharge is directed to the highest active cell which can be either layer 1 or 2 since layer 1's active cell domain is not inclusive of all recharge cells because it does not cover all surface features of the model area.

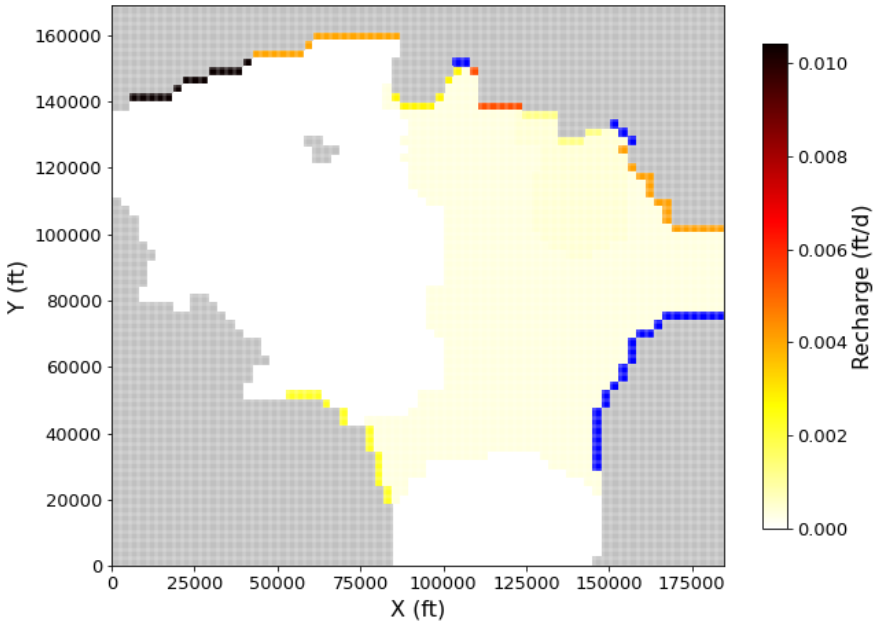

Figure 3.11: Spatial Distribution of Recharge in LA Model (ft/d) (fixed heads shown in blue)

Horizontal Flow Boundary (HFB) HFB data is used to represent geologic faults in the model that mostly trend northwest. There are 1097 cells used to represent the faults and their impediment to flow. The HFB conductances range from 4.3·10-5 ft^2/d to 0.86 ft^2/d.

3.1.2.2. Aquifer Parameters

The BCF package was used to specify flow parameters for the aquifers. The horizontal hydraulic conductivity and leakance values are shown in Table 3.1. Appendix Figures A.1-A.8 show the spatial distribution of hydraulic conductivity for each layer. Vertical hydraulic conductivity was specified to be a fraction of the horizontal hydraulic conductivity. K_z/K_h ranges from 0.10 in the top layer forebay to 0.0005 in layers 2 and 3 in the inland part of the basin. There are no separate vertical confining units or aquitards. All layers are assumed to be isotropic.

	K_h (ft/d)			L=K_z /ΔL (d^{-1})		
Layer	**Min**	**Max**	**Average**	**Min**	**Max**	**Average**
1	13	800	30.9	$8 \cdot 10^{-6}$	0.22	$4.9 \cdot 10^{-3}$
2	0.1	130	15.7	$7 \cdot 10^{-7}$	$7 \cdot 10^{-2}$	$5.9 * 10^{-3}$
3	0.6	140	22.1	$2 \cdot 10^{-6}$	$4 \cdot 10^{-2}$	$6.3 \cdot 10^{-2}$
4	1	50	13.3			

Table 3.1: Aquifer Properties of Los Angeles Model

3.1.3. Transformed Model

The model was transformed following the method of Bakker and Schaars (2013) outlined in Chapter 2. In the transformed model, all layers are modeled as BCF layer type 3. Figures 3.12-3.14 show cross-sections of the transformed model along lines mapped in Figures 3.3-3.4. The model top now ranges from -2.1-39.0 ft AMSL whereas the original model top was a constant 339 ft AMSL. The very bottom of the model is now fixed at -8.5 ft AMSL contrary to the original model bottom ranging from -1561 to 83 ft AMSL. It may be useful to compare Figures 3.5-3.7 with Figures 3.12-3.14. It can be seen that the colorbar (depicting K) in the transformed model cross-sections is set to a scale greater than the original model's colorbar by a factor α. The y-axis (depicting elevation) can also be seen to have been scaled inversely by α and the ordering of the layers has been flipped as well. The leakance parameters are not altered as the change in vertical conductivity is matched by the change in cell thickness. The boundary conditions are inverted with their respective layers.

3.1.4. Interface Results

Interface results are shown in Figures 3.15-3.18 and Figures 3.24-3.26. Figures 3.15-3.18 show the depth of the interface in the context of the model's boundary conditions as well as the location of the interface tip and toe in each layer. Figures 3.24-3.26 show the model cross-section of the interface location for various lines shown in Figures 3.3 through 3.4.

The interface shows expected behavior, deepening as it moves inland. Due to the sea interacting with the aquifer from two fronts, the gradient has more of a east-west direction in the northwest and a north-south direction in the southeast of the model domain. Where the interface from San Pedro Bay meets the interface from Santa Monica Bay, the gradient direction merges into more of a diagonal direction to the northeast. Towards the northern-most section of the model, north of Santa Monica Bay,

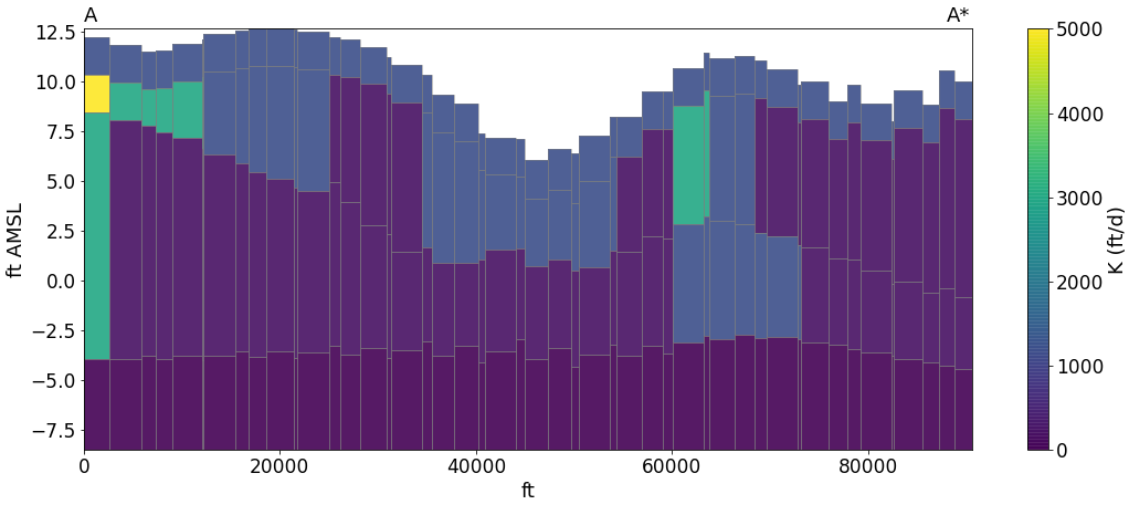

Figure 3.12: Cross-section of transformed model along line A colored by hydraulic conductivity

the gradient is oriented fully to the east, bending to the south. In the eastern part of the model domain, just south of the Whittier Narrows, the gradient is nearly oriented north. Both of these patterns seem to be strongly influenced by the high values of the GHB cells representing the underflow through the Los Angeles and Whittier Narrows. In Figure 3.17, there is a section of the toe that is shaped like an oval between the tip and landward toe location. This is a consequence of the lithology as the layer bottom–in a round shape–of layer 3 starkly rises in contrast to the lower elevations around it causing a toe. This unique geological feature is shown in Appendix Figure A.7. Otherwise, the interface elevation change in this area is not unique in this region–it is only due to the layer elevation rise that this strange pattern in the toe occurs, however that could still have implications for local and regional water management depending on the location of extraction and injection wells.

The impact of the faults is significant in the gradient distribution. The faults act as a barrier to flow and thus there is a significant gradient that builds up on the inland sides of the fault. The cross-section plots of the interface depth shown in Figures 3.24-3.26 also demonstrate the impact of the faults as barriers to flow. Just as it impedes freshwater flow from inland to the coast, the model tells us that it is also able to act as a barrier to seawater intrusion causing a sharp increase in interface depth once it encounters the fault zone. This impact of the faults in creating steep gradients is also apparent just from looking at the map view of the interface results where there is a concentration of lines along the HFB cell locations.

There is also a significant gradient that occurs near the GHB cells that represent groundwater underflow through the Whittier and Los Angeles Narrows in the northern part of the model domain. This can be explained by the high values of around 300 ft AMSL that the GHB cells are set to that lead to a

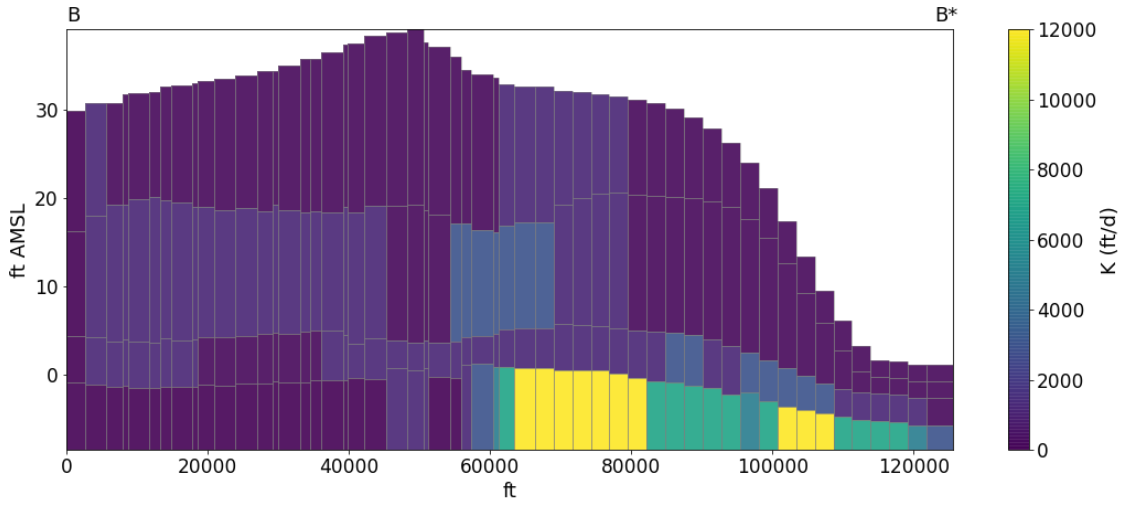

Figure 3.13: Cross-section of transformed model along line B colored by hydraulic conductivity

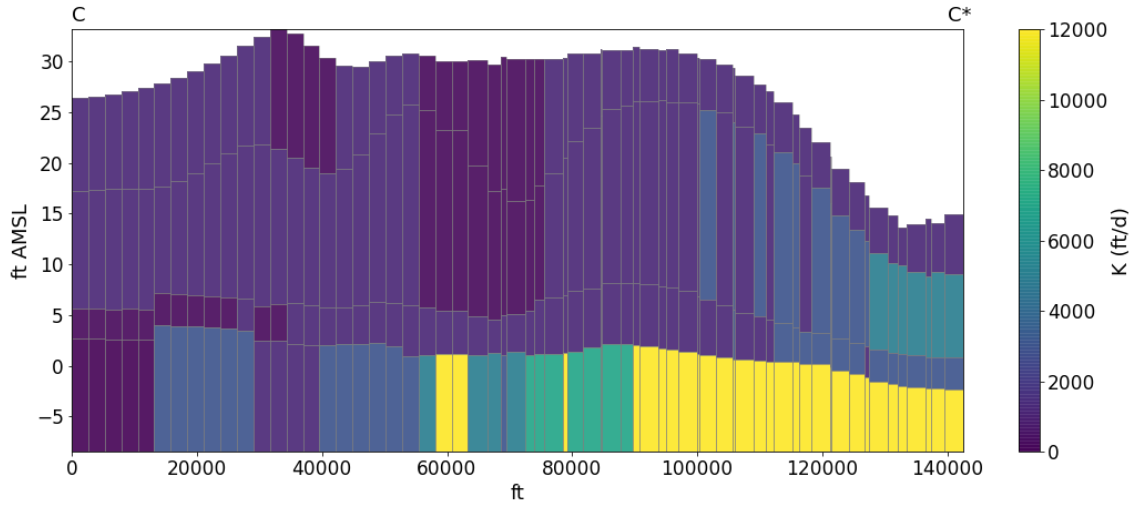

Figure 3.14: Cross-section of transformed model along line C colored by hydraulic conductivity

rapid increase in head near these GHB locations leading to a very deep interface.

The boundary conditions of the GHB cells representing the groundwater flows of the two Narrows, the HFB cells representing the fault system caused by the NIU, and the GHB cells representing the head at sea play the biggest role in the position and depth of the interface as described above. In between the faults and the Narrows and seaward of the faults, the interface/head gradient is milder. These patterns generally match expectations as the faults are impediments to lateral flows. This restriction to flow that acts as protection against further inland seawater intrusion fits the conceptual model understanding. However, such intense gradients near the faults may not be realistic as the model predicts that there is a drop of several hundred feet across the faults in interface depth. In reality, there may be some leaky areas across the faults to mitigate this build-up that this model has attempted to account for with the

conductance terms.

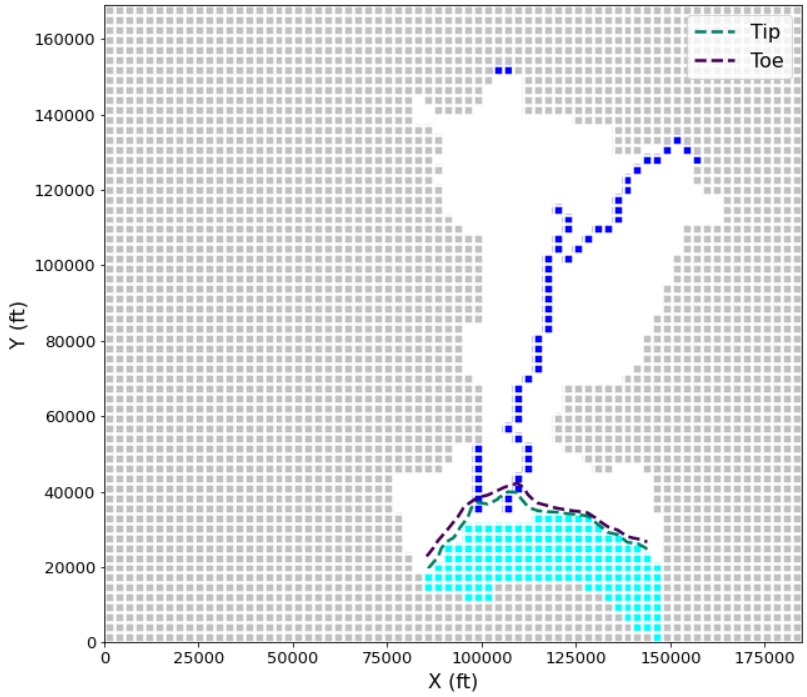

Figure 3.15: Interface tip and toe location for layer 1 of LA model with GHB and CHD boundary conditions included

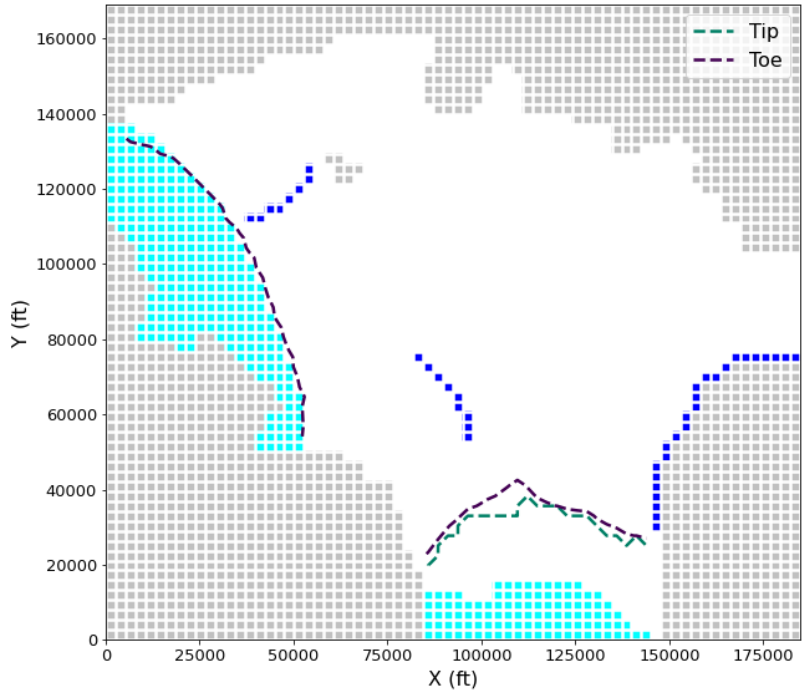

Figure 3.16: Interface tip and toe location for layer 2 of LA model with GHB and CHD boundary conditions included

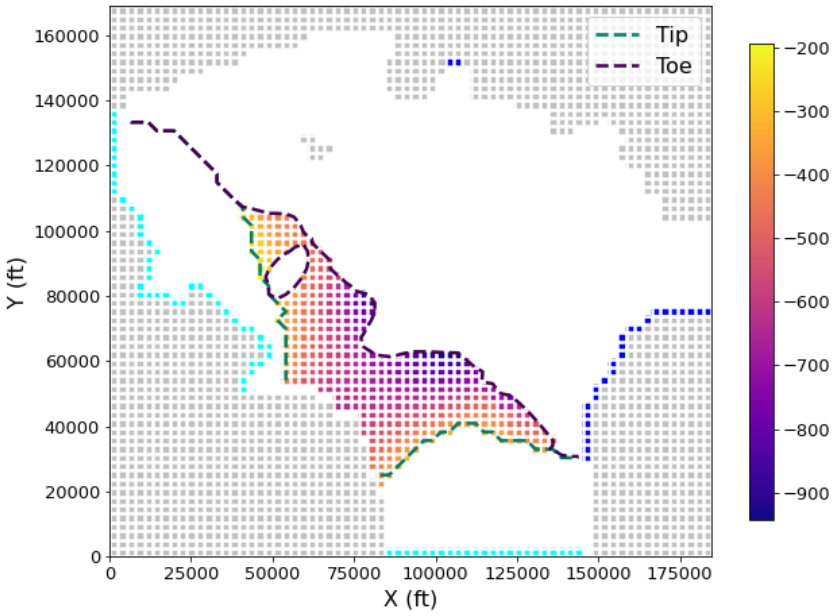

Figure 3.17: Interface tip, and toe location and depth (indicated by the colorbar in ft AMSL) for layer 3 of LA model with GHB and CHD boundary conditions included

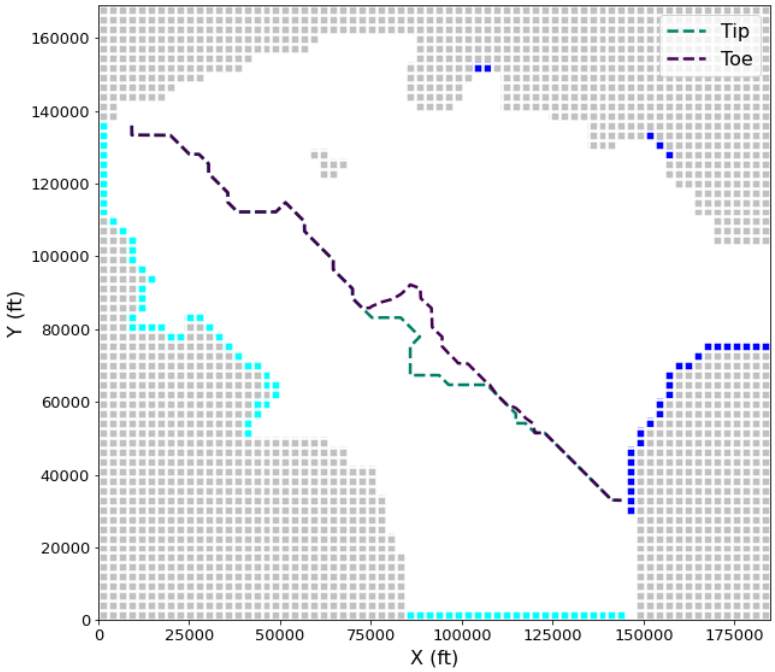

Figure 3.18: Interface tip and toe location for layer 4 of LA model with GHB and CHD boundary conditions included

Mendenhall (1905) reported on the state of the basin in 1905 and thus provides basic information to compare results. Figure 3.19 shows manually drawn contours of freshwater head near the coast. Figures 3.20-3.21 show freshwater contours as produced by the Bakker-Schaars method (prior to converting to interface depth) for the top two layers which represent the most relevant conditions since Mendenhall (1905) only included information from wells 25 ft deep or less. In general, there are similar values seen in heads near the coast and near the Narrows. In between these two areas, the gradient appears to be slightly higher on the seaward side based on the location of the 100 ft contour in each figure. The heads in Mendenhall are slightly higher in some areas but overall similar patterns to give confidence to the model's results. Furthermore, there can be seen some jaggedness in the contours in the middle of the basin of Mendenhall's map that seem similar to the jaggedness produced by the faults in the model. Mendenhall also describes "... a fold that acts as a dam to waters seeking a way seaward beneath the surface... In consequence, groundwater levels are much higher above this ridge than below it." He is unable to quantify any specific changes in groundwater levels across the ridge however.

Mendenhall attributes the possibility of the then-artesian aquifers to this ridge. It is now known he was describing the Newport-Inglewood Uplift, but the impact of this ridge on the water levels was well noted. Mendenhall also comments on the regularity of the gradient inland of the anticlinal ridge as compared to the gradient seaward of the ridge which is less uniform. In the modeled freshwater contours, this irregularity is not as noticeable but Mendenhall does also leave room for the explanation of this irregularity to be attributed to a lack of data.

3.1.4.1. Pumping Optimization

A location for a hypothetical pumping well is chosen at row 43 and column 51 for optimization following the methods in Section 1.5. Figure 3.27 shows the location of the cell containing the well in the model. The location of the well was chosen because it was past the extent of all toes in the model so it would begin as totally freshwater. In some locations inland of the HFB barriers, the interface was incapable of connecting past the HFB no matter the magnitude of pumping but this location was near enough to the toe and the lateral flows from Orange County that it was able to find a critical pumping rate. Once the location was chosen, the model was iterated following the methodology in Section 2.5 until the surrounding cells were dry–representing saltwater intrusion.

The well is set in layers 2 and 3 and the pumping rate is split between the layers proportional to the transmissivity of each layer. The iterative procedure was followed and cross-sectional plots were checked to ensure that there was connectivity from the well area to the sea when intrusion occurred in the well area. The critical pumping rate is found to be 1,917,000 ft^3/d (44 acre-ft/d or 54,283 m^3/d)

Figure 3.19: Contours of freshwater head from Mendenhall (1905)

for this location. The interface tip and toe locations are shown in Figures 3.28-3.31 where the red cell represents the cell that the well is in and the light blue again represents GHB cells. Figure 3.30 again shows the round toe area as a consequence of an elevated layer bottom in that region. Figure 3.32 also shows a cross-section view of the interface along column 51 of the model, the same column in which the well is positioned. This shows the the well draws the interface in deeper until it rises up above layer 2 due to the significant pumping and causes saltwater intrusion.

This critical pumping rate is a high value for pumping but it should be recalled that this is the only pumping well in the model. For reference, Reichard et al. (2003) reported that the mean pumping out of the basin from 1971-2000 was nearly 31 million ft^3/d (708 acre-ft/d or 873,000 m^3/d), approximately 16.1 times as much but most of that pumping occurs inland of the fault zone. There is also active injection that accounts for roughly 4.2 million ft^3/d (96 acre-ft/d or 118,000 m^3/d). Including injection barrier wells, the net pumping out of the basin is approximately 27 million ft^3/d, approximately 14.2 times as much as the optimized pumping rate, and the basin in Reichard experiences protection from seawater intrusion as well. Considering the location of much of that pumping and injection in comparison to the

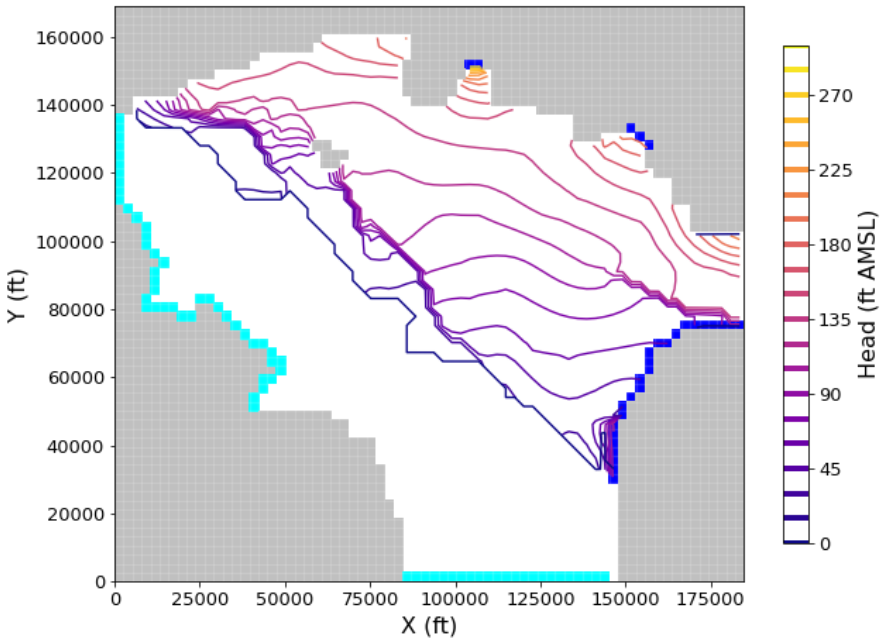

Figure 3.20: Freshwater head contours for LA model layer 1

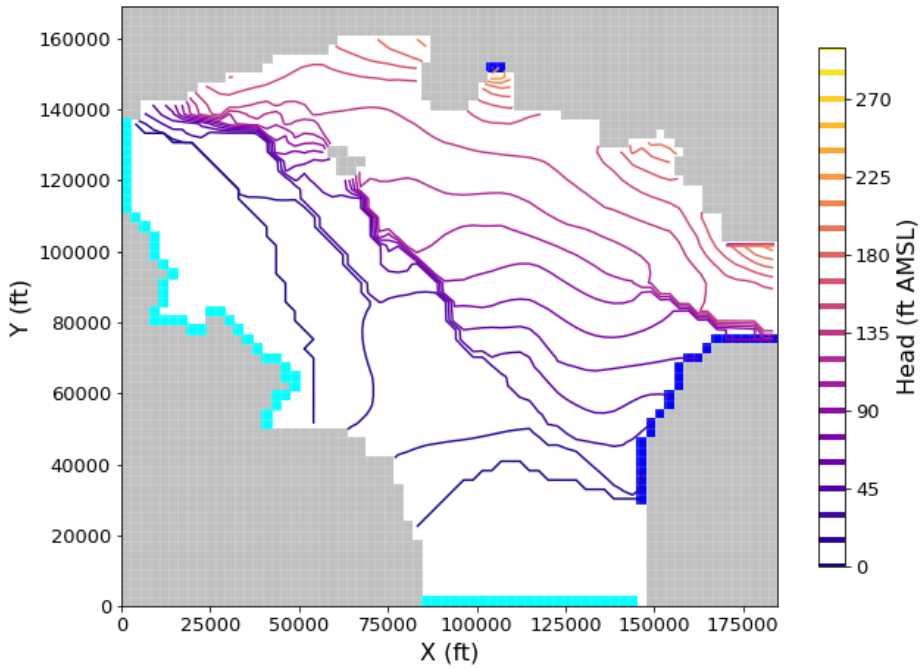

Figure 3.21: Freshwater head contours for LA model layer 2

optimized well that is nearer the sea, the optimized pumping value seems realistic even if from just one well. Figure 3.31 shows the impact of the well best because it shows the difference in the toe location

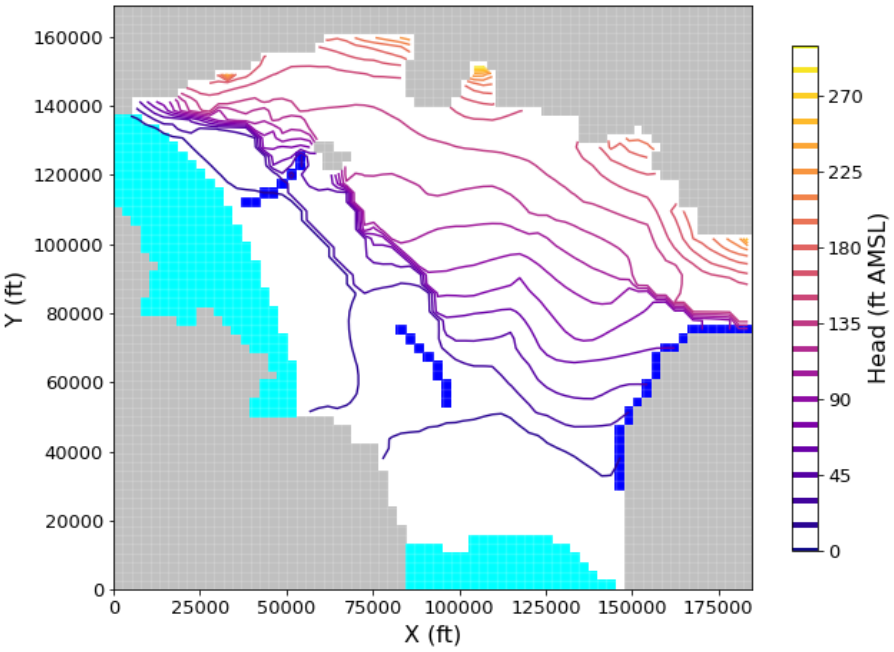

Figure 3.22: Freshwater head contours for LA model layer 3

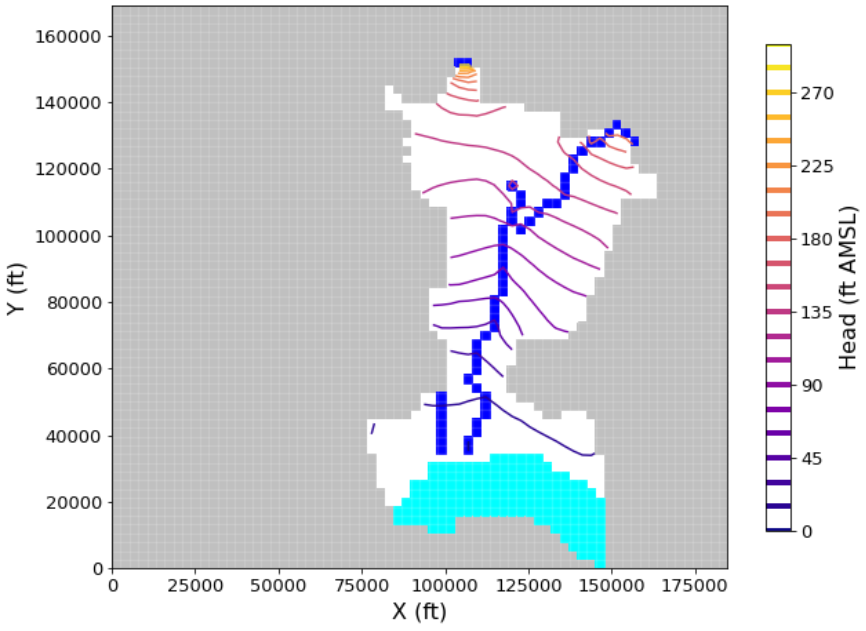

Figure 3.23: Freshwater head contours for LA model layer 4

once the optimized well is included. In this plot, the optimized toe location is pulled further inland so that there is seawater intrusion just beneath the well. Figure 3.32 shows the cross-section of the model

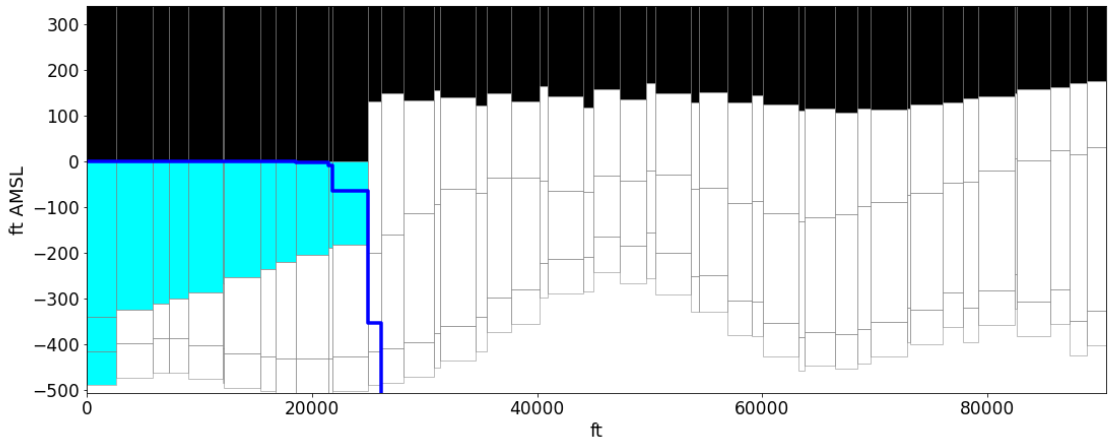

Figure 3.24: Cross-section of interface along line A

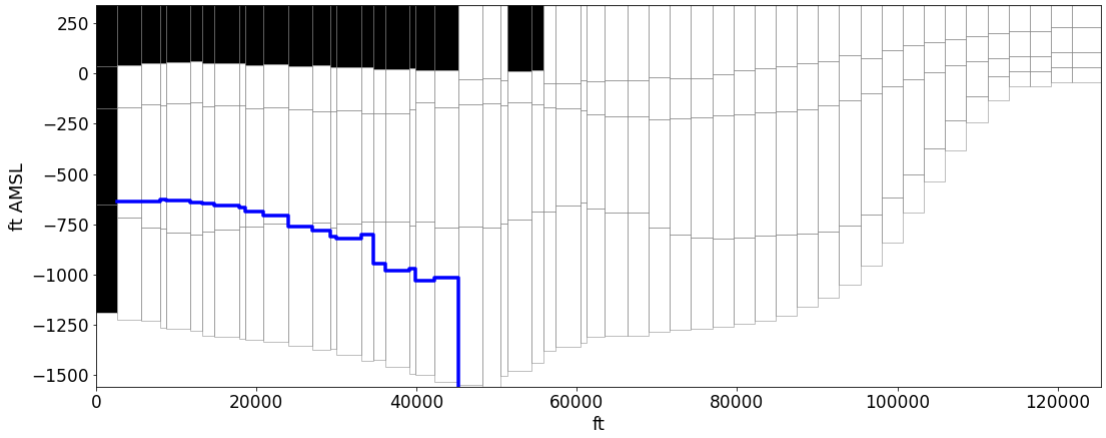

Figure 3.25: Cross-section of interface along line B

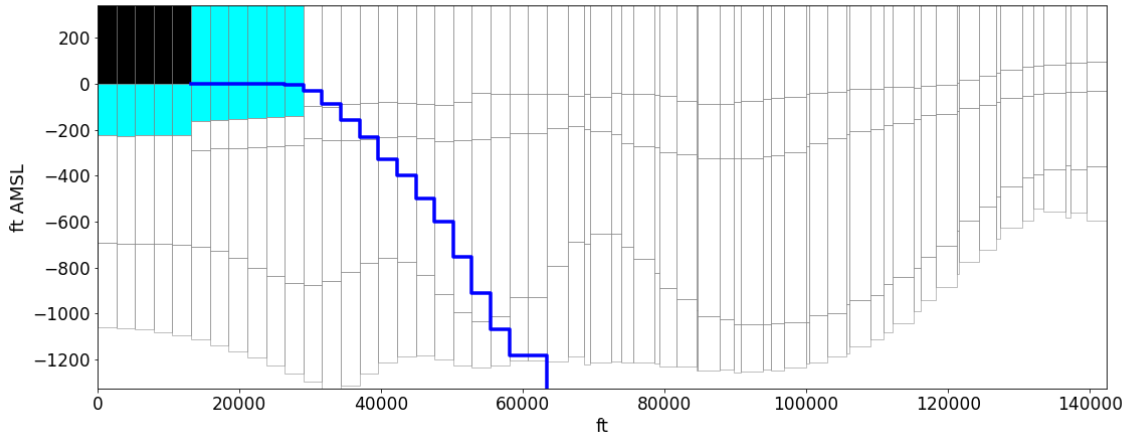

Figure 3.26: Cross-section of interface along line C

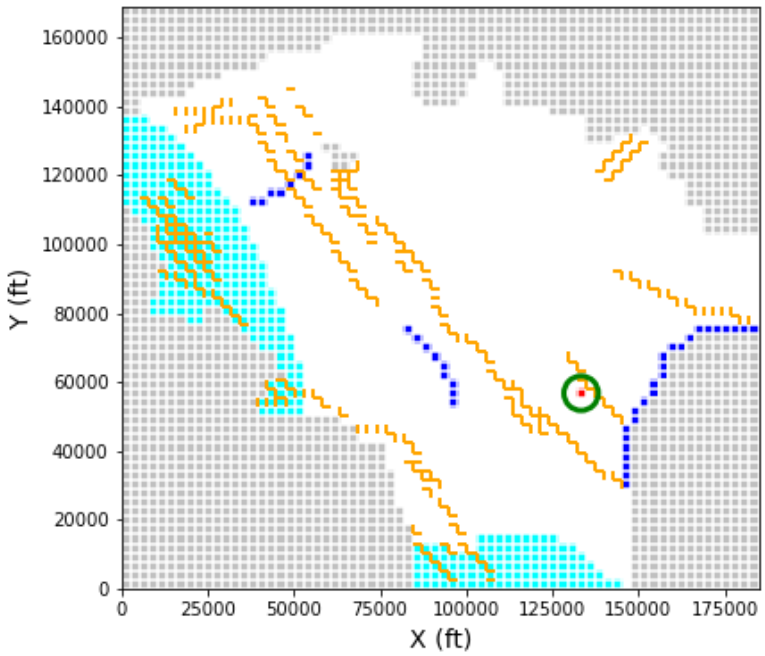

Figure 3.27: Location of well to be optimized in context of model layer 2 and surrounding boundary conditions (Well is shown in red and circled in green; HFB boundaries shown in orange, constant head boundaries in blue, GHB shown in light blue, and no-flow cells are grey)

in the same column as the well (column 51). This figure shows how the well has drawn the interface further in and upwards toward the well, just before intrusion occurs. Besides layer 4, the plots of the tip and toe of each scenario are not very different. In some cases the tip or toe may be marginally inland due to the well but the well's impact is localized. Once seawater intrusion were to occur however, the impact may be more widespread–if pumping were to exceed the critical pumping rate.

It should be cautioned that the well's proximity to the fixed head cells to the east could influence the critical pumping rate. The fixed heads can act as an infinite source which is unrealistic and may inflate the critical pumping rate.

3.1.5. Summary

- A realistic interface is computed with minimal seawater intrusion representing pre-development conditions given the basic conceptual understanding of the model and through comparison with Mendenhall (1905).
- The interface shows nearly no seawater intrusion in the top two layers but some intrusion extending to the fault system in the bottom two layers.
- The fault system represented by the HFB package plays a highly influential role in the protection

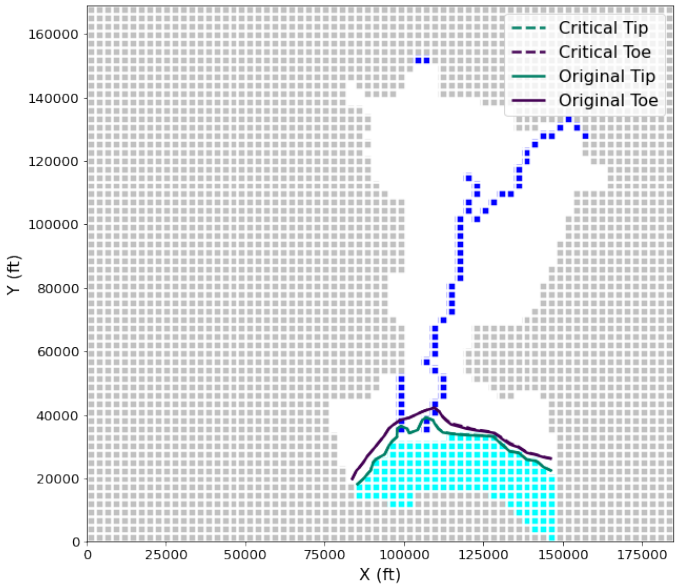

Figure 3.28: Interface tip and toe location for scenario with optimized well at critical pumping rate and initial transformed model (Base) for layer 1 of LA model

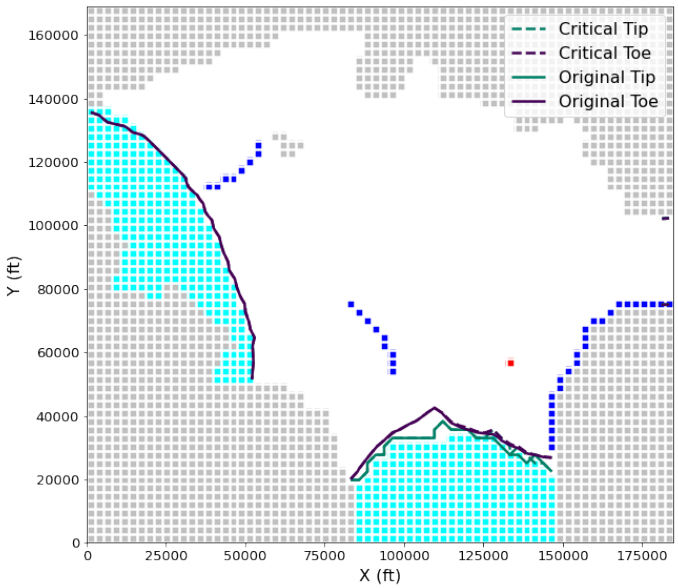

Figure 3.29: Interface tip and toe location for scenario with optimized well at critical pumping rate and original transformed model (Base) for layer 2 of LA model (well indicated by red-colored cell)

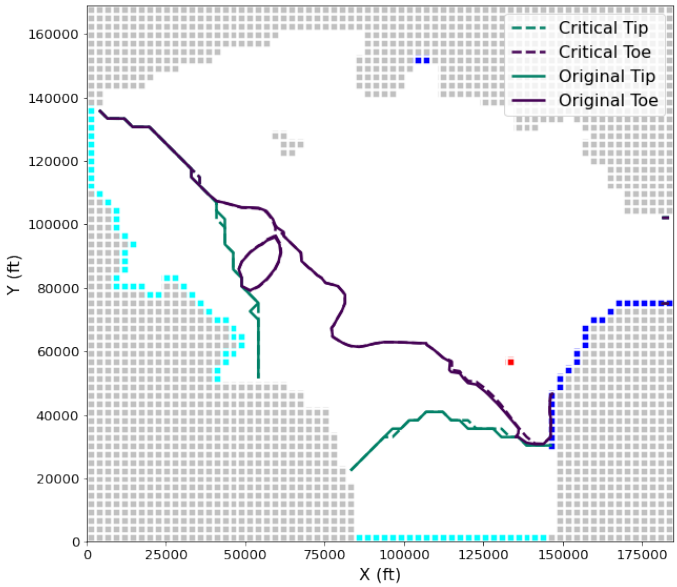

Figure 3.30: Interface tip and toe location for scenario with optimized well at critical pumping rate and original transformed model for layer 3 of LA model (well indicated by red-colored cell)

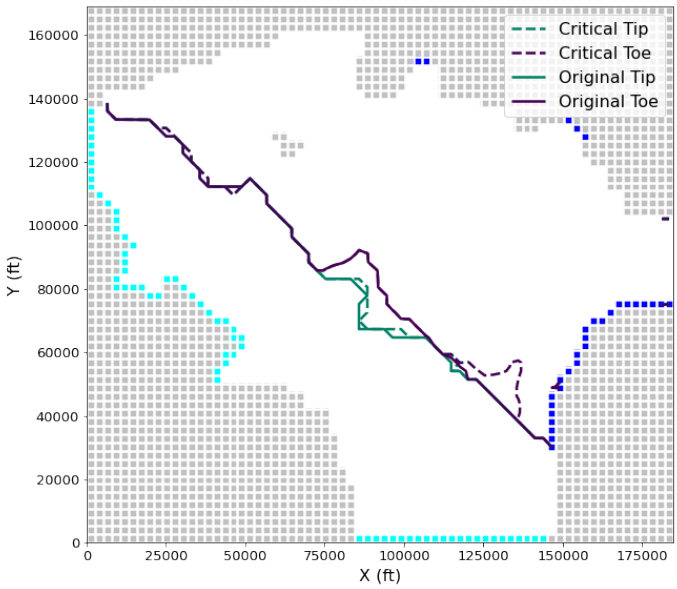

Figure 3.31: Interface tip and toe location for scenario with optimized well at critical pumping rate and original transformed model for layer 4 of LA model

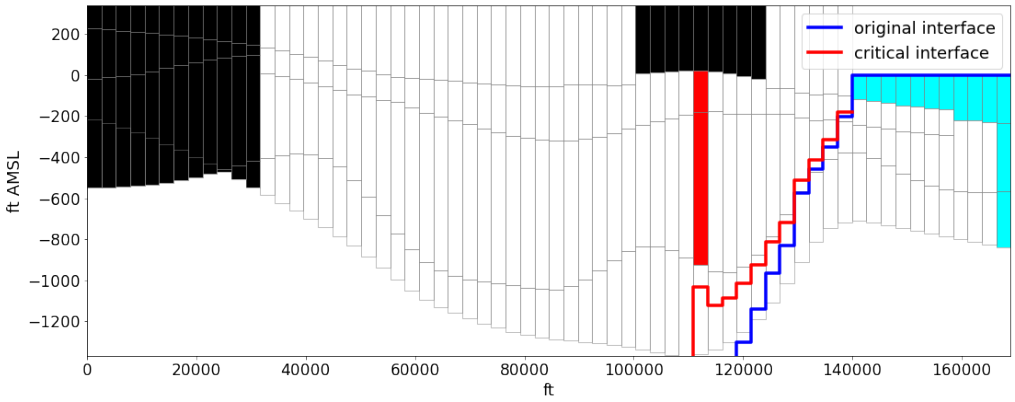

Figure 3.32: Interface of critical pumping rate scenario (red) and original transformed model with no pumping (blue) along column 51 of the Los Angeles model

of the basin from seawater intrusion, primarily for deeper layers and when there is pumping.

- A critical pumping rate is computed for a hypothetical well of 1,917,000 ft^3/d (44 acre-ft/d or 54,283 m^3/d). This hypothetical well had a localized effect in which the interface position mostly only changed near the well and in the lowest layer. The proximity to the fixed heads to the east should caution the results however.

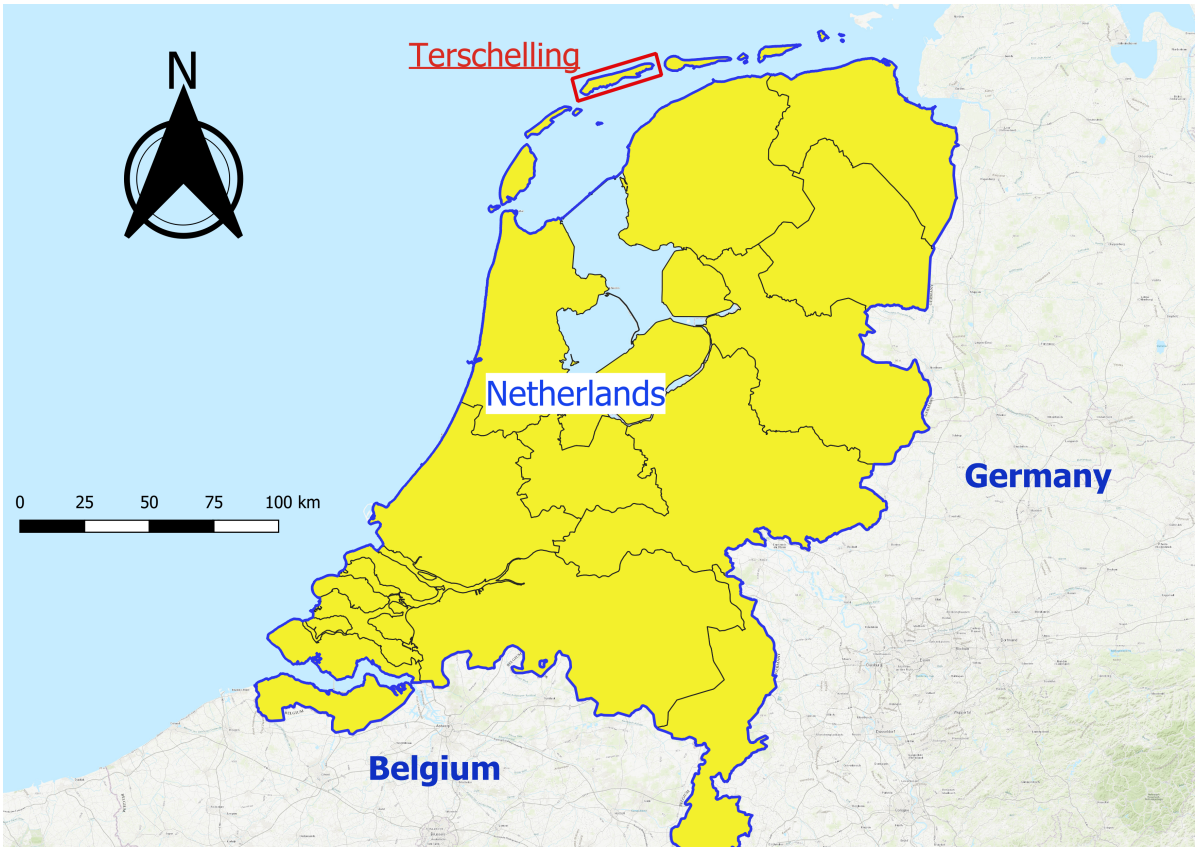

Figure 3.33: Map of Geographical Context (Netherlands, yellow) indicating where the model area, Terschelling, is (red box)

3.2. Terschelling

3.2.1. Area Description

Figures 3.33 and 3.34 show the location of the Terschelling model area. Terschelling is an island in the chain of barrier islands on the Northwestern border of The Netherlands known as the Frisian Islands. The island has an area of 674 km^2, of which 85 km^2 are land and the rest (589 km^2) is water. Bordered on the northwest by the North Sea, the border of the island facing the mainland is surrounded by the Wadden Sea. The Wadden Sea is very shallow and protected by the barrier formed by the Frisian Islands causing it to have usually a higher level of seawater than the North Sea-facing portion of the island. The inland-facing part of Terschelling is made up of a polder area reclaimed from salt marshes lying below sea level. The rest of the island is covered by dunes with variable elevation. Figure 3.35 shows the variable elevation of the island. The island aquifer is used to supply a portion of the municipal and agricultural use on the island.

The island geology can be described in two main layers. The uppermost aquifer is comprised of Holocene marine deposits as well as the Eem deposits which are mostly made up of fine to medium sands and is underlain by silty beds and clay lenses. The Urk I and II sediments form the lower layer

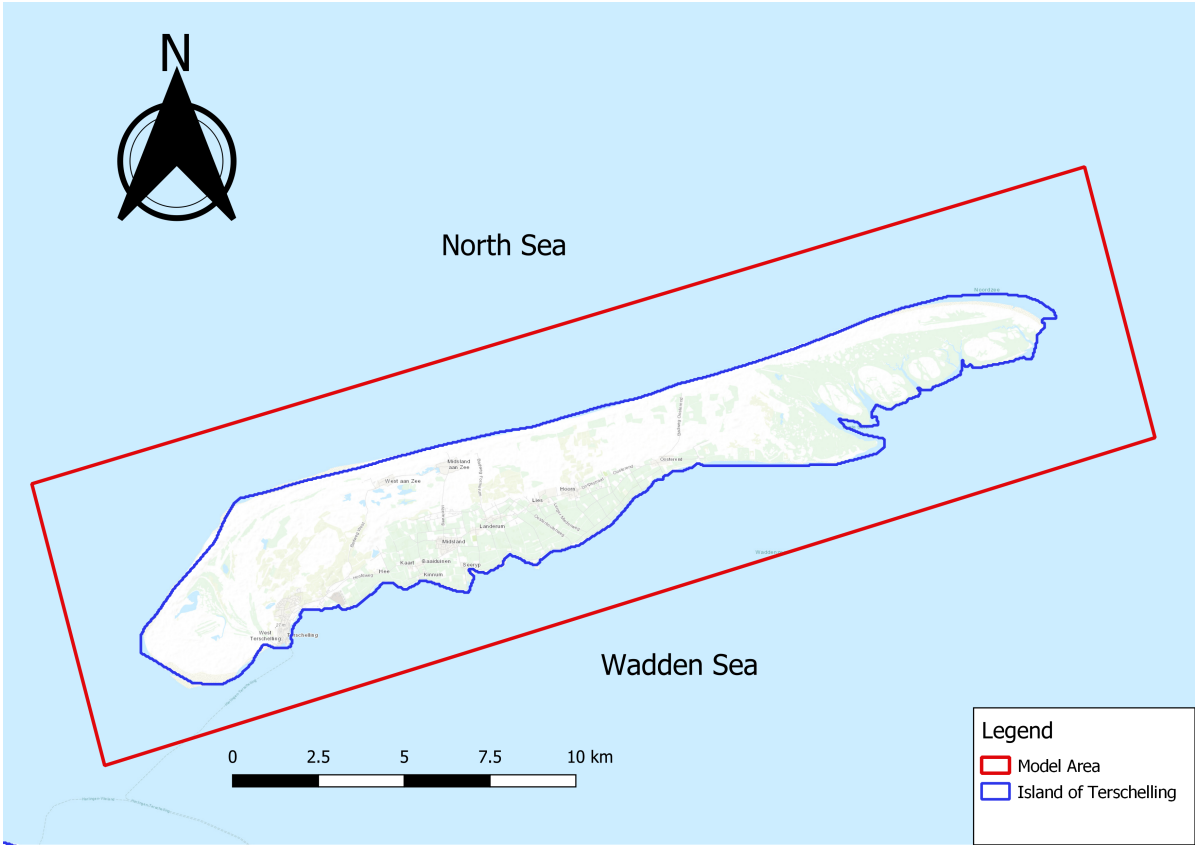

Figure 3.34: Map of Terschelling Model Area

and are comprised of fine to coarse sands. There are no faults of folds in the geology of the area and the layers are deposited atop one another so that the layer interfaces are approximately horizontal.

3.2.2. Model Description

A MODFLOW (Harbaugh, 2005) model was developed for the Terschelling Island by the consulting firm, Artesia in Schoonhaven, The Netherlands. The model is comprised of three homogeneous aquifers and two aquitards and simulated transient flow. The top aquifer is included only to account for geographical storage effects that hold the water for some time rather than letting it discharge from the surface immediately. The model top is also the only non-flat boundary elevation. The model bottoms are all horizontal. The top aquifer is has variable thickness due to the variable model top but reaches a constant depth of -3 m AMSL. The aquitard in-between the top and middle aquifers is set to 1 m thickness. The middle aquifer layer is 26 m thick, reaching a depth of -30 m AMSL and is comprised of sands. The aquitard separating the middle and bottom aquifer is also set to 1 m thick. The bottom-most layer is 119 m thick reaching a depth of 150 m below MSL. The model has 150 rows and 490 columns. The model uses the LPF (Layer-Property Flow) package to represent flow parameters in the model. The top model layer is set as a convertible layer type between unconfined and confined (LPF layer type

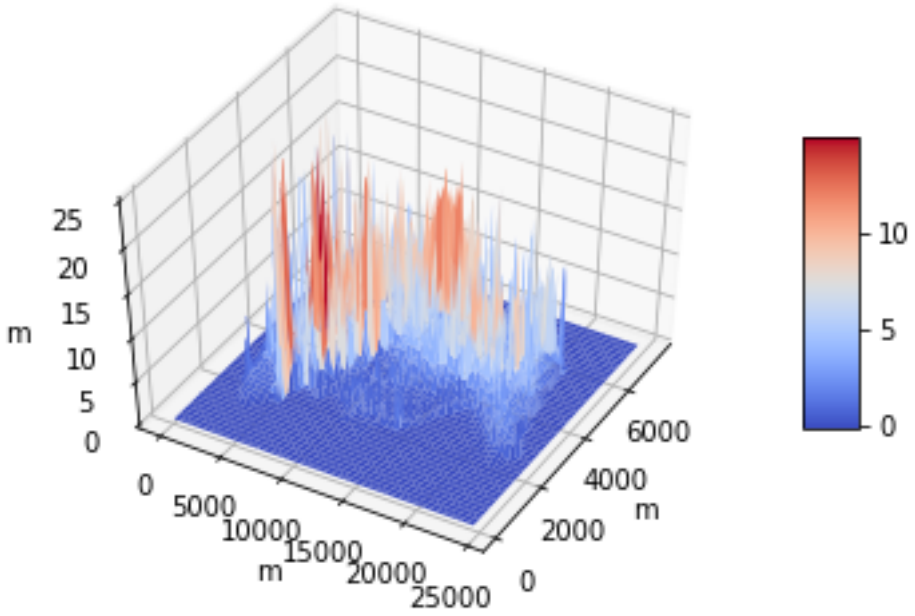

Figure 3.35: Model Surface Elevation of Terschelling Island Model

1) and the bottom two aquifers are set to confined (LPF layer type 0).

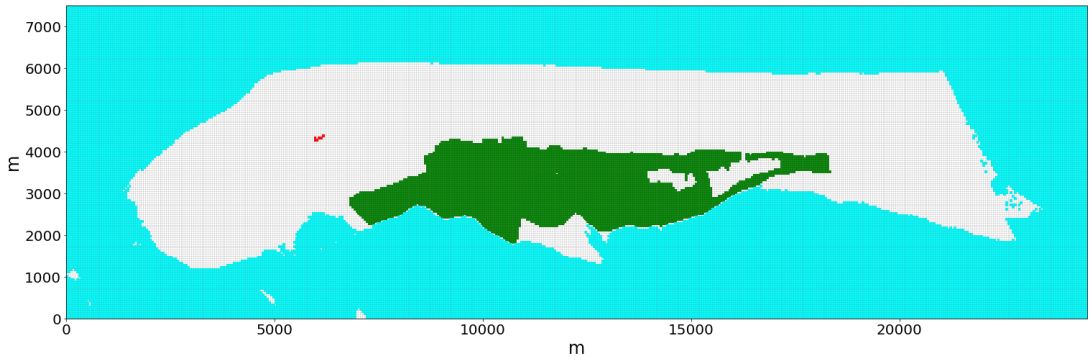

Figure 3.36: Boundary Conditions for original Terschelling model Green - RIV (layer 1), Red - WEL (layers 1 and 2), Light blue - GHB (layers 1 through 3))

3.2.2.1. Boundary Conditions

The Terschelling Model has no no-flow cells and no fixed-head cells (included in the IBOUND parameter). The lateral model boundaries are assumed impermeable and all cells in the model are active. The model has five BC packages: WEL, DRN, RIV, RCH, and GHB. The DRN (drain) package of the model is removed for this thesis. Figure 3.36 shows a map of the different locations of the different boundary conditions except for GHB cells which surround the island and are shown in Figure 3.37.

GHB The 67,815 GHB cells in the model are primarily used to represent the sea level elevation. There are two different elevations of the sea-level in the model. The first is the same as the datum, 0 cm AMSL, and the second is 7.5 cm AMSL. Figure 3.37 shows the spatial variability of the sea level around Terschelling. The GHB cells are all set to 0 cm AMSL to avoid the problem of moving saltwater.

Well (WEL) There are 14 well cells included in the model. Their positions are shown below in 3.36 in red. The default transient model is converted to steady-state by calculating an average of each well's discharge. This results in all well cells having an equal discharge of -39.1 m^3/d. The wells have seven x, y locations penetrating the first two layers so each well is represented in layers 1 and 2 to combine for 14 well cells. The wells' x, y position is seen in Figure 3.36 in red. It can be seen that the wells' positions are very concentrated into one area of the model.

River (RIV) There are 7,446 head-dependent flux river cells in the model. The cells are implemented to represent the surface-water bodies on the top of the model that interact with the water table. When the river stage is above the head in that groundwater cell, there is infiltration; when the opposite occurs, there is flow out of the cell. In contrast to the GHB element, there is a defined lower limit controlling the flux into the model once the head drops below the river bottom. On Terschelling, this package is largely used to represent the polder area of the model. Figure 3.36 shows the location of the RIV cells in green. Some of the river cells have stage values below sea level due to the polder area on the south-central portion of the island. For instance, the minimum stage of the river cells is -0.55 m AMSL while the maximum is 2.51 m AMSL. The mean stage in the model is 0.13 m AMSL.

The river conductances vary considerably with a mean value of 22.66 m^2/d. The minimum is 0.17 m^2/d and the maximum is 185.20 m^2/d. 85% of the conductances are less than the mean indicating that there only a few cells with large conductivity values.

Figure 3.37: GHB cells and their corresponding values used to represent sea level in the model

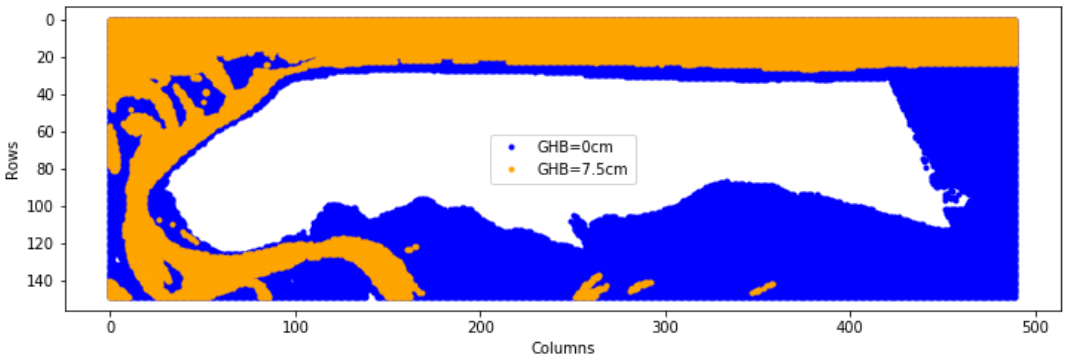

Recharge (RCH) Recharge is directed towards only the top layer of the model and ranges in value from $0.40 \cdot 10^{-3}$m/d to $16.78 \cdot 10^{-3}$m/d on the island. Off the island, there is no recharge. Figure 3.38 shows the spatial distribution of recharge.

Figure 3.38: Spatial Distribution of Recharge in m/d

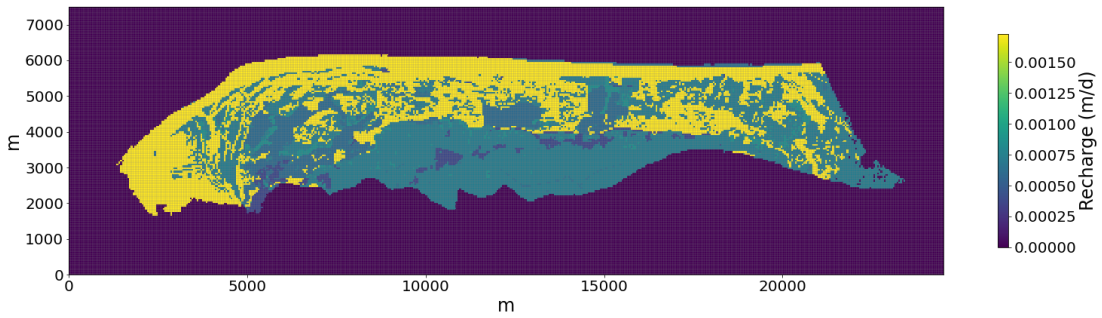

3.2.2.2. Aquifer Parameters

As stated earlier, the Terschelling model uses the LPF package. All layers are homogeneous and isotropic. The aquifer parameters are shown in Table 3.3. The vertical hydraulic conductivity wihtin each aquifer layer is set to 10 m/d everywhere except for the confining units where the K_v is listed in the table. There is no K_v for the bottom layer because the bottom of the model is impermeable and no vertical flow occurs beneath the bottom layer. The original model had a confining unit thickness set to 0.01 m, but this was changed to 1 m for this model. These confining units are only used for vertical flow and do not carry parameters pertaining to horizontal flow. Figures 3.40 and 3.41 show cross-sections of the original model and the transformed model, respectively, with the colors of the layers corresponding to the hydraulic conductivity. The cross-sections are shown for row 64. Figure 3.39 shows the location of rows on the model used for cross-sections later on.

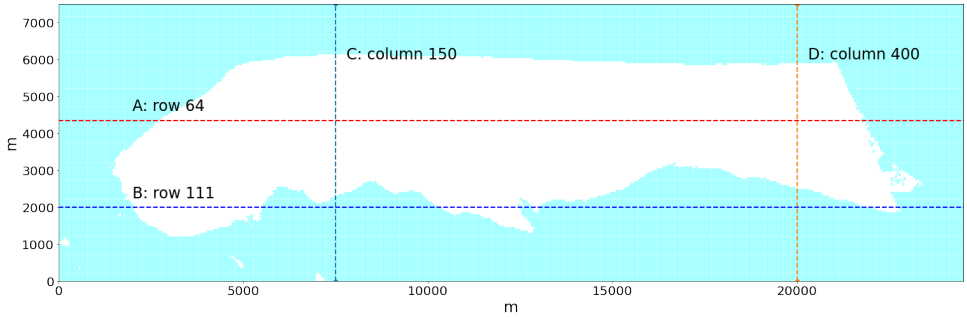

Figure 3.39: Map view of rows and columns used for cross-sections

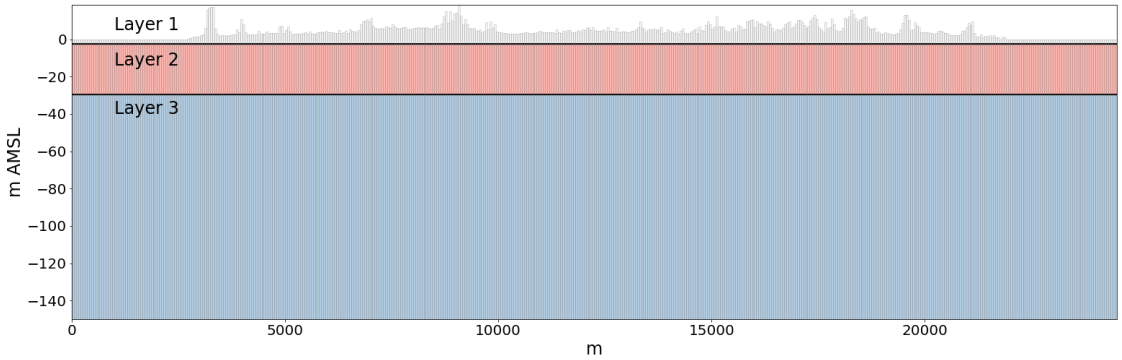

Figure 3.40: Cross section of Terschelling along row A showing layer elevations (aquitards colored in black)

Layer	K (m/d)	K_v* (m/d)
1	10.6	$2.8{\cdot}10^{-4}$ - $6.7{\cdot}10^{-3}$
2	10.1	$6.7{\cdot}10^{-4}$ - $1.2{\cdot}10^{-2}$
3	14.2	N/A

Table 3.2: Aquifer Properties of Terschelling Model
* - refers to the vertical hydraulic conductivity the confining aquitards beneath each respective layer

3.2.3. Transformed Model

The model was transformed following the method of Bakker and Schaars (2005) outlined in Chapter 2. In the transformed model, all layers are modeled as layer type 1 (unconfined). Figure 3.41 shows a cross-section of the transformed model along line A (row 64). Figures 3.40 and 3.41 can be compared to note the differences between the original and transformed model. The range of the y-axis is shortened by α in the transformed cross-section and the hydraulic conductivities are scaled by α as compared with the original model properties. The thickness of the confining units is 0.025 m in the transformed model.

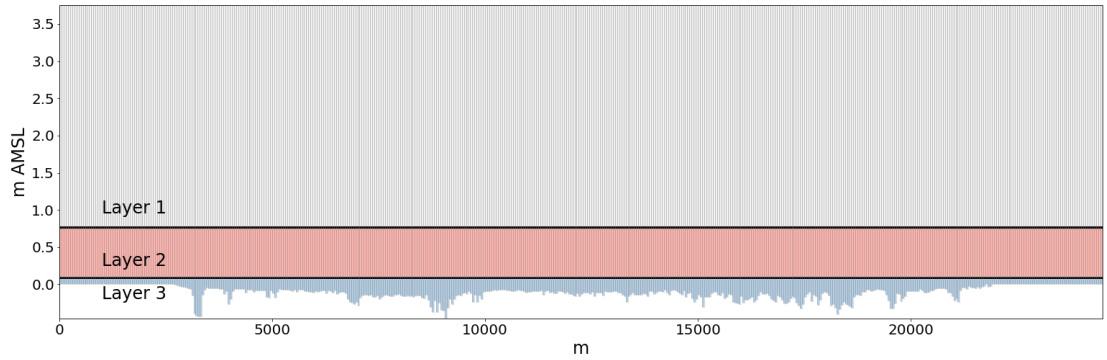

Figure 3.41: Cross section of transformed Terschelling model along row A showing layer elevations (aquitards colored in black)

Layer	K (m/d)	K_v* (m/d)
1	568	$1.7{\cdot}10^{-5}$ - $3.1{\cdot}10^{-4}$
2	404	$6.9{\cdot}10^{-6}$ - $1.7{\cdot}10^{-4}$
3	424	N/A

Table 3.3: Aquifer Properties of transformed Terschelling Model

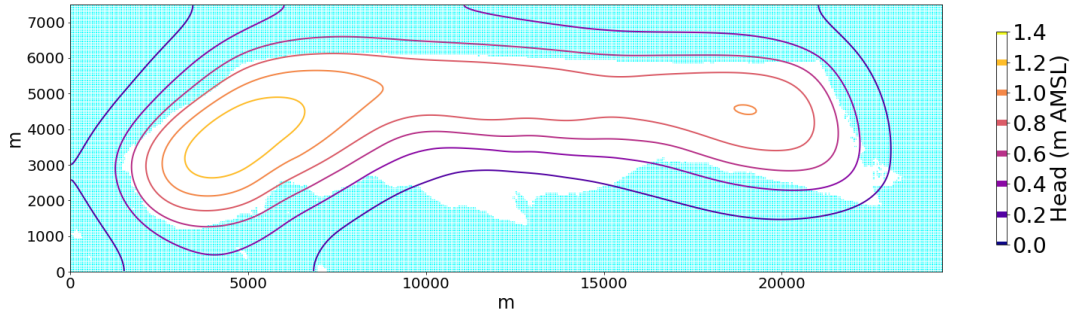

Figure 3.42: Heads for Terschelling from transformed model for layer 1 (light blue cells represent sea GHB cells)

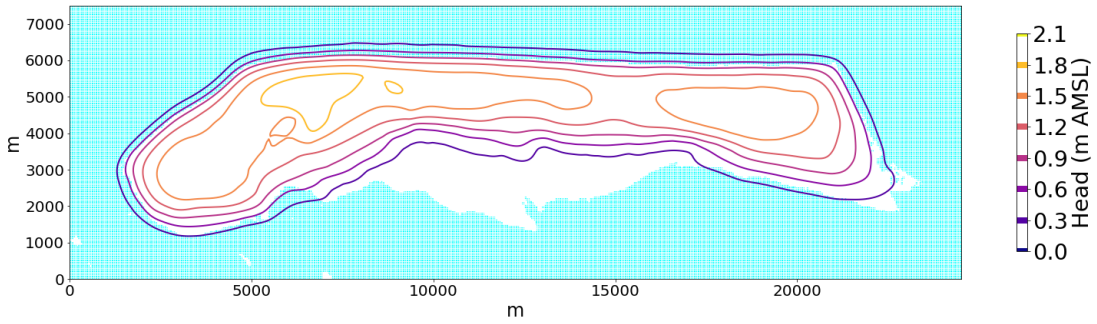

Figure 3.43: Heads for Terschelling from transformed model for layer 2 (light blue cells represent sea GHB cells)

3.2.4. Interface with Constant Sea Level

Figures 3.42-3.44 show the freshwater heads resulting from the transformed model. Figures 3.45-3.47 show the location of the tip and toe and the interface depth between the tip and toe for each model layer. For layer 3, only the interface tip and interface depths are shown since the interface does not reach the bottom of the aquifer. Figures 3.52 and 3.51 show cross-sections of the interface depth across the layers for rows 64 and 100 and columns 150 and 400 as shown in the map of these rows in Figure 3.39. The lowest interface depth is -147 m AMSL. As shown in Figure 3.52, the dominant features of the interface are the two troughs that occur on the eastern and western portions of the

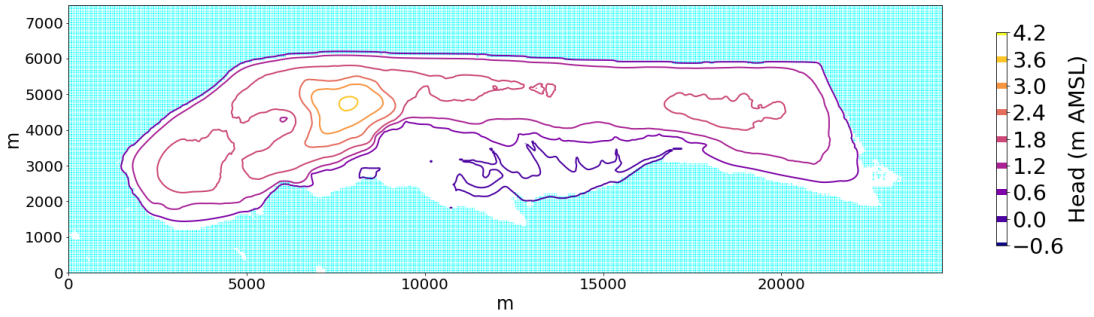

Figure 3.44: Heads for Terschelling from transformed model for layer 3 (light blue cells represent sea GHB cells)

island. These troughs and their relative depths can also be observed well in Figures 3.50 and 3.51. The western trough is the deepest interface feature whereas the eastern trough is milder. The cross-sectional plot in Figure 3.49 shows that in the south-central portion of the island, the interface exceeds the land surface which is attributed to the polder area which does lie below sea level. This polder area is represented mostly by the RIV package which has very low stage values.

The cross-section in Figure 3.52 shows that the wells do have an impact with their default pumping amounts, pulling the interface towards the surface near the deepest trough. The reason for the significant difference in the troughs' magnitudes could likely be attributed to recharge. Reviewing Figure 3.38 shows how there is more recharge on the western portion of the island than the eastern portion. This is consistent with the trend seen in the interface depth from the transformed model so it seems likely to play a major role.

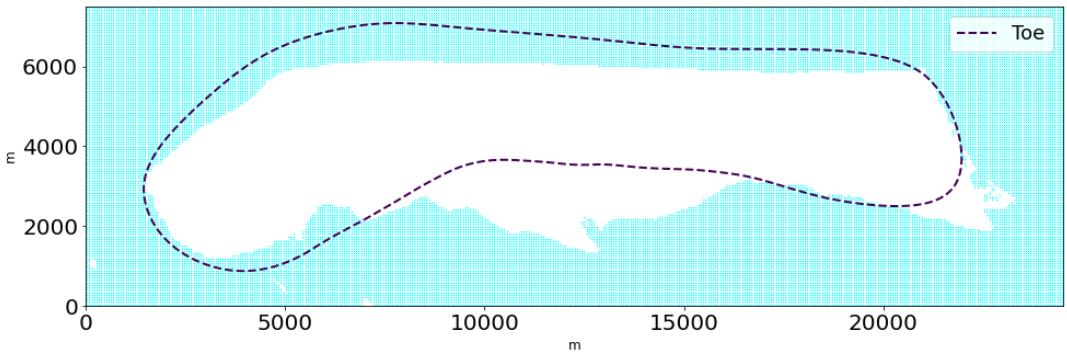

Figure 3.45: Locations of interface tip and toe for layer 1 of model as well as interface depth (light blue cells represent sea GHB cells)

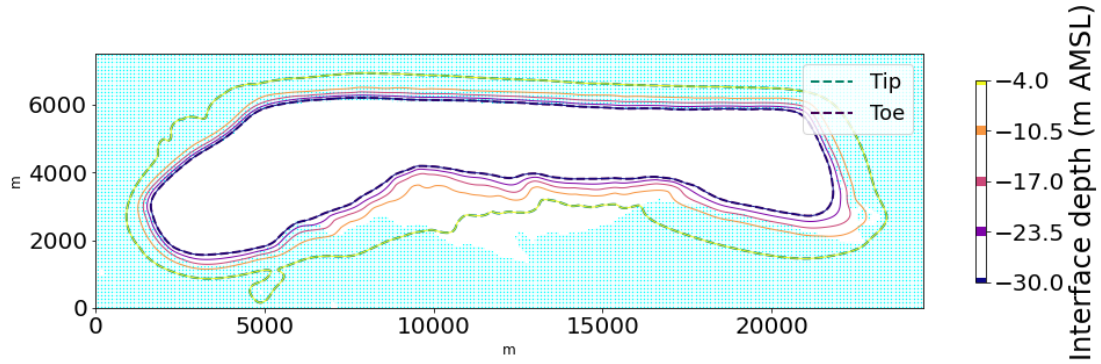

Figure 3.46: Locations of interface tip and toe for layer 2 of model as well as interface depth (light blue cells represent sea GHB cells)

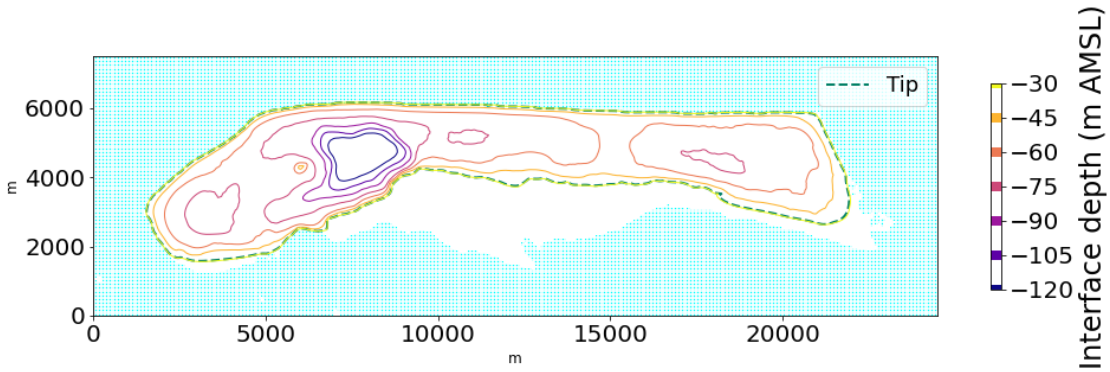

Figure 3.47: Locations of interface tip for layer 3 of model as well as interface depth (light blue cells represent sea GHB cells)

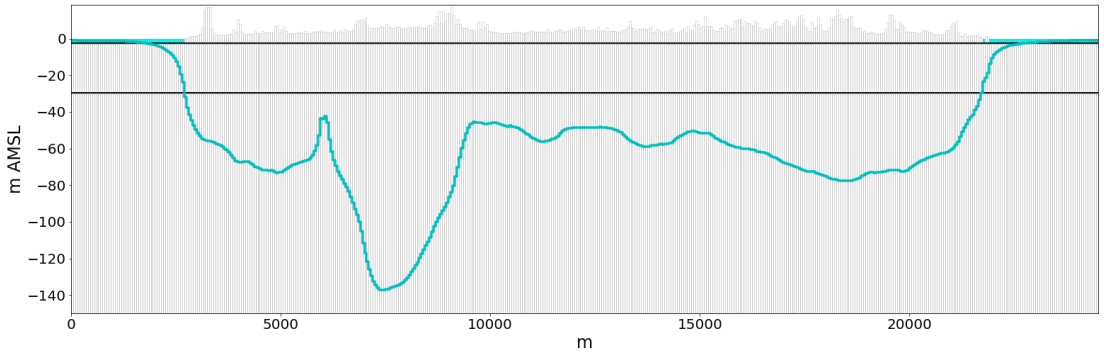

Figure 3.48: Cross-section of the interface along row A for Terschelling

3.2.4.1. Pumping Scenarios

The existing wells in the model were optimized to find the critical pumping rate just less than the amount that would cause saltwater intrusion to enter the well using the transformed model. Wells are assumed

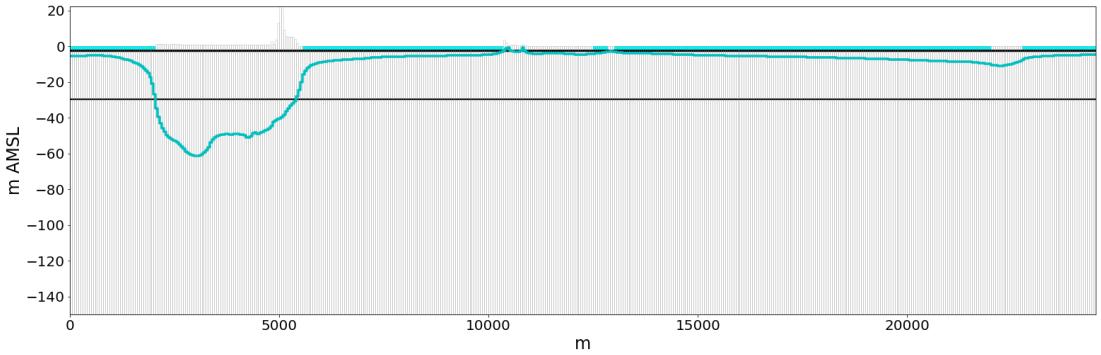

Figure 3.49: Cross-section of the interface along row B for Terschelling

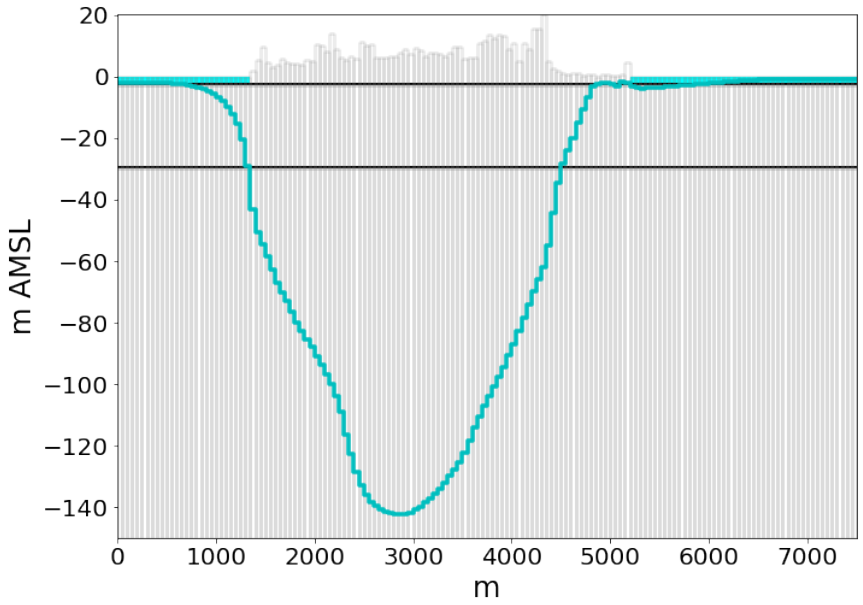

Figure 3.50: Cross-section of the interface along column C for Terschelling

to be fully penetrating so once the interface coincides with the bottom of the layer and position that the well is in, saltwater intrusion is assumed to occur. The critical pumping rate is defined as the maximum pumping rate at which saltwater intrusion does not occur for any well in the model. Each of the seven wells was optimized with each well occupying both the first and second layer of the original model while holding constant the other wells' pumping rates. All of the wells were also optimized together. This was done by increasing the pumping rate for each well proportionally to the transmissivity of the layer that each well is found in until saltwater intrusion occurred.

Table 3.4 gives values of maximum average pumping rates each well can exploit before seawater intrusion occurs while holding pumping in other wells constant at 78 m^3/d of extraction. When all wells are optimized together, the total pumping that the aquifer system can withstand is 5,990 m^3/d of

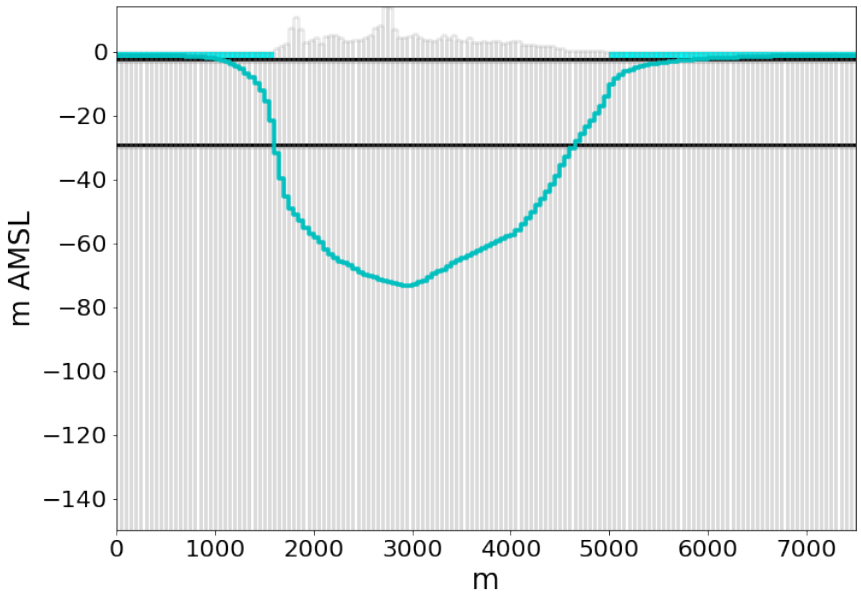

Figure 3.51: Cross-section of the interface along column D for Terschelling

extraction before seawater intrusion occurs. Because the layers have the same thickness and hydraulic conductivity at the pumping locations, the proportion of pumping between layer 1 and 2 is the same for every well. When finding the critical pumping rate of all the wells together, 83% (4,998 m^3/d) of the pumping occurs in the second layer.

Compared to the average pumping rates in the original model the maximum individual critical pumping rate is approximately 15 times greater than what is currently sustained. The critical pumping rate of all wells when optimized together is 11 times greater than the sum of current average pumping rates in the model. This should indicate that according to the model, the area is not at serious risk of overpumping to the extent of causing saltwater intrusion. If large pumping wells were placed however on the eastern portion of the island, the result would likely be different and the island would be less likely to achieve a significant supply of freshwater without causing seawater intrusion.

3.2.5. Interface with Different Sea Levels

Terschelling has different mean sea levels implemented through GHB cells (Figure 3.37). Therefore, the saltwater head beneath the interface varies which impacts the interface position. To solve for this unknown discrepancy, the method in Section 2.6 is used. After the initial interface position is estimated by using a transformed model with constant sea level, the saltwater model and freshwater model are then shaped by that interface as the model top and bottom, respectively. Figures 3.53 and 3.54 show the first iteration model cross-sections for the freshwater and saltwater models, respectively. These

Row,Column	Pumping Rate (m^3/d)
64,120	1140
64,119	1165
63,119	1195
64,120	1140
63,121	1170
63,122	1175
62,123	1230

Table 3.4: Maximum steady pumping rate until seawater intrusion occurs for each Well

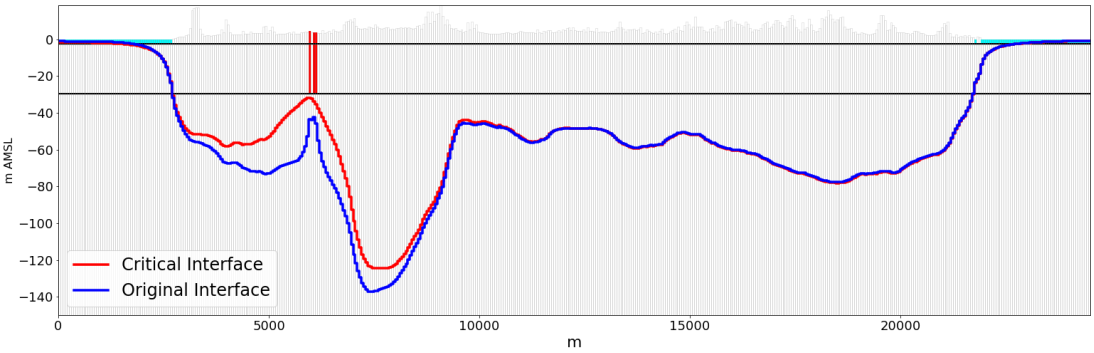

Figure 3.52: Cross-section of the interface along row 64 for Terschelling for the transformed model and then the critical pumping scenario

figures show how the interface estimate is used as the model top or boundary while maintaining the hydraulic parameters of each layer of the original model.

The presented methodology is limited in how it is implemented as when the interface is used as the model boundary, the outer cells are assigned to be inactive as can be seen in Figure 3.53. Once these cells are assigned as inactive, the heads can only be solved within that boundary and there is no way to expand the area. This part of the model that is sloping from the edge to the bottom of the interface represents the outflow zone and because its shape is unknown, it becomes misrepresented and incorrectly warped. The active model area can only move inward because outer cells cannot be reassigned as active so the heads can only be solved in the progressively smaller area with each iteration. This causes a steep interface near the model boundary and an incorrectly deep interface. The incorrectly deep interface is due to a smaller active model area adjusting to the same model inputs so the model must result in higher heads. What can be estimated by this method at least is qualitatively where the interface should deepen in response to the different sea levels by comparing the first results of the method with the constant sea level interface solution. The first results can be used because the model active area has not begun to contract and so it will still be operating realistically. The actual

change in heads in the methods should not be used though.

Figures 3.55 and 3.56 show the first iteration of the different sea level model results compared with the constant sea level interface. These results have not converged so they should not be used as explicit figures. Figure 3.57 shows a map view of the difference in head between the constant sea level model and the first iteration of the different sea level model. These results give a first indication where the interface moves to. It is seen that the western end of the island experiences more interface deepening. As shown in Figure 3.55, another notable result is the interface in the polder area becoming shallower and exceeding the land surface even more. This could be mis-portrayed due to the removal of the DRN (drain) cells that may remove water in this area. Figure 3.57 shows that interface underneath the land portions of the island all deepen and in most areas bordering the island, the interface becomes shallower due to the different sea levels. This represents a shortening of the outflow zone as discussed earlier as a consequence of the methodology. The area with minimal interface interface changes are the areas with fixed boundary conditions including the GHB cells representing drainage and the RIV cells. The implication is that the areas that deepen to compensate for the areas that become shallower on the island edge are best defined as the areas without boundary conditions, particularly freshwater inputs.

Overall, the method is challenged by the fact that once the active model area and discharge area contracts, it has no way of expanding to allow for all possible areas of the model to become active again and reflect the original model. Due to this challenge, the actual final interface cannot be solved for using this method, but qualitative assessments as to where the interface position will change can be made using the first iteration of the proposed methodology.

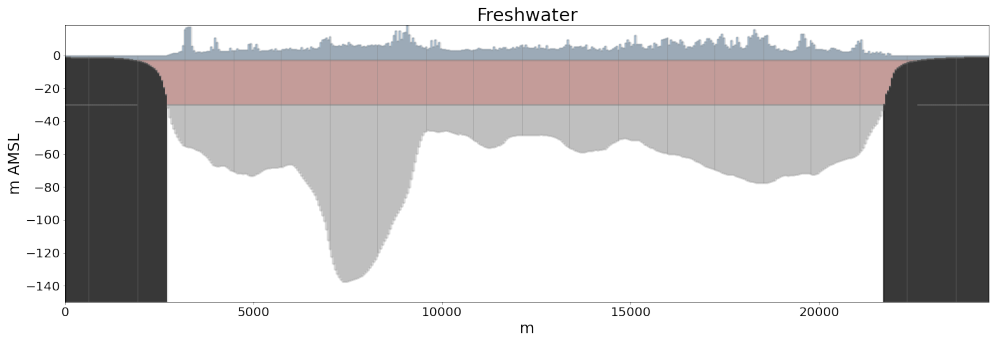

Figure 3.53: Model cross-section using original interface as bottom to model only freshwater

3.2.6. Summary

- Using a transformation of the original model, a realistic interface is successfully computed.

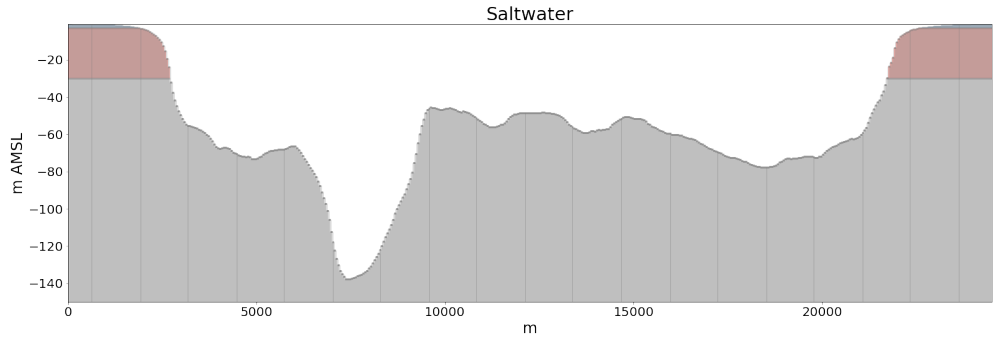

Figure 3.54: Model cross-section using original interface as top to model only seawater

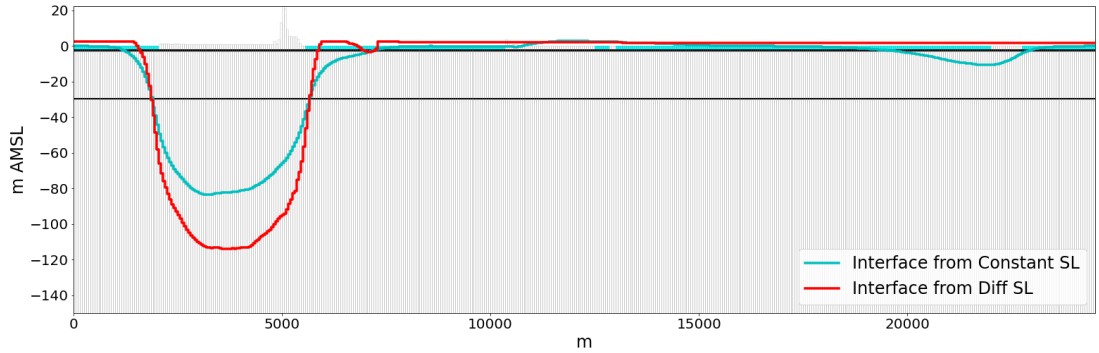

Figure 3.55: Cross-section of interface position of constant sea level (blue) and first iteration of different sea levels (red) along row 111 of Terschelling

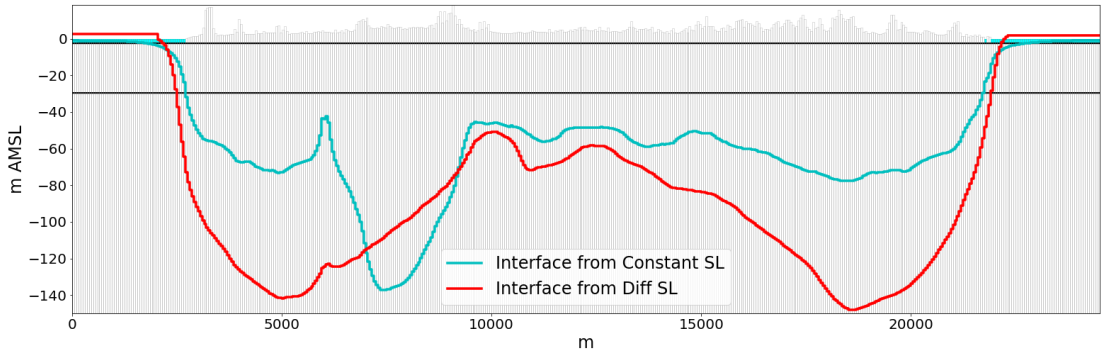

Figure 3.56: Cross-section of interface position of constant sea level (blue) and first iteration of different sea levels (red) along row 64 of Terschelling

- The model predicts an interface for constant sea level with two deep pockets of freshwater on the east and west sides of the island due to recharge from precipitation and the width of the island. The interface is deepest (-147 m AMSL) on the western region of the island.

- The island section near the Wadden Sea has a predicted interface that exceeds land surface. This may be due to the impact that the removed DRN cells have.

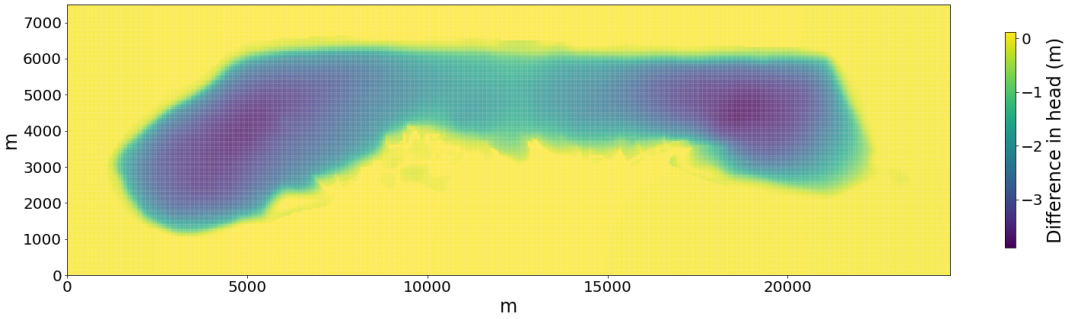

Figure 3.57: Difference in heads between constant sea level transformed model and first iteration of variable sea level model

- The existing model wells are optimized to calculate a critical pumping rate for all wells combined and each well individually. The maximum critical pumping rate for an individual well holding all other pumping constant is 1,230 m^3/d, approximately 15 times greater than the current average individual pumping rate.
- The method to predict an interface with moving saltwater is attempted but incapable of computing a result.Instead, a qualitative assessment can be made regarding where the interface position will change and how it may change.
- The comparison of the first iteration of the variable sea level method and the constant sea level interface show that in the western region of the island, the interface is expected to deepen significantly in response to the moving saltwater and that on the land portion of the model, it is expected to deepen everywhere. Consequently, the interface is expected to become shallower near the island boundary.

3.3. Alamitos

The Alamitos model was developed by the consulting firm INTERA, inc. using MODFLOW (Harbaugh, 2005) in conjunction with the Orange County Water District and the Water Replenishment District based in Southern California, USA. The model is much smaller and is designed to represent much finer geological detail with smaller discretization. The model focuses on the Alamitos Gap injection wells which are a set of injection wells that act as a barrier to seawater intrusion. The model was developed for analyzing whether or not there is saltwater intrusion inland of some partially penetrating wells in the barrier injection system and also for analyzing the travel time of injected water to municipal pumping wells as recycled water is used at the injection sites to supplement water supply so it needs sufficient travel time to qualify for water treatment purposes.

The Alamitos model was unsuitable for the methodology here to try to compute the interface position. The model has a unique relationship where the saltwater has a thin-to-none connection with the active model area. This connection occurs only through the top aquifer. Ultimately, since the model lacks enough connection to the ocean throughout, it is unsuitable. The method is incapable of solving for situations in which there is a disconnect between the sea and the active cells. Because the model does not fit the needs of the methodology, only a brief model description followed by a description of the challenges faced are included.

3.3.1. Area Description

The Alamitos model is located on the eastern border of the Los Angeles model. The Alamitos model focuses on a series of barrier injection wells that straddle the Central Basin in Los Angeles County and the Orange County Groundwater Basin in California. This geologic setting is known as the Alamitos Gap.

In the basin there are two surface water features: the San Gabriel River and Los Cerritos Channel. The other main features of the basin are related to the Newport-Inglewood Uplift (NIU) from the Los Angeles model geology. The NIU caused the Seal Beach Fault which acts as an impediment to lateral flows that mostly keep freshwater heads inland higher and keep seawater intrusion at bay.

3.3.2. Model Description

The model uses a rectilinear MODFLOW grid of 100 ft by 100 ft cells. The model has 200 rows, 365 columns, and 13 layers (7 aquifers, 6 aquitards) for a model length and width of 6.9 and 3.8 miles (11.1 and 6.1 km), respectively. Originally, the model was delivered as a transient model so all boundary conditions that are transient underwent averaging for as a steady-state model.

The area where seawater intrusion is expected to occur in the lower aquifer layers is at the mergence zone where aquifer and aquitard layers pinch out and have the minimally defined thickness of 0.1 ft. The mergence zone is also represented by high vertical hydraulic conductivity values. The injection wells are located in the mergence zone to protect deeper aquifers from saline intrusion through the top aquifer.

3.3.2.1. Boundary Conditions

The landward lateral boundaries are represented by fixed heads using the CHD package for time-varying fixed heads. The ocean level is represented by fixed IBOUND cells (-1) set to 0 m AMSL in layer 1. To represent the inhibition of flow at the Seal Beach Fault, all cells in layers 2-13 seaward of the fault are set as no-flow from the fault line to the ocean boundary. Layer 1 is the only layer with a direct connection to the ocean so all seawater is assumed to come through this layer and then downward to other layers further inland. This conceptual set-up is the primary source of the diconnect between the model and the sea. The inland boundary is set using constant-head (CHD) boundaries to represent lateral flows to and from the model are. The model contains three boundary condition packages: WEL, CHD, and RCH.

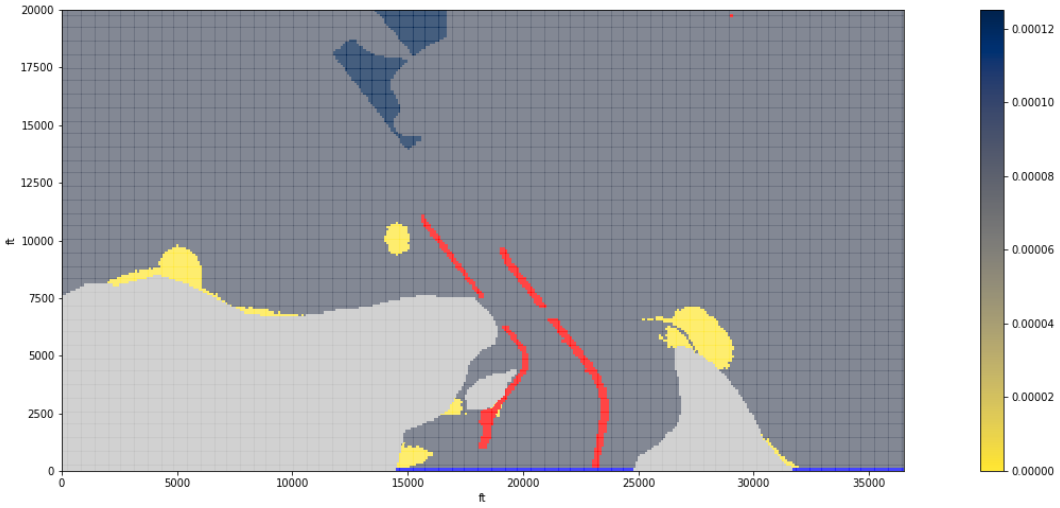

Figure 3.58: Boundary conditions of layer 1 of the Alamitos model: grey cells are inactive cells; blue cells are fixed head; red cells are wells; cells ranging from yellow to dark blue represent recharge values

WEL There are 856 wells in the model. The wells in the model are either extraction wells, injection wells, or even focused recharge cells from channel leakage. There are 21 injection wells represented in layers 5, 7, and 9 and 504 wells used to represent focused recharge from surface channels. The injection wells average inputs of 10,840 ft^3/d. The focused recharge wells have positive rates of 80

ft^3/d and 120 ft^3/d. This leaves 69 wells used for extraction, averaging 17,480 ft^3/d of pumping. The net flux from wells is 478,000 ft^3/d of extraction. Figure 3.58 shows a map layout of the boundary conditions for layer 1 where the red cells represent the wells and the two main collective features of wells are representing focused recharge from the San Gabriel River and Los Cerritos Channel. In the initial model runs, these wells are excluded to simplify the model and to aim for ”pre-development” conditions.

CHD CHD cells were added to represent the lateral model boundaries as time-varying fixed heads. The data came from existing monitoring wells and underwent temporal and vertical interpolation to estimate reasonable boundaries. The data also needed to be interpolated to the relevant active boundary cells. The CHD cells are meant to represent lateral fluxes from inland boundaries but due to data availability, head boundaries were used instead.

CHD cells are averaged for every layer across the length of the boundary and time to give a representative specified head for each time step and layer. Table 3.5 shows these heads for each layer with the added context of the mean bottom layer at the model border where the CHD cells are defined.

Aquifer (Layer)	CHD head (ft AMSL)	Bottom elevation at landward border (ft AMSL)
1(1)	1.1	-102.9
2(3)	-1.5	-213.3
3(5)	-5.1	-310.2
4(7)	-8.9	-463.9
5(9)	-13.9	-704.6
6(11)	-20.7	-1280.2
7(13)	-23.4	-1673.9

Table 3.5: Average values of CHD–specified heads–for each layer and for all stress periods

RCH The areal recharge is applied to the top layer of the model and is equal to 0.37 in/yr (0.94 cm/yr) in most areas. In areas where there is likely to be less runoff, such as large parks, the recharge is set to 0.55 in/yr (1.40 cm/yr). The total amount of recharge is equal to approximately 400 ac-ft/yr (493,400 m^3/yr).

3.3.3. Interface Results

Figures 3.59 and 3.60 show the cross-section of the model layering. These figures demonstrate how the majority of the model’s active area is disconnected with the ocean causing the method to be invalid for this model. Due to the disconnect caused by the fault system of the regional geology, there isn’t

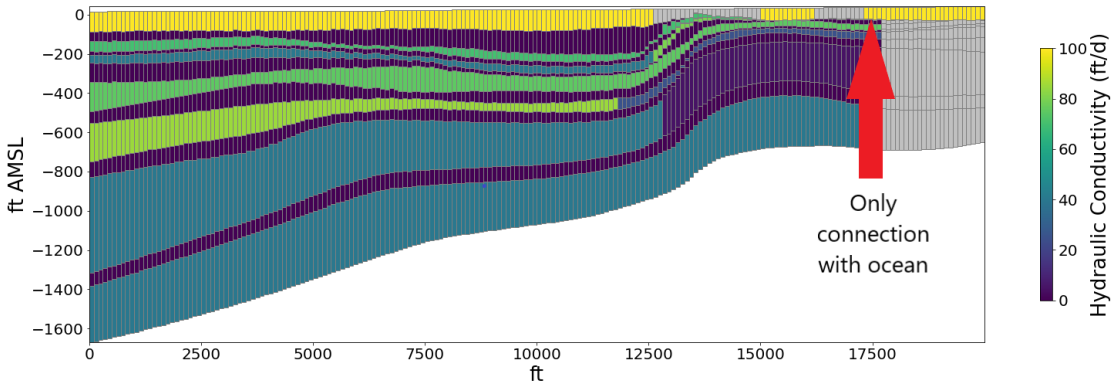

Figure 3.59: Cross-section of Alamitos model column 178; colors correspond to horizontal hydraulic conductivity with grey representing no-flow cells

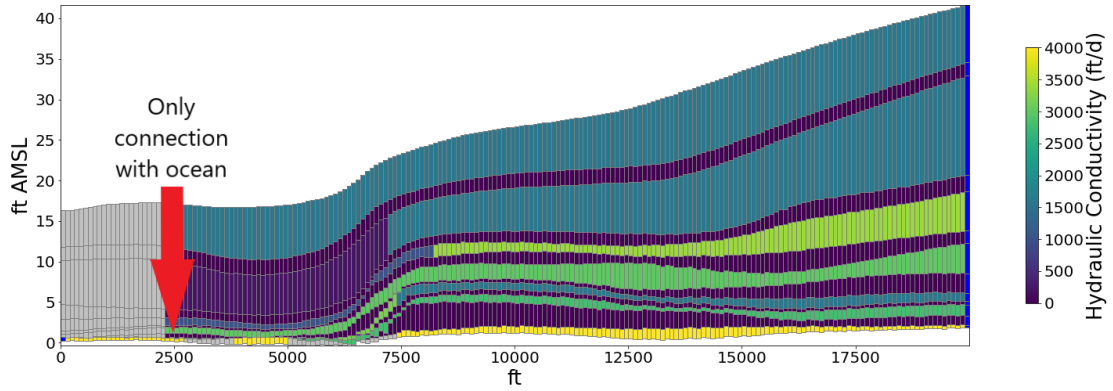

Figure 3.60: Cross-section of transformed Alamitos model column 178; colors correspond to horizontal hydraulic conductivity with grey representing no-flow cells

enough connection between the ocean and the active model area. Before this was fully understood, the model was attempted to run and encountered other challenges as outlined below.

The transformed Alamitos model ultimately fails when it attempts to run. This is because the model is trying to define fixed heads for layers below those layers' bottom elevations causing the model cells to dry out.

The CHD boundary condition on the inland border was adjusted to maintain wet cells by fixing the specified heads to be above the transformed model layer bottoms. This means that it has to be even higher than the top of the normal model due to the model flipping about sea level. The model works for this scenario but realistic results are not available. No seawater intrusion occurs because by definition of this model, the heads are above the inverted and scaled model bottoms which means when the Ghyben-Herzberg relation is applied to the computed heads, the interface position will be completely below the normal model layer bottoms.

In response to this, a flux boundary was employed. It was attempted to determine a flux boundary

that can match the heads computed using the specified head boundary condition. First, the flux had to be determined for the untransformed model that would match the original model results. The flux would be applied through the use of the WEL package. Next, that flux must be applied to the transformed model. However, the transformed model did not give successful results. The pre-determined flux boundary conditions resulted in the drying of the model, which perhaps is realistic given that using original CHD values resulted in the drying out of the model. This represents full saltwater intrusion which also makes sense if all heads except for the top fixed head are below sea level. To try and find what could represent perhaps a pre-development scenario or one in which there is seawater intrusion partially into the aquifer system, the lateral flux at the landward boundary was increased.

3.3.4. Summary

- The Alamitos model represents a smaller area with much finer geological detail and grid cell discretization than the other two models. The main features of the model are injection wells designed to prevent further seawater intrusion.
- All of the model layers except for the surface layer are disconnected from the sea due to faulting.
- This disconnect between the aquifer system and the sea precludes the Bakker and Schaars (2013) method for this setting.

4

Discussion and Conclusions

4.1. Discussion

4.1.1. Implications

In this research it is found that the Bakker and Schaars' (2005) method to estimate the steady interface using single-density groundwater codes applies to real-world, complex models. The method was able to give estimates of the interface position for both models of the Los Angeles' Central and West Coast Basins and of Terschelling Island. The method was applied relatively simply and was able to mitigate concerns over computational expense. The Terschelling model and Los Angeles model were both able to run successfully in under 6 seconds. Computational times of this order are able to effectively and easily be used for management and optimization scenarios.

It is noted that particularly geologically complex areas may be difficult for a simple approach to solve accurately. Geological complexities such as many impermeable faults, or dramatic folds can cause effects of disconnected saltwater plumes which require separate handling. The Alamitos model also demonstrated that areas of minimal connection to the sea can cause problems as well.

While the method is able to apply to models and estimate the steady interface position reliably, there still is significant uncertainty in the actual position of the interface. There is a lack of accurate monitoring and measurement of seawater intrusion in not just these areas, but many around the world. The lack of data and previous models to compare to make it difficult to assess these models accurately.

In the Los Angeles model, the Mendenhall report (1905) was used as a comparison, but there is very limited quantitative data from that report and the boundary conditions are difficult to assess to fit with the hydrology of that time. The Los Angeles model primarily uses data from 1971-2000 which is after the development of the basin where production wells and injection wells had been in place for over a decade and urban landscapes expanded significantly, impacting the natural regime. The boundary heads, particularly in the south-eastern region of the model, can likely result in an interface location that is farther inland than pre-development.

Because of the transport processes involved with saltwater interacting with freshwater, seawater intrusion is complex which makes it difficult to measure. These transport processes are complicated by tidal influences, storm surges, wave swash, and other event-driven influences on saltwater intrusion. In a steady model, these effects are not considered but, depending on the model area, they can play a role. The complex geology discussed above can impact other important model approximations, particularly the neglecting of dispersion. Areas with high dispersion may not be applicable to interface modeling as explained in Chapter 2 assumptions but such areas are impossible to identify with the modeling approached used in this thesis.

The Terschelling model seems to be simple enough to qualify well for the assumptions made in the model except for the approximation that saltwater is not moving. It is isotropic, homogeneous and has nearly all horizontal layer elevations. The moving saltwater approximation is dealt with by fixing the sea level around the island as constant and then attempting to solve for the variable mean sea level. While the method used to solve for the moving saltwater-scenario interface was unsuccessful, this research can help others perhaps complete this iterative approach to compensate for the movement of saltwater.

The Los Angeles model has heterogeneity in aquifer parameters as well as highly variable model elevations. However, the hydraulic conductivity in the Los Angeles model does not vary by more than two orders of magnitude across all layers which gives credence to the transition zone approximations and limits the impact that macro-heterogeneity may have on dispersion. However, the Dupuit approximation may not hold well in the Los Angeles model since there are areas of the model that experience steep head gradients, primarily due to the faults.

4.1.2. Research Objectives Evaluation

Objective 1:

The first objective of this thesis is to evaluate whether the method in Bakker and Schaars (2013) is able to be applied to real-world coastal aquifers by using single-density groundwater codes (MODFLOW).

Evaluation: The first research objective is fulfilled successfully. The method is able to be applied to real-world complex models despite the failure of the Alamitos model. The Alamitos model had a significant disconnect between the sea and the rest of the model preventing the method from working.

Objective 2:

The second objective of this thesis is to evaluate whether the interface can be estimated when saltwater beneath the freshwater is also moving using a novel iterative technique.

Evaluation: The second research objective was not successfully achieved. The method faced a challenge of the model active area contracting without being able to re-expand to include more of the original model active area. However, a qualitative assessment of where the interface position will change and how it will change was made.

4.1.3. Method Implementation Challenges

When the methodology to compute a steady interface was implemented for the different models, key challenges arose that required adjustments. The first common challenge was related to the elevation of boundary condition heads. This refers both to starting heads and also heads in either fixed head boundary condition packages or head-dependent fluxes (GHB, DRN, RIV, etc.). Since the model is transformed (which included flipping each layer about sea level), its model bottom is likely to be higher than it was initially (a likely exception is for the top layer of a model in which some cells are completely above sea level). The starting heads or heads used in boundary condition packages have not been altered so it is possible that some, or all, of these heads are now below the transformed layer bottom automatically translating to a cell that dries out. A dry cell indicates seawater intrusion, but consider the following example:

A model layer with a top of -40 m AMSL and a bottom of -100 m AMSL and a fixed head of 0.5 m AMSL. This model transformed now has a top of 2.5 m AMSL and a bottom of 1 m AMSL with that same fixed head of 0.5 m AMSL. This model will necessarily dry out and indicate saltwater intrusion, but the fixed head tells us that this should not be the case.

This problem was faced specifically in Alamitos because the inland boundary constituted of fixed heads all lower than sea level–which normally would definitively lead to total saltwater intrusion–but instead, the injection wells seaward of this boundary condition protects these low groundwater levels in reality. Similarly, in the Los Angeles model, the starting heads needed to be adjusted to be significantly higher than the default. The original starting heads were low because they were trying to represent relatively recent conditions. For this kind of steady model, the starting heads are not important as long

as they allow the model to run successfully.

The second challenge relates to the correction of layer types. This is an issue addressed in Bakker and Schaars (2005) where they mention that the top layer must be able to be represented as confined. Some models, when transformed, respond differently to the different layer types and in some cases, all layers may be modeled as confined to get accurate solutions. It is important to understand the different layer types and to test the different options out to best represent the given system while understanding the relevant repercussions of those options.

4.1.4. Future Research

To build on this thesis, it is recommended to further validate the Bakker and Schaars (2005) method by building models of the same area using common seawater intrusion modeling codes including SEAWAT (Langevin et al., 2008) and SWI2 (Bakker and Schaars, 2005). A comparison of the results from these more complex modeling tools with the results here would provide insight as to how the method stacks up against other more advanced tools. Similarly, the method used in this thesis to compute the steady interface position for moving saltwater should also be compared to models that solve fully combined flow and transport equations such as SUTRA (Voss and Provost, 2010) and SEAWAT.

More techniques to handle moving saltwater should be investigated as well. This thesis attempts one method but ultimately was unsuccessful and could only provide qualitative indication of where the interface depth should deepen or become shallower. This is an area of research that has yet to find a solution and because of this, it is not yet known how much moving saltwater would even impact the interface depth in comparison with results for a constant sea level model (Bobba, 1993).

A modification to this presented methodology could offer a potential solution. While iterating with the freshwater model and saltwater model to solve for the freshwater and saltwater head components of the solution, the unknown outflow zone causes for the outer cells in the freshwater to become inactive and then it is impossible to reactivate them later on, contracting the active model area incorrectly. Instead of iterating between the freshwater and saltwater models after estimating an initial interface depth, just the saltwater flow could be simulated which would give a saltwater head. This saltwater head could then be used as the sea level in the transformed domain to solve for an interface. That interface could then be used as the top of the saltwater model boundary and iterated between these two steps until a solution is converged upon. There was no time to test this method but it may work and would not have the problems of a contracting active model area.

Improved saltwater intrusion monitoring would also greatly improve the ability of models to represent situations accurately by providing enough reliable data to calibrate with. This is an active area of research that should be expanded in application (Dhar and Datta, 2009; Goebel et al., 2019). There

are geophysical methods using electrical resistivity measurements to go alongside conventional water density and chloride concentration measurements that can provide higher resolution data. Techniques such as airborne electromagnetic imaging also provide potential to fill this gap (Aucken at al., 2010). However, airborne electromagnetic imaging can not be used in highly urbanized areas such as Los Angeles. Using this data helps modelers create more accurate models in a field, seawater intrusion, that is significantly lacking in data. It would be incredibly valuable to apply cheaper, easy-to-use methods to help managers and modelers together understand local saltwater intrusion.

Lastly, it would be interesting to include some, or all, of the injection and extraction wells that exist in the Los Angeles model to see how they are impacting seawater intrusion. These could also then be optimized to prevent seawater intrusion in a steady model.

4.2. Conclusion

Bakker and Schaars (2005) offer a method for steady saltwater intrusion interface modeling. The method requires only a single-density flow model (MODFLOW) in a coastal area. This method has not been applied to real-world models until now. This thesis applied the method to three different models: 1) Los Angeles Basin, 2) Terschelling Island, and 3) Alamitos Gap. The method was successful in determining the interface position for the first two models. There was limited-to-no data available for calibration validation of the models so their accuracy can be improved with improved monitoring data. For the Alamitos model, the connection to the sea was too restricted exposing a known limitation of the methodology.

A new iterative method to compute the steady interface position for a situation in which the saltwater is also moving is also presented and attempted. This relaxes a common assumption of interface modeling and usually represents a situation with different sea levels affecting an area–commonly, an island. The method was unsuccessful due to uncertainties about the outflow zone and the active model area becoming restricted in each iteration. The method was able to provide an indication of the direction of change in the interface depth at each horizontal position in response to the different sea levels as compared to constant sea level results. However, methods using similar styles of iteration schemes may be able to find success with different arrangements avoiding the issues this methodology faced.

Flopy proved a very efficient tool when manipulating models and transforming them. The methodology of Bakker and Schaars (2005) faced a learning curve when implemented to real-world models and some challenges faced are described here to help future modelers accelerate their development. Some boundary conditions must be modified to accommodate for the transformed model including both specified head and head-dependent-flux boundaries. Also, conditions of no-flow causing signifi-

cant disconnect can limit the method's applicability. This method can be improved and validated further in next steps by comparison to other saltwater intrusion model techniques (SEAWAT, SWI). It is also suggested that saltwater intrusion data gathering and monitoring efforts are improved and advanced as it is a severe limitation in saltwater intrusion modeling, particularly when issues of calibration and validation are already glaring.

Bibliography

Auken, Esben, et al. The Use of Airborne Electromagnetic for Efficient Mapping of Salt Water Intrusion and Outflow to the Sea. 2010, p. 4.

Bakker, M., et al. “Scripting MODFLOW Model Development Using Python and FloPy.” Groundwater, vol. 54, no. 5, 2016, pp. 733–39. Wiley Online Library, doi:10.1111/gwat.12413.

Bakker, Mark, and Frans Schaars. Modeling Steady Sea Water Intrusion with Single□Density Groundwater Codes - Bakker - 2013 - Groundwater - Wiley Online Library. 2013, https://ngwa.onlinelibrary.wiley.com/doi/epc 6584.2012.00955.x.

Barlow, Paul M. “Ground Water in Freshwater-Saltwater Environments of the Atlantic Coast.” Circular, 1262, 2003. pubs.er.usgs.gov, doi:10.3133/cir1262.

Bedekar, Vivek, et al. “Approaches to the Simulation of Unconfined Flow and Perched Groundwater Flow in MODFLOW.” Groundwater, vol. 50, no. 2, 2012, pp. 187–98. Wiley Online Library, doi:https://doi.org/10.1111/j.1745-6584.2011.00829.x.

Biddle, Kevin T. The Los Angeles Basin: An Overview. AAPG Special Volumes, 1991

Bobba, A. G. “Mathematical Models for Saltwater Intrusion in Coastal Aquifers.” Water Resources Management, vol. 7, no. 1, Mar. 1993, pp. 3–37. Springer Link, doi:10.1007/BF00872240.

Carrera, Jesus, et al. “Computational and Conceptual Issues in the Calibration of Seawater Intrusion Models.” Hydrogeology Journal, no. 18, Oct. 2009, pp. 131–45, doi:10.1007/s10040-009-0524-1.

Cheng, A. H. D., et al. Pumping Optimization in Saltwater□intruded Coastal Aquifers. 1 Aug. 2000, https://agupubs.onlinelibrary.wiley.com/doi/abs/10.1029/2000WR900149.

Dausman, Alyssa M., et al. A Comparison between SWI and SEAWAT – the Importance of Dispersion, Inversion and Vertical Anisotropy. 2010, p. 4.

Dhar, Anirban, and Bithin Datta. “Saltwater Intrusion Management of Coastal Aquifers. II: Operation Uncertainty and Monitoring | Journal of Hydrologic Engineering | Vol 14, No 12.” Journal of Hydrologic Engineering, vol. 14, no. 12, Dec. 2009, https://ascelibrary.org/doi/full/10.1061/%28ASCE%29HE.1943-5584.0000155?casa_token=bzYHmIeaK3MAAAAA%3AQQVTdZsG7U6vdrt131DC-QkYxTGzTP4VVYSrsllYvmAw-H1afuo9iOPuPsKloLodxFXdV6H2-A.

Goebel, Meredith, et al. “Mapping Saltwater Intrusion with an Airborne Electromagnetic Method in the Offshore Coastal Environment, Monterey Bay, California.” Journal of Hydrology: Regional Studies,

vol. 23, June 2019, p. 100602. ScienceDirect, doi:10.1016/j.ejrh.2019.100602.

Gottschalk, Ian, et al. “Using an Airborne Electromagnetic Method to Map Saltwater Intrusion in the Northern Salinas Valley, California.” GEOPHYSICS, vol. 85, no. 4, Society of Exploration Geophysicists, June 2020, pp. B119–31. library.seg.org (Atypon), doi:10.1190/geo2019-0272.1

Harbaugh, Arlen W., et al. “MODFLOW-2000, The U. S. Geological Survey Modular Ground-Water Model-User Guide to Modularization Concepts and the Ground-Water Flow Process.” Open-File Report. U. S. Geological Survey, vol. 92, 2000, p. 134.

Harbaugh, Arlen W. “MODFLOW-2005, the US Geological Survey Modular Ground-Water Model—the Ground-Water Flow Process: US Geological Survey Techniques and Methods 6-A16.” A16, 2005, p. Variously Paginated.

Kummu, Matti, et al. “Over the Hills and Further Away from Coast: Global Geospatial Patterns of Human and Environment over the 20th–21st Centuries.” Environmental Research Letters, vol. 11, no. 3, IOP Publishing, Mar. 2016, p. 034010. Institute of Physics, doi:10.1088/1748-9326/11/3/034010.

Langevin, Christian D., et al. “Documentation for the MODFLOW 6 Groundwater Flow Model.” Documentation for the MODFLOW 6 Groundwater Flow Model, vol. 6-A55, USGS Numbered Series, 6-A55, U.S. Geological Survey, 2017. pubs.er.usgs.gov, doi:10.3133/tm6A55.

Mantoglou, Aristotelis. Pumping Management of Coastal Aquifers Using Analytical Models of Saltwater Intrusion - Mantoglou. 4 Dec. 2003, https://agupubs.onlinelibrary.wiley.com/doi/full/10.1029/2002WR001891.

Mendenhall, Walter C. Development of Underground Waters in the Western Coastal Plain Region of Southern California. Water-Supply and Irrigation Paper No. 139, USGS, 1905.

Mercer, James W., et al. “Simulation of Salt-Water Interface Motion.” Groundwater, vol. 18, no. 4, 1980, pp. 374–85. Wiley Online Library, doi:https://doi.org/10.1111/j.1745-6584.1980.tb03412.x.

Pool, Maria, and Jesus Carrera. A Correction Factor to Account for Mixing in Ghyben□Herzberg and Critical Pumping Rate Approximations of Seawater Intrusion in Coastal Aquifers. 7 May 2011, https://agupubs.onlinelibrary.wiley.com/doi/full/10.1029/2010WR010256.

Reichard, E. G., et al. Geohydrology, Geochemistry, and Ground-Water Simulation-Optimization of the Central and West Coast Basins, Los Angeles County, California. Water-Resources Investigations, 03–4065, USGS, 2003, https://pubs.usgs.gov/wri/wrir034065/wrir034065.html.

Shamir, U., and G. Dagan. “Motion of the Seawater Interface in Coastal Aquifers: A Numerical Solution.” Water Resources Research, vol. 7, no. 3, 1971, pp. 644–57. Wiley Online Library, doi:https://doi.org/10.1029/WR007i003p00644.

Werner, Adrian D., et al. “Seawater Intrusion Processes, Investigation and Management: Recent Advances and Future Challenges.” Advances in Water Resources, vol. 51, Jan. 2013, pp. 3–26. ScienceDirect, doi:10.1016/j.advwatres.2012.03.004.

Yerkes, R.F., et al.. Geology of the Los Angeles Basin, California: -An Introduction. U.S. Government Printing Office, 1965.

A

Los Angeles Model Data

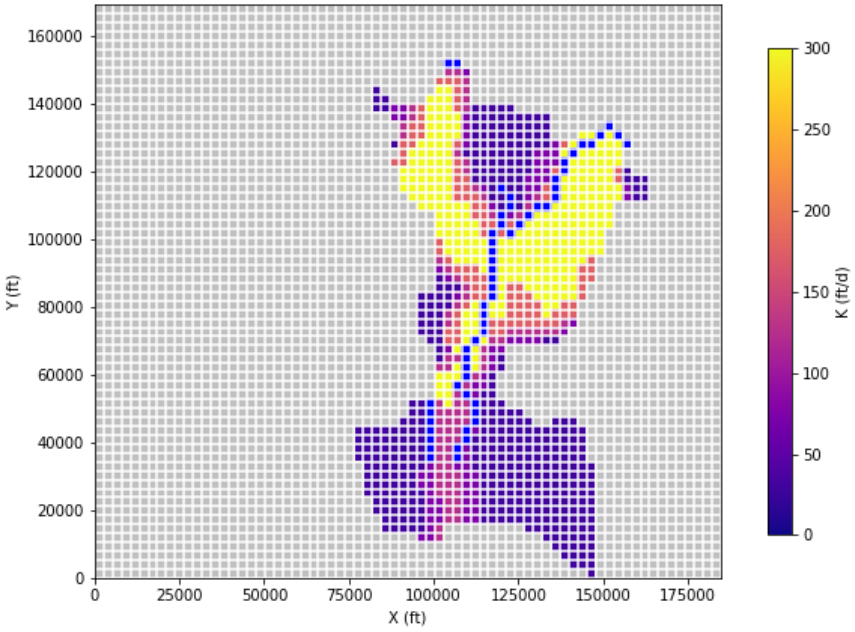

Figure A.1: Hydraulic Conductivity for Layer 1 of the Los Angeles model (ft/d)

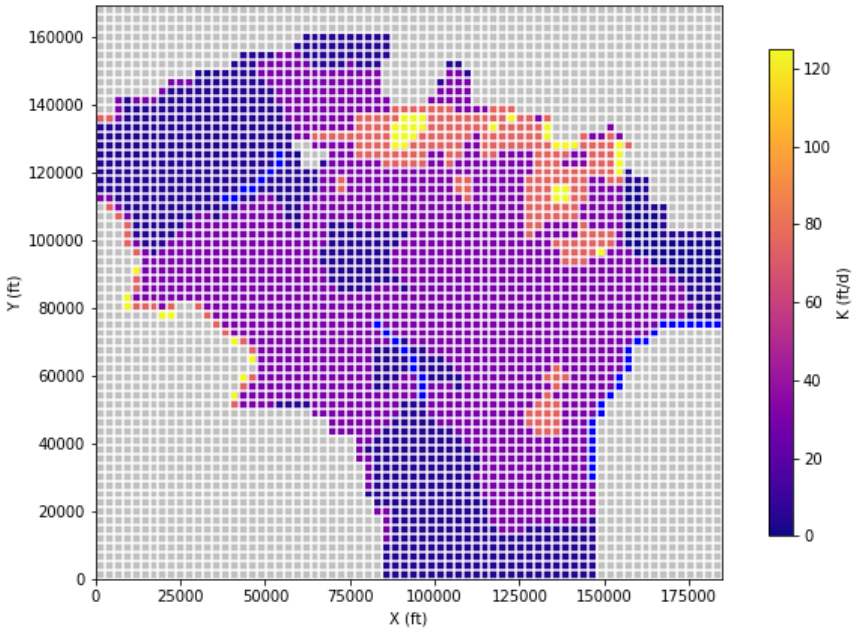

Figure A.2: Hydraulic Conductivity for Layer 2 of the Los Angeles model (ft/d)

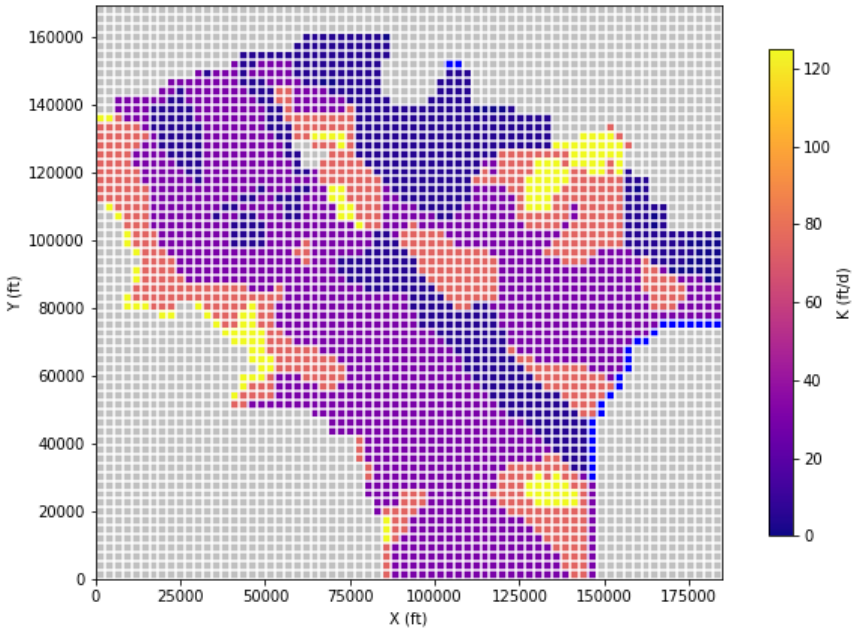

Figure A.3: Hydraulic Conductivity for Layer 3 of the Los Angeles model (ft/d)

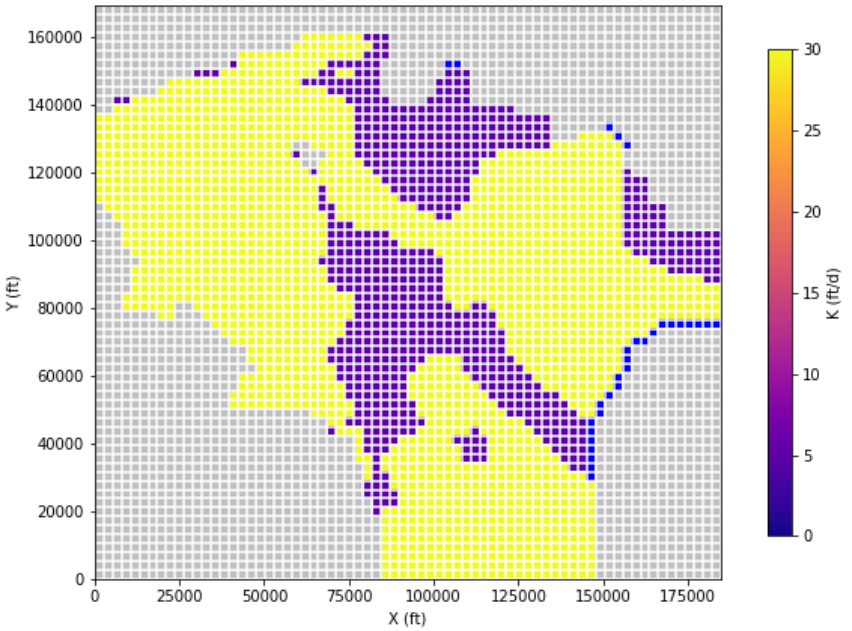

Figure A.4: Hydraulic Conductivity for Layer 4 of the Los Angeles model (ft/d)

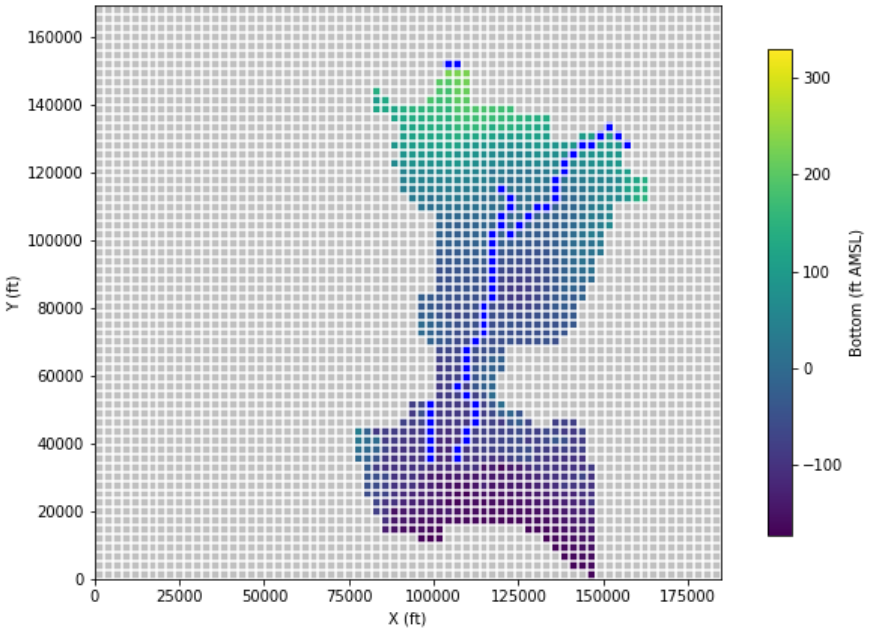

Figure A.5: Bottom Elevations of Layer 1 of the Los Angeles model (ft)

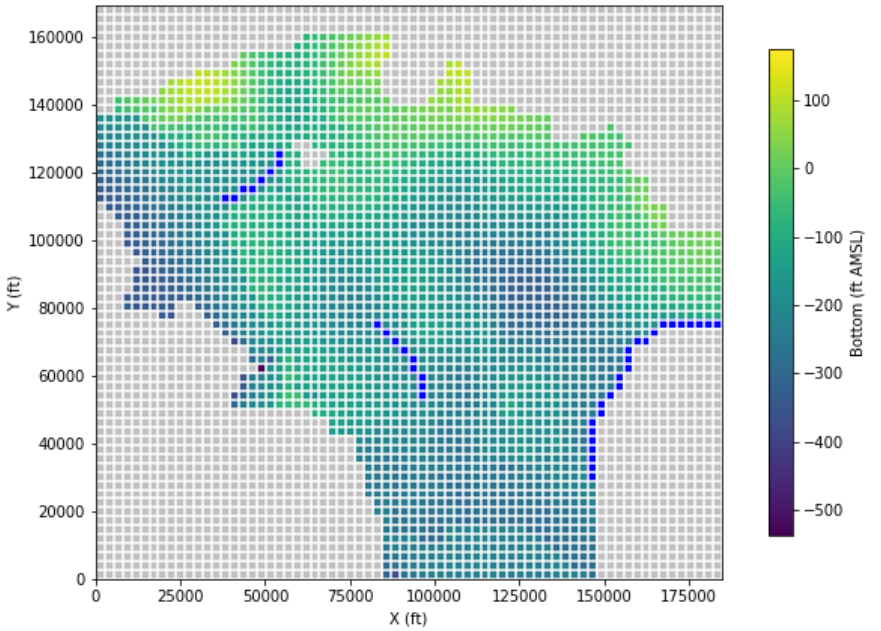

Figure A.6: Bottom Elevations of Layer 2 of the Los Angeles model (ft)

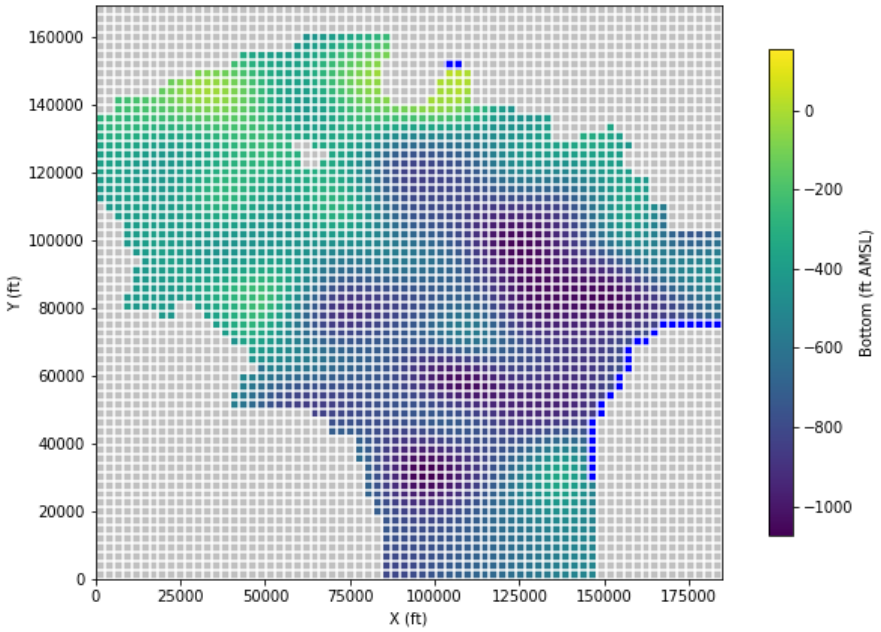

Figure A.7: Bottom Elevations of Layer 3 of the Los Angeles model (ft)

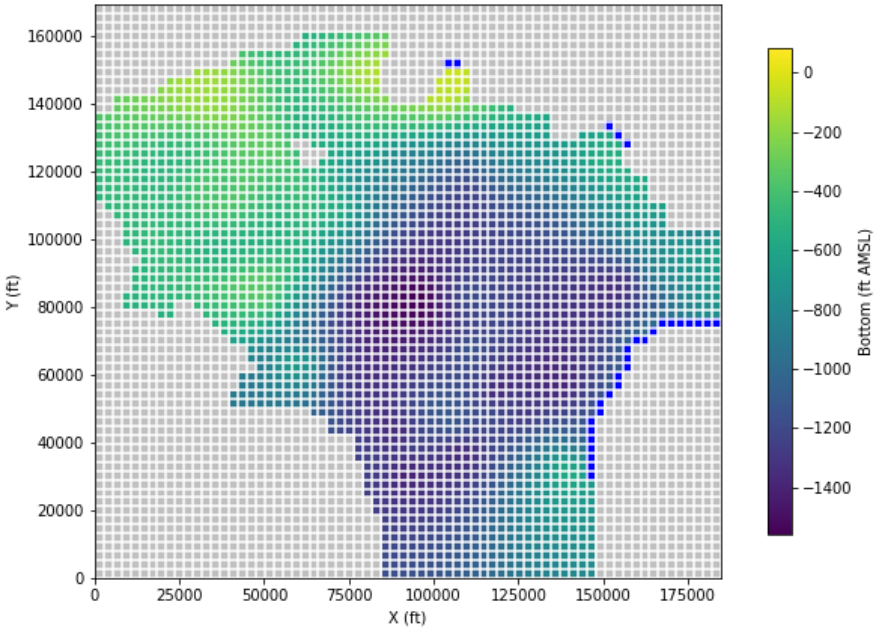

Figure A.8: Bottom Elevations of Layer 4 of the Los Angeles model (ft)